MODELING THE RESPONSES OF LIGHT-ACTIVATED SHAPE MEMORY POLYMERS

A Dissertation

by

ZHI YUAN

Submitted to the Office of Graduate and Professional Studies of
Texas A&M University
in partial fulfillment of the requirements for the degree of

DOCTOR OF PHILOSOPHY

Chair of Committee,	K.R.Rajagopal
Co-Chair of Committee,	Anastasia Muliana
Committee Members,	Alan Freed
	Raytcho Lazarov
Head of Department,	Andreas A. Polycarpou

December 2017

Major Subject: Mechanical Engineering

ABSTRACT

The aim of this study is to model the macroscopic response of light-activated shape memory polymers (LASMPs) subject to mechanical loadings and exposure to light at certain wavelengths and frequencies. When exposed to external stimuli of mechanical, thermal, photochemical and other origins, polymers undergo microstructural changes, e.g., scission, crosslinking, crystallization, etc. These microstructural changes affect the macroscopic performance of the polymers. In this study, in order to incorporate the effect of microstructural changes on the macroscopic response of light-activated shape memory polymers, we formulate constitutive models based on the notion that the natural configuration of the body under consideration evolves during its response. The theoretical framework appeals to a multi-network approach consisting of two microstructural networks, which are the original network and the new network formed owing to a light activation. Firstly two different nonlinear elastic models are considered based on photo-tunable molecular crosslinks (PMC) LASMPs. The first model assumes the two networks are isotropic. The second model takes into account the directional preference owing to the anisotropy of the second network that is formed. Several classical boundary value problems involving homogeneous and inhomogeneous deformations are studied. We also investigate two nonlinear constitutive relations and different loading modes. The results highlight the differences in the responses when isotropic and anisotropic models are considered.

Furthermore, with a view toward incorporating two different mechanisms and determining the effect of the viscoelasticity of the polymers, a single integral model is adopted to incorporate the viscoelastic response in the original and second networks. We study the response of viscoelastic light-activated shape memory polymers subject to uniaxial and biaxial tension. Parametric studies are carried out to obtain a better understanding of the effect of quantities such as relaxation time and the ratio of the relaxation modulus to the instantaneous modulus. Finally, the model is used to describe the stress relaxation behavior of photo-induced network rearrangement (PNR) LASMPs reported in the literature.

In order to solve boundary value problems with complex geometries and boundary conditions, the constitutive models based on the multi-network configuration are implemented in user material subroutines (UMAT) within ABAQUS finite element analysis. Finite element is then used to simulate and investigate the response of the structures integrated with LASMPs, such as folding in flexible structures to mimic morphing wings and shape changes in lattice structures.

ACKNOWLEDGEMENTS

I would like to express my deepest appreciation to my advisor, Professor K.R.Rajagopal. Without your guidance, maybe I will never have a chance to walk into the world of mechanics. Your richness of knowledge, dedication to research and integrity will inspire me for my whole life. Sincerely thank you for always giving me encouragement and freedom to pursue and implement the ideas about the research work and career development.

I also want to send my deepest gratitude to my co-advisor, Professor Anastasia Muliana. I will never forget the discussion moments with you, whenever I had what kinds of problems about research, you were always so patient to help me sort out the ideas and provide valuable discussions which really broadened the horizon to mechanics. Without your support, I cannot complete my research so smoothly.

I would like to thank Professor Alan Freed and Professor Raytcho Lazarov for serving as my committee members. You are always so kind whenever I need help from you.

I want to thank my friends, lab mates and all people I met during the past five years. Here I won't list all your names, but the acknowledgement for your help is sent from my heart and you are very important for me.

Finally I want to send my special thanks to my family members. Thank my father and brother for unconditional support and understanding. Thank my parents-in-law for everything you have done for me, you were sacrificed so much. I want to thank my wife,

Yan Pan, for giving me so much love, understanding, encouragement and tolerance in these 5 years hard time. I am also grateful for my two dear kids, Alice and Allen, you always can bring me sunshine in the darkness and happiness in the difficulty, I am proud of you. Love you all.

CONTRIBUTORS AND FUNDING SOURCES

This work was supervised by a dissertation committee consisting of Professor K.R.Rajagopal (advisor), Anastasia Muliana (co-advisor), and Alan Freed of the Department of mechanical engineering and Professor Raytcho Lazarov of the Department of Mathematics.

All work for the dissertation was completed by the student, under the advisement of Professor K.R.Rajagopal and Anastasia Muliana of the Department of mechanical engineering.

This work was made possible in part by the Air Force Office of Scientific Research (AFOSR) under grant FA9550-14-1-0234.

TABLE OF CONTENTS

Page

LIST OF FIGURES

Page

LIST OF TABLES

Page

CHAPTER I

INTRODUCTION[*]

The development of new materials is one of important aspects in science and technology that allows overcoming current technological limitations and adding new functional capabilities. Material development often starts at the laboratory scale before they are being used in practical engineering applications. This presents several challenges with regards to material characterization, which is often done at the laboratory scale, and prediction of the overall response of real structures, such as limited information that can be gained from lab-scale material characterization and lack of systematic analyses, design and manufacturing [1]. Different applications also require different material performance and characteristics [1-6] in addition to constraints due to cost and aesthetic aspects, which can further complicate the material development and engineering design. There is clearly a need for analytical and design tools that are capable in capturing the response of structures during service conditions, while incorporating proper material behaviors under various external stimuli.

Recent advances in smart or intelligent materials open doors to the development of adaptive structures that are actively and efficiently responding to external stimuli. For

[*] Part of this section is reprinted with permission from "Modeling the response of light-activated shape memory polymers" by Zhi Yuan, Anastasia Muliana, and Kumbakonam Ramamani Rajagopal, 2017. Mathematics and Mechanics of Solids, 22(5), pp.1116-1143. Copyright 2017 by SAGE Publications.

[*] Part of this section is reprinted with permission from "Quasi-linear viscoelastic modeling of light-activated shape memory polymers" by Yuan Zhi, Anastasia Muliana, and K. R. Rajagopal, 2017. Journal of Intelligent Material Systems and Structures, p.1045389X17689936. Copyright 2017 by SAGE Publications.

example, integrating smart or intelligent materials in engineering structures allows to control various properties (mechanical, electrical, thermal, etc.) and functions of the structures to meet the performance needs [7]. Shape memory material is one kind of smart materials which is able to recover their original shape at the presence of right stimulus. This study focuses on modeling response of shape memory polymers, activated by light irradiation.

1.1 Shape memory materials

Shape memory materials (SMMs) have been widely used and studied in virtue of their unique properties. They can be programmed to have two or more different configurations and change back and forth between these different configurations due to mechanical and non-mechanical stimuli, such as heat, light, magnetic, electric, and water/solvent [8]. Roughly SMMs can be divided into shape memory alloys (SMAs) and shape memory polymers (SMPs).

SMAs are now being used in many applications in military, commercial, and biomedical fields because of their obvious advantages like high strength and fast actuations [9]. However, the limitations of SMAs also restrict their applications such as high cost, limited recoverable strains, challenging processing conditions, and inflexible transition temperatures. Hence SMPs have been developed alternatively to overcome some of the drawbacks in SMAs, especially the appealing characteristics of biocompatibility and biodegradability of SMPs can widely extend their potential applications in biomedical applications such as smart implants, internal sutures and

micelles used for targeted drug delivery [10-12]. Other proposed functions include robotics [13], artificial muscles[14], smart textiles and apparels [15], and sensors and actuators [16], candidate materials for morphing aircraft and satellite structures [17, 18], and so on.

The initial class of SMPs, similar to SMAs, use heat as a stimulus, which is often referred to thermally activated SMPs (TASMPs). They use the glass transition mechanism or the melt transition mechanism to switch between the rubbery phase and glassy/crystalline phase, which have different mechanical properties [19]. Several studies related to experiments, modeling and applications of TASMPs have been documented in the literature [60, 61]. Another class of SMPs use light irradiation to switch between the different phases, known as light activated SMPs (LASMPs). Compared to the heating protocol, light technology can be spatially controlled in a precise manner by selecting suitable wavelengths, polarization directions and intensity, and they can be easily operated from afar. Also it is reported that LASMPs need much less energy input to trigger network changes comparing with TASMPs (the amount of heat required for TASMPs is between 16.4 J/g and 324.2 J/g, the LASMPs require only ~1.4 J/g [20][21]). It is possible to functionalize shape memory response at ambient temperature with athermal stimulus which can benefit many applications [17]. For example in minimally invasive surgery, LASMPs have the advantages of avoiding the tissue damage or injury due to overheating by providing the sufficient operation space.

1.2 Current research on LASMPs

In LASMPs light is used as a stimulus to induce deformations in the polymers through microstructural changes. Depending on the type of LASMPs different mechanisms of microstructural changes are observed:

1. Photothermal SMPs. They use light as a heat source to increase the temperature to the switch transition temperature in order to trigger the shape recovery. Typically particles or composites such as carbon blacks and CNTs are incorporated to improve the light absorption efficiency [22-24]. This kind of polymers is actually based on the thermally activated mechanisms.
2. Photochemical SMPs. This type of SMPs can change shape or respond under light activation due to chemical structure alterations. They can be further divided into two categories based on the material responses [25]. The first type is the one that starts in an initial stress free state, and exert a force on their surroundings when stimulated, and then return to their initial state when the stimulus is removed, without the use of external forces. For example, azobenzene-containing liquid-crystal elastomers were found to be photo-responsive and since azobenzenes are photoisomerizable molecules, which can have cis- and trans- conformations under exposure to light of a specific wavelength [26, 27]. Triphenylmethane leuco derivatives can form ionization reactions and ion-pair formation under UV irradiation; thus, polymers incorporated with these molecules can have the property of photo-induced swelling and shrinkage [28, 29]. The second one is a little different which needs external forces to deviate from their initial state. The photosensitive molecules in the

polymers can form or cleave a new crosslink resulting in the shape memory effects due to modulus change under the irradiation of the light with some specific wavelength or frequencies that realize. In this thesis, the LASMPs of the second type of photochemical SMPs are studied.

1.2.1 Experimental observation

In 2005 Lendlein et al. [30] discovered LASMPs with photo-tunable molecular crosslinks (PMC) where cinnamic acid or cinnamylidene acetic acid moieties work as light-triggered switches incorporated into the polymer architecture. Upon exposure to UV light of $\lambda > 260nm$, a new network is formed by the photoresponsive molecules, and reversibly cleaved by irradiation with UV light of $\lambda < 260nm$. Cyclic photomechanical experiments on LASMPs with two different strategies were carried out under both stress control and strain control conditions. In this LASMP stress relaxation behavior is rather insignificant. The grafted polymer has the maximum strain-fixity rate (R_f) of 52% and the strain-recovery rate (R_r) of 95%, while for the interpenetrating network R_f is 33% and R_r is 98%.

Scott et al. [31] developed LASMPs which display photo-induced stress relaxation which is attributed to photo-induced network rearrangement (PNR) wherein cleavage of the residual photoinitiator molecules are formed by light instigation from free radicals, which can react and produce addition-fragmentation chain and transfer through functional groups in the polymer backbone. There are three control experiments

carried out to study the behavior of PNR LASMPs. All of them were subjected to the same mechanical loading history, namely extension for 12 minutes at the rate of 0.5% strain per minute and then keeping the strain constant for around one hour, but differ either in the weight percentage of Irgacure 184 or in the irradiation treatment. The first specimen is not a standard PNR LASMPs because it had no Irgacure 184 which is a photo initiator although subjected to light irradiation, so it is impossible to form a new network. It is not within the scope of this study. The second specimen which is the standard setting of PNR LASMPs received both light irradiation and consists of 3 wt% Irgacure 184, there is a very dramatic decrease in stress, up to 70%. The third specimen contained 3 wt% Irgacure 184 but did not receive light irradiation, 3% decrease of the stress is observed. As discussed in this article depending on the external stimuli prescribed, the material can experience significant stress relaxation.

For the above two LASMPs, thermal effects are insignificant and neglected. Polymers of similar structure to the LASMPs have specific heats ranging from 103.4 to 215.3 J/mol*K [32]. But only a portion of the incident optical energy is absorbed as heat, the remaining are reflected, transmitted, and utilized for crosslinking, with a portion of that heat being diffused to the sample's surroundings, so the temperature changes very little to affect the property [25]. However, the thermal effects are possible to be important for some conditions including strong absorption of LASMPs, large intensities, insulating boundary conditions, highly exothermic photochemistry and so on [33]. In our study we will not consider the impact factor of temperature change to the mechanical property of LASMPs.

The physical mechanism of PMC LASMPs can be described by the process depicted in Fig. 1: in the initial configuration or permanent shape, the body is composed of only one network wherein the photosensitive molecules are disconnected; this is then loaded by a force till the body comes to a deformed shape, followed by exposing the material to light of a certain wavelength or frequency, the photosensitive molecules begin to connect to each other and form a new network; by releasing the force completely, the body will not go back to the original shape but attains a temporary shape, that is, there is some residual stretch retained in the body; further by exposing the material to light of another wavelength, the newly formed network will be cleaved which leads to the body returning gradually back to the original shape. In PMC LASMPs, formation of a new network due to irradiation is associated with connecting photosensitive molecules and it does not affect the structures of the original network. The mechanism of PNR LASMPs is shown as Fig. 2. Instead of the second network forming due to the pendant photoinitiators directly, in PNR LASMPs the embedded photo initiator molecules in the original network need to be cleaved under the irradiation of light and dissociated into free radical fragments which leads to subsequent fragmentation of the polymer backbone. This type of photo-induced network rearrangement transfers one network to another new network resulting in stress relaxation, which is observed macroscopically. Thus, in PNR LASMPS, as a new network is forming, the amount of the original network is decreasing. More details will be presented in the constitutive modeling and application part (Chapter II).

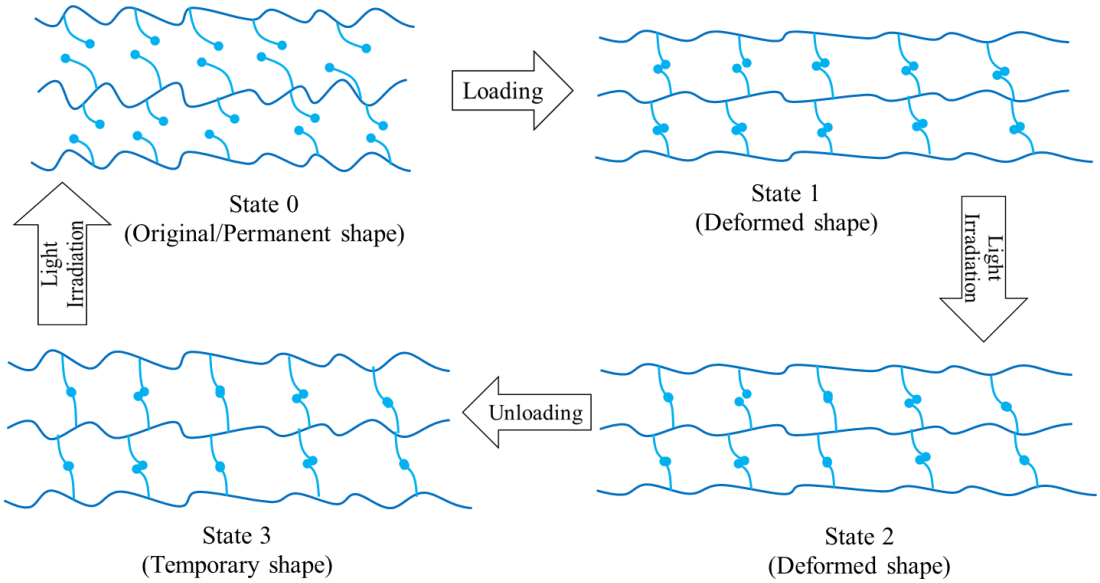

Fig. 1 Schematic plot of the mechanism of PMC LASMPs

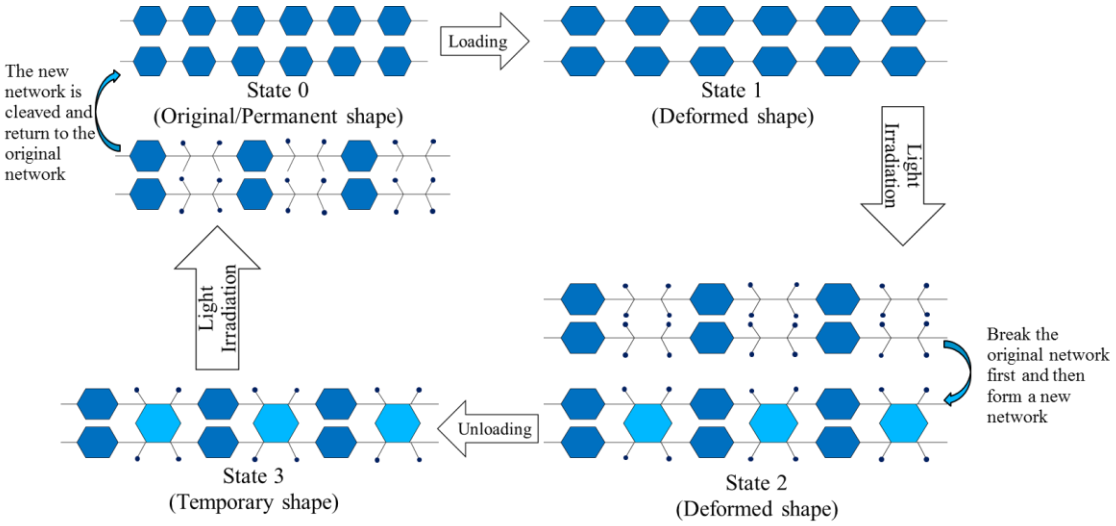

Fig. 2 Schematic plot of the mechanism of PNR LASMPs

1.2.2 Modeling approach

There are currently few studies devoted to modeling the mechanical behavior of LASMPs. Beblo and Weiland [34] proposed a standardized in situ method for characterizing the temporal and spatial variations inherent in both the light stimulus and propagation in materials. The experimental results validated that the absorption of light in the polymers followed the Beer-Lambert-Bouguer Law. A chemical kinetic model is presented to predict the through –thickness evolution of Young's modulus of the polymers. Further Beblo and Weiland [35, 25] provided a multiscale model based on molecular structures to predict the soft and hard state moduli of the polymers which can aid the design and development of LASMPs. This model firstly used rotational isomeric state theory to build a molecular model of a single polymer chain, then calculated the entropy with respect to strain via probability density function which was needed to use statistical mechanics to predict the modulus of the polymer. Finally to ensure macroscopically fitting with property of the LASMPs, they adopted the junction constraint theory to consider the interaction or entanglement with neighboring chains. The results showed that the predicted Young's modulus can match well with the one determined experimentally in soft state but not good in hard state. Li et al. [36, 37] improved this chemical kinetic model and adopted it for active vibration controls by manipulating the frequencies of elastic beams and cylindrical shells coupled with LASMPs patches.

Sodhi and Rao [38] considered multiple natural configurations [39, 40] in order to describe the macroscopic behavior of LASMPs under mechanical loading and light activation. Their work mainly focuses on the isotropic elastic behavior of the materials, although they discussed the possibility of deformation-induced anisotropy in the response of LASMPs as they undergo large deformations. Also, in this study, Sodhi and Rao [38] assumed that the intensity of light was homogeneous and they also considered homogeneous deformations. In a recent paper, Sodhi, Cruz and Rao [41] considered inhomogeneous light intensity and also inhomogeneous deformations.

Long et al. [42] developed a three-dimensional finite deformation model to simulate the photomechanical behavior of LASMPs with various operative mechanisms by incorporating light propagation through the solids, photochemistry that is responsible for shape memory cycle, chemical-mechanical coupling and mechanical deformation. They also implemented their model in a finite element setting and their model was capable of predicting the behavior of photo-induced stress relaxation and bending. In this model, they used the Arruda–Boyce eight-chain hyperelastic model to represent the mechanical behavior of all networks and assumed the second network was stress free at the moment of its creation which was also referred to follow the theory of natural configurations. By following this framework, they explored more about the photomechanics that can facilitate shape change and actuation technologies [43, 44]. However, this model neglected the possible anisotropy property when the polymers undergo large deformations, and ignored the inherent viscoelastic characteristics.

Most of the existing LASMPs models are based on isotropic hyperelasticity and do not consider the time dependent responses of polymers. However, the additional crosslinkings are formed based on a deformed state which may cause the second network has some preferred orientation and shows anisotropic performance macroscopically. As LASMPs undergo microstructural changes during loadings and exposure to light radiations, constitutive models will be derived based on multiple natural configuration approach. The theory of the multiple natural configurations has been used to model response of various materials undergoing microstructural changes such as metal plasticity [45], twinning induced deformation [46], viscoelastic solids and fluids [47], solid-to-solid phase transition [48], polymer crystallization [49], and anisotropic liquids [50]. It allows capturing the mechanical behavior during the process of phase transformation and furthermore taking the anisotropy change into consideration.

1.3 Research objectives and scope

The main objective of this study is to develop a constitutive model to describe the mechanical behavior of the LASMPs and obtain the solutions to the boundary value problems either analytically or numerically, depending on the complexity of the problems. The constitutive model is derived based on the theory of multiple natural configurations, firstly considering hyperelastic behavior for each network and then incorporating the viscous effect by adopting quasi-linear viscoelastic model. Both isotropic and anisotropic behaviors will be considered. Specific research tasks include:

1. Develop a nonlinear elastic constitutive framework to model full cycle of the mechanism of the LASMPs. Since the formation of the second network takes place on a deformed configuration, two elastic models will be considered, firstly both networks are assumed isotropic, and the other is to study the effect of anisotropic behavior induced by the second network.

2. Develop a viscoelastic model to capture the relaxation behavior of the LASMPs. By assuming the formation of the second network can change the mechanical properties of LASMPs such as shear modulus or relaxation characteristic time, we aims to unify both PMC and PNR mechanisms into one framework by considering the PNR mechanism may cause obvious stress relaxation while PMC does not. Then use the model to capture the experimental data of LASMPs available in literature.

3. Implement the above constitutive models in ABAQUS finite element via user subroutines. For the problems with more complex geometry or boundary conditions, it is almost impossible to obtain analytical solutions. Finite element method is used to obtain approximate solutions to boundary value problems.

4. Simulate shape changes in several structural components consisting of LASMPs under various loading conditions and geometries using finite element method. This tool can be used to analyze and design structural components with shape changing capabilities.

1.4 Dissertation organization

Chapter II presents the details of constitutive framework to model the mechanical behavior of LASMPs. Isotropic and anisotropic elastic models are developed based on PMC mechanism. Then some one-dimensional boundary value problems are carried out to observe the shape memory behavior and highlight the anisotropic effects. Next a general viscoelastic model is developed to capture the stress relaxation behavior of LASMPs. This model can be applicable to describe both PMC and PNR LASMPs which have different underlying physical mechanisms by assuming the formation or breakage of the networks causes the changes of the mechanical properties. Parametric studies are investigated for PMC LASMPs, and stress relaxation behavior is captured to calibrate the experimental data of PNR LASMPs.

Chapter III implements the constitutive models in ABAQUS FE using user subroutines. The formulations are derived based on the strain energy in terms of invariants of stretch tensors. The validations of the subroutines are conducted by simulating simple deformation processes and compared the response to the ones obtained from analytical solutions.

Chapter IV presents several simulations on the shape reconfiguration responses of LASMP-integrated structures under different loading conditions.

Chapter V summaries the research outcomes and provides some recommendation for the future work.

CHAPTER II

CONSTITUTIVE MODELING OF LIGHT-ACTIVATED SHAPE MEMORY POLYMERS[†]

In this chapter, related works are performed on understanding responses of LASMPs, considering both elastic and viscoelastic behaviors. The constitutive model is based on a multi-network approach consisting of two microstructural networks, which are the original network and the second network that is formed due to light irradiation. A single integral model is adopted to incorporate the viscoelastic responses in the original and second networks. Parametric studies are carried out in order to obtain a better understanding of the effect of quantities such as material anisotropy, different nonlinear elastic responses, relaxation time and the ratio of the relaxation modulus to the instantaneous modulus. Several examples of boundary value problems are presented.

2.1 Preliminaries

This section summarizes the general kinematics and balance equations that are necessary for our study. Let us consider an abstract body B placed in a three dimensional Euclidean space $\mathcal{E}$ through a one parameter family of placers κ_λ. Let $\kappa_R(B)$ be a

[†] Part of this section is reprinted with permission from "Modeling the response of light-activated shape memory polymers" by Zhi Yuan, Anastasia Muliana, and Kumbakonam Ramamani Rajagopal, 2017. Mathematics and Mechanics of Solids, 22(5), pp.1116-1143. Copyright 2017 by SAGE Publications.

[†] Part of this section is reprinted with permission from "Quasi-linear viscoelastic modeling of light-activated shape memory polymers" by Yuan Zhi, Anastasia Muliana, and K. R. Rajagopal, 2017. Journal of Intelligent Material Systems and Structures, p.1045389X17689936. Copyright 2017 by SAGE Publications.

reference configuration of the body and let $\kappa_t(B)$ denote the configuration of the body at time *t*. The placers are assumed to be one to one mappings and hence we can associate a function χ, referred to as the motion, assigns to each point of the body in a reference configuration a point in the current configuration of the body at time *t*. For any particle P belonging to the abstract body, let $\boldsymbol{X}$ be the position of the particle in some reference configuration, and $\boldsymbol{x}$ be the position at current configuration, then the motion of the body is expressed as:

$$\boldsymbol{x} = \boldsymbol{\chi}_{\kappa_R}(\boldsymbol{X}, t) \tag{2.1}$$

The deformation gradient is then given as:

$$\boldsymbol{F}_{\kappa_R}(\boldsymbol{X}, t) = \frac{\partial \boldsymbol{\chi}_{\kappa_R}}{\partial \boldsymbol{X}} \tag{2.2}$$

The left and right Cauchy-Green tensors are defined through (for notational convenience we shall henceforth drop the suffix κ_R):

$$\boldsymbol{B} = \boldsymbol{F}\boldsymbol{F}^T, \ \boldsymbol{C} = \boldsymbol{F}^T\boldsymbol{F} \tag{2.3}$$

For homogeneous incompressible materials, the balance of mass reduces to:

$$\det \mathbf{F} = \mathbf{1} \text{ or } div(\mathbf{v}) = 0 \tag{2.4}$$

Here, $\mathbf{v}$ is the velocity of the body. The balance of linear momentum is given by:

$$\rho[\frac{\partial \mathbf{v}}{\partial t} + \nabla \mathbf{v} \cdot \mathbf{v}] = div\boldsymbol{\sigma}^T + \rho \boldsymbol{b} \tag{2.5}$$

where $\boldsymbol{\sigma}$ is the Cauchy stress and $\boldsymbol{b}$ is the specific body force. For quasi-static motion, in the absence of body forces, the above equation is reduces to

$$div\boldsymbol{\sigma}^T = 0 \tag{2.6}$$

The balance of angular momentum leads to symmetric of the Cauchy stress tensor:

$$\boldsymbol{\sigma} = \boldsymbol{\sigma}^T \tag{2.7}$$

and thus

$$div\boldsymbol{\sigma} = 0 \tag{2.8}$$

2.2 The notion of multiple natural configurations

A detailed discussion of the notion of natural configurations can be found in Rajagopal [34], and Rajagopal and Srinivasa [35]. Here, we shall merely motivate the main aspects of the same. One can think of the natural configuration as a configuration that a body takes in the absence of any external stimuli. The classical theory of elasticity presumes that an elastic body has one natural configuration, which is the stress free state. In bodies that are capable of producing entropy (within a purely mechanical context capable of dissipation), the natural configuration of the body changes as the body undergoes a dissipative process. Such is indeed the case in a variety of situations such as inelastic and viscoelastic response of materials, twinning, phase transition, growth, etc.

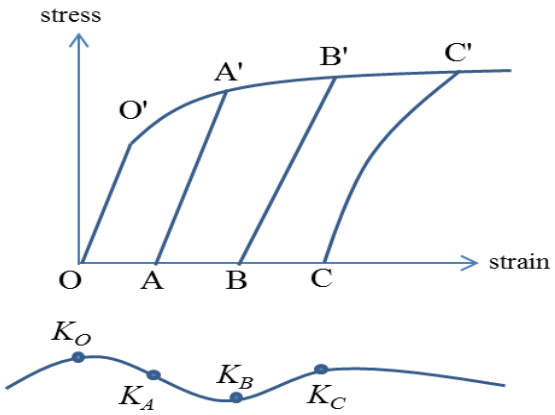

Fig. 3 A schematic sketch showing the notion of natural configurations

In order to clearly illustrate the notion of the evolution of natural configurations we discuss the inelastic response of bodies as depicted in Fig. 3. When the material is deformed so that its configuration lies outside its initial elastic domain OO', dissipation takes place. Then upon unloading, the material will display a different elastic response which has a new elastic domain and range, such as AA', BB' or CC'. For instance, traditional elastic-plastic response, as depicted in Figure 3, can be considered as a class of elastic responses from an evolving set of natural configurations. Within a thermodynamic framework, the evolution of the natural configuration is determined by the maximization of entropy production.

It is noted that the evolution of natural configurations has been used successfully to describe classical plasticity [45], twinning [46], the response of viscoelastic solids and fluids [47], solid-to-solid phase transition [48], polymer crystallization [49], response of single crystal super alloys [80], and anisotropic liquids [50] by Rajagopal and his coworkers. The most important aspect of the framework that is relevant to this study is

the manner in which the material symmetry of the body can change during the process that the body is subject to, and this is described in detail later.

The LASMPs are assumed to be isotropic and homogeneous bodies with regard to their mechanical response, in their initial configuration. It is also assumed that the bodies are initially free of stress and strain. When loaded from the initial unstrained state the LASMPs comprised of the original network undergoes deformation and the materials symmetry changes as in that of a simple material. However, when light of certain wavelength is applied to the polymers, a second network is formed. It is noted that the second network is formed with a certain directional preference that is dependent on the state of deformation at which exposure to light is initiated, that is, the second network is formed so that it is anisotropic. On further deformation, the response of the body is a combination of that due to the original network and the new network that is formed. The response of LASMPs undergoing loading, light irradiation, and unloading is described below.

2.3 Elastic model

2.3.1 Elastic constitutive model

2.3.1.1 Loading of the original network

SMPs are capable of undergoing large deformations due to the twist and stretch of the polymeric chains. In this study, the LASMPS are assumed to be incompressible bodies. In the natural configuration, the stress tensor of the LASMPs associated with the original network can be written in the following form:

$$\boldsymbol{T} = -p\mathbf{I} + \boldsymbol{f}_{Ka}(\boldsymbol{B}_{Ka}) \tag{2.9}$$

where $p\mathbf{I}$ is the indeterminate part of the stress due to incompressibility, $\boldsymbol{f}$ is a tensor valued function , and $\boldsymbol{B}_{Ka}$ is left Cauchy-Green tensor from the evolving natural configurations. We shall assume that the constitutive equation for the original network is that for a neo-Hookean material:

$$\boldsymbol{T} = -p\mathbf{I} + \mu\boldsymbol{B}_{Ka} \tag{2.10}$$

We also consider the original network being comprised of a Mooney-Rivlin model whose stress is given as:

$$\mathbf{T} = -p\mathbf{I} + \mu_a\mathbf{B}_{Ka} + \mu_{aa}\mathbf{B}_{Ka}^{-1} \tag{2.11}$$

2.3.1.2 Formation of the second network and response due to a mixture of two networks

When exposing the material to the light of specific wavelength, the photo-sensitive molecules such as cinnamic acid [52] and cinnamylidene acetic acid [53] can be activated to form an extra network. To capture the variation of light intensity travelling across the media, the standard Beer's correlation is used here:

$$\frac{I_o}{I_i} = e^{-al} \tag{2.12}$$

where I_i , I_o are the incident and transmitted optical intensities, and a is the absorption coefficient, l is the thickness. So from (2.12) we can see $\frac{I_o}{I_i} \approx 1$ when the material

sample is very thin, that means the light intensity is constant in the material. Our study only focuses on very thin bodies and does not consider the variation of light density within the thickness of the material. Therefore, for a body with homogeneously distributed photo-sensitive molecules, the formation of the second network under light activation is at the same percentage with the same formation rate throughout the thickness.

After the completion of the formation of the second network, the body is treated as a constrained mixture of two networks, namely the original network and new network that is formed due to light irradiation co-exist and are constrained to move together. We assume the two networks are uniformly distributed and are constrained to have the same displacement. The stress at a material point is assumed to be

$$\mathbf{T} = -p\mathbf{I} + \mathbf{T}_1 + \mathbf{T}_2 \tag{2.13}$$

where $\mathbf{T}_1$ and $\mathbf{T}_2$ denote the Cauchy stresses in the original and newly formed networks, respectively. We follow the framework outlined in [54] [50] to describe the multi-network model. Once the second network is formed, assumptions have to be made about the nature of the second network and configuration in which it is formed. We suppose the new network is formed in a stress-free state, that is, the deformed state of the original network in the body is the natural configuration (unstrained/unstressed state) for the second network. Thus when further deformation takes place, the new network will also deform based on its own natural configuration. Thus, in the material after light irradiation the total stress can be written as:

$$\boldsymbol{T} = -p\mathbf{I} + \boldsymbol{f}_{Ka}(\boldsymbol{B}_{Ka}(t)) + \alpha \boldsymbol{f}_{Kb}(\boldsymbol{B}_{Kb}(t)) \tag{2.14}$$

where α is the percent formation (volume fraction) of the second network. We should also notice that the second network is formed based on a deformed configuration at which the polymer is being irradiated; therefore, it makes sense to assume that the second network should have some directional preference, which will induce anisotropic response of the body. We consider two types of models with regard to the material symmetry. The first model considers both networks as isotropic, while the second model assigns a specific anisotropy for the second network.

a) Isotropic networks

We shall assume that both the networks can be modeled as neo-Hookean bodies. Then, the total stress is given by

$$\boldsymbol{T} = -p\mathbf{I} + \mu_a \boldsymbol{B}_{Ka} + \alpha\mu_b \boldsymbol{B}_{Kb} \tag{2.15}$$

where $\boldsymbol{B}_{Ka}$ and $\boldsymbol{B}_{Kb}$ are the left Cauchy-Green tensor associated with the deformation of the original and new network based on deformation from their own natural configurations, and, μ_a and μ_b are the moduli of the materials associated with the original and second network. We represent the two natural configurations as Ka and Kb.

b) Anisotropic model

The anisotropy of the second network depends on the deformation history of the material, which depends on the orientation of the molecules at the time of the formation of the second network at time, say $t = \tau$. We assume that the second network is orthotropic and the tensor $\boldsymbol{B}_{Ka}(\tau)$ includes the information we need such as the three principal directions of $\boldsymbol{B}_{Ka}(\tau)$. We use these mutually perpendicular principal directions to determine the directions of anisotropy in the second network. The principal directions can be quantified by any two of the three eigenvectors of $\boldsymbol{B}_{Ka}(\tau)$ or $\boldsymbol{B}_{Kb}$, which we shall refer to as $\boldsymbol{n}_{Kb}$ and $\boldsymbol{m}_{Kb}$.

We shall assume that the orthotropic incompressible elastic material that is comprised of the second network to be represented by:

$$\mathbf{T}_2 = -p\mathbf{I} + \alpha\mu_b\mathbf{B}_{Kb} + \alpha\mu_{c1}\mathbf{F}_{Kb}(J_1 - 1)\boldsymbol{n}_{Kb} \otimes \boldsymbol{n}_{Kb}\mathbf{F}_{Kb}^{\ T} + \alpha\mu_{c2}\mathbf{F}_{Kb}(K_1 - 1)\boldsymbol{m}_{Kb} \otimes \boldsymbol{m}_{Kb}\mathbf{F}_{Kb}^{\ T} \quad (2.16)$$

where $\mu_b, \mu_{c1}, \mu_{c2}$ are the material moduli related to the formation of the second network that depends on the eigenvalues of $\boldsymbol{B}_{Kb(\tau)}$, and $J_1 = \boldsymbol{n}_{Kb} \cdot \mathbf{C}_{Kb}\boldsymbol{n}_{Kb}$, $K_1 = \boldsymbol{m}_{Kb} \cdot \mathbf{C}_{Kb}\boldsymbol{m}_{Kb}$.

Finally, the total stress is the combination of the stresses in the two networks:

$$\mathbf{T} = -p\mathbf{I} + \mu_a\mathbf{B}_{Ka} + \alpha\mu_b\mathbf{B}_{Kb} + \alpha\mu_{c1}\mathbf{F}_{Kb}(J_1 - 1)\boldsymbol{n}_{Kb} \otimes \boldsymbol{n}_{Kb}\mathbf{F}_{Kb}^{\ T} + \alpha\mu_{c2}\mathbf{F}_{Kb}(K_1 - 1)\boldsymbol{m}_{Kb} \otimes \boldsymbol{m}_{Kb}\mathbf{F}_{Kb}^{\ T} \quad (2.17)$$

During the unloading, due to the two networks being present, and on assuming that there is no conversion of the networks taking place during the unloading, the body will tend to a natural state that is different from the natural configuration that

corresponds to a body fully comprised of the original network. In other words, the body will be in a strained state with respect to the original natural configuration.

2.3.2 Boundary value problems

within the context of elastic constitutive model, several simple boundary value problems are discussed based on some assumptions: the material sample is relatively thin so that the light irradiation is homogeneous across the bodies; the second network is formed in a stress free configuration; however, its anisotropic response depends on the deformation state of the material at the time when light irradiation occurs.

2.3.2.1 Uniaxial tension

Consider a rod subjected to uniaxial tension, as illustrated in Fig. 4. For an incompressible isotropic body, the motion of the body under a uniaxial tension can be assumed to be:

$$x = \Lambda X, \quad y = \frac{1}{\sqrt{\Lambda}} Y, \quad z = \frac{1}{\sqrt{\Lambda}} Z \tag{2.18}$$

and the stresses are:

$$T_{11}(t) = T(t), \quad T_{22}(t) = T_{33}(t) = 0 \text{ and } T_{ij}(t) = 0 \ (i \neq j) \tag{2.19}$$

where X, Y, Z denote a typical point in the reference configuration, x, y, z describe the same point in the current configuration, Λ is the stretch ratio along the loading direction, which is in the x direction. The deformation gradient and stretch tensors are given as:

$$\mathbf{F}_{Ka} = diag(\Lambda, \frac{1}{\sqrt{\Lambda}}, \frac{1}{\sqrt{\Lambda}}), \quad \mathbf{B}_{Ka} = \mathbf{C}_{Ka} = diag(\Lambda^2, \frac{1}{\Lambda}, \frac{1}{\Lambda}) \tag{2.20}$$

Fig. 4 Schematic plot of uniaxial tension

We recall that the original network is assumed a Neo-Hookean material. Then the governing equation of the motion is obtained from the balance of linear momentum as:

$$\frac{\partial T_{xx}}{\partial x} = 0 \quad \Rightarrow \quad T_{xx} = C \tag{2.21}$$

The other two equations of balance of a linear momentum are satisfied automatically. Prescribing the boundary conditions, the parameter p is determined from imposing $T_{yy} = T_{zz} = 0$, and finally the axial stress corresponding to the uniaxial stretch is:

$$T_{11} = \mu_a(\Lambda^2 - \frac{1}{\Lambda}) \tag{2.22}$$

After the cylinder is deformed to a specified amount of axial stretch, the rod is exposed to light irradiation with a specific wavelength or frequency, which activates the photo-sensitive molecules in the material and the second network is formed. After completion of light activation, the material now comprises of two networks with different reference configurations. The deformation gradients satisfy:

$$\mathbf{F}_{Ka}(t) = \mathbf{F}_{Kb}(t)\mathbf{F}_{Ka}(\tau) \tag{2.23}$$

Therefore, we have

$$\mathbf{F}_{Kb} = diag(\frac{\Lambda}{\Lambda_1}, \sqrt{\frac{\Lambda_1}{\Lambda}}, \sqrt{\frac{\Lambda_1}{\Lambda}}) \quad \mathbf{B}_{Kb} = \mathbf{C}_{Kb} = diag((\frac{\Lambda}{\Lambda_1})^2, \frac{\Lambda_1}{\Lambda}, \frac{\Lambda_1}{\Lambda}) \quad (2.24)$$

where Λ is the total stretch, Λ_1 is the new stretch after the formation of the second network. Then using the theory of constrained mixtures, the total stress in the rod at the current state is the summation of the contribution of the two networks. In this study, we consider both isotropic and anisotropic elastic models for the second network, while the original network is isotropic. When both the original and second network are isotropic, the total axial stress is:

$$T_{11} = \mu_a(\Lambda^2 - \frac{1}{\Lambda}) + \alpha\mu_b((\frac{\Lambda}{\Lambda_1})^2 - \frac{\Lambda_1}{\Lambda}) \quad (2.25)$$

When the mechanical responses of polymers associated with the second network are modeled as anisotropic, the axial stress when both networks are present is given as:

$$\begin{aligned} T_{11} &= \mu_a(B_{Ka11} - B_{Ka22}) + \alpha\mu_b(B_{Kb11} - B_{Kb22}) + \alpha\mu_c(J_1 - 1)(\frac{\Lambda}{\Lambda_1})^2 \\ &= \mu_a(\Lambda^2 - \frac{1}{\Lambda}) + \alpha\mu_b((\frac{\Lambda}{\Lambda_1})^2 - \frac{\Lambda_1}{\Lambda}) + \alpha\mu_c((\frac{\Lambda}{\Lambda_1})^2 - 1)(\frac{\Lambda}{\Lambda_1})^2 \end{aligned} \quad (2.26)$$

In the above equations, α is the extent of formation of the second network, Λ is the total stretch, Λ_1 is the new stretch after the formation of the second network. Finally, the second network can be cleaved by further application of light, so that the body returns to its original shape.

Figure 5 illustrates the complete loading history of the uniaxial load considering both isotropic and anisotropic models for the second network. The simulations consider three percentages of the new network: $\alpha = 1, \alpha = 0.66, \alpha = 0.33$ and the material

parameters are $\mu_a = 5, \mu_b = 20, \mu_c = 40$. In the case of an anisotropic second network we have a different unloading path than when it is isotropic. For the specific case considered here, the anisotropic second network leads to a smaller reduction of stretch after stress is released. The amount of the difference depends on the modulus μ_c.

Furthermore, we perform three case studies with a view towards understanding the behavior of the LAMSP cylinder under different boundary conditions for different constitutive models. In the first case study, we examine different modes of loading, i.e., force control, and compare the responses to the mixed-mode loading presented above. In the second case study, we consider a Mooney-Rivlin model for the LASMPs. In the third case study, we consider several cycles of loading.

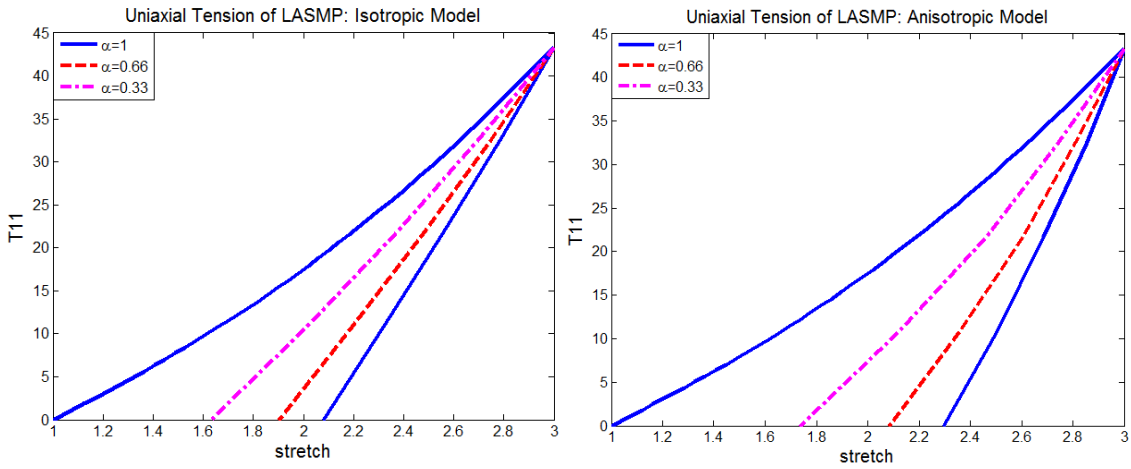

Fig. 5 Stress vs. stretch curve for uniaxial tension of LASMP: Isotropic (Left) and Anisotropic (Right)

Case 1 Comparison of different loading modes

In the above discussion, we considered mixed-mode loading, i.e., during the loading we stretch the rod, in which the deformation is prescribed (displacement control), while unloading we release the stress (force control). It is noted that when the displacement is prescribed, using the above constitutive models, the stress can be immediately determined. In a situation when a force is prescribed, the Cauchy stress is not necessarily straightforward to determine. For incompressible materials the volume should be preserved, thus $A_0 L_0 = A_t L_t \Rightarrow A_t = \frac{A_0}{\Lambda}$; where A_0 and A_t are the original and current section area of rod, respectively, and L_0 and L_t are the original and current length, respectively. The axial stress is then given as:

$$\begin{aligned} T_{11} &= \frac{\mathrm{F}_{ext}}{A_t} = \frac{\mathrm{F}_{ext}\Lambda}{A_0} = -p + \mu\Lambda^2 \\ \Rightarrow \frac{\mathrm{F}_{ext}\Lambda}{A_0} &= \mu(\Lambda^2 - \frac{1}{\Lambda}) \\ \Rightarrow \frac{\mathrm{F}_{ext}}{A_0} &= \mu(\Lambda - \frac{1}{\Lambda^2}) \end{aligned} \tag{2.27}$$

The left side of the above equation $\frac{\mathrm{F}_{ext}}{A_0}$ is the 1st Piola-Kirchhoff stress, which is easily determined. From the expression, we can see the relations between the 1st Piola-Kirchhoff stress and stretch is nonlinear, and we use a numerical method (bisection method) to determine the corresponding stretch. After calculating the stretch, the corresponding Cauchy stress can be determined. Based on the above discussion, the constitutive equation in the original network when force is prescribed is:

$$\frac{\mathrm{F}_{ext}}{A_0} = \mu_a(\Lambda - \frac{1}{\Lambda^2}) \tag{2.28}$$

and upon formation of the second network, the axial stress in the rod becomes:

$$\frac{\mathrm{F}_{ext}}{A_0} = \mu_a(\Lambda - \frac{1}{\Lambda^2}) + \alpha\mu_b(\frac{\Lambda}{\Lambda_1^{\,2}} - \frac{\Lambda_1}{\Lambda^2}) \tag{2.29}$$

Alternatively, the constitutive model can be given for stretch or strain that is expressed in terms of stress. So here we also present a constitutive model for the stretch in terms of the 1st Piola-Kirchhoff as the independent variable. The nonlinear elastic model for isotropic incompressible bodies becomes:

$$\mathbf{B} = \frac{1}{\mu}(\mathbf{P}\mathbf{F}^T + p\mathrm{I}) \tag{2.30}$$

where **P** is the 1st Piola-Kirchhoff stress, $\mathbf{P} = J\boldsymbol{\sigma}\mathbf{F}^{-T}$. Thus, for the uni-axially loaded cylinder comprised of the original network, the stretch is

$$\begin{cases} \Lambda^2 = \dfrac{1}{\mu}(P_{11}\Lambda + p) \\ \dfrac{1}{\Lambda} = \dfrac{1}{\mu}(P_{22}\sqrt{\dfrac{1}{\Lambda}} + p) \end{cases} \Rightarrow \Lambda^2 = \frac{1}{\mu}P_{11}\Lambda + \frac{1}{\Lambda} \tag{2.31}$$

When two networks are present in the body, for each component of two networks, the stretch is

$$B_{kb} = \frac{1}{\mu_b}(P_2F_{kb}^T + p_2\mathrm{I})\,,\quad B_{ka} = \frac{1}{\mu_a}(P_1F_{ka}^T + p_1\mathrm{I}) \tag{2.32}$$

and the theory of constrained mixture gives the following stress:

$$P_1F_{ka}^T + \alpha P_2F_{kb}^T = PF_{ka}^T$$

The constitutive model when the two networks are present is given as:

$$\frac{\alpha B_{kb}}{\mu_a} + \frac{B_{ka}}{\mu_b} = \frac{1}{\mu_a \mu_b}(PF_{ka}^T + p\mathrm{I}) \tag{2.33}$$

For the uni-axially loaded rod, the response becomes:

$$\frac{\alpha}{\mu_a}(\frac{\Lambda}{\Lambda_1})^2 + \frac{\Lambda^2}{\mu_b} = \frac{P_{11}}{\mu_a \mu_b}\Lambda + \frac{\alpha}{\mu_a}\frac{\Lambda_1}{\Lambda} + \frac{1}{\mu_b}\frac{1}{\Lambda} \tag{2.34}$$

In the above case, Steffensen's method [59] is used to solve the above constitutive relation. From the result shown in Fig. 6, we can see the three different loading modes give the same stress-stretch responses.

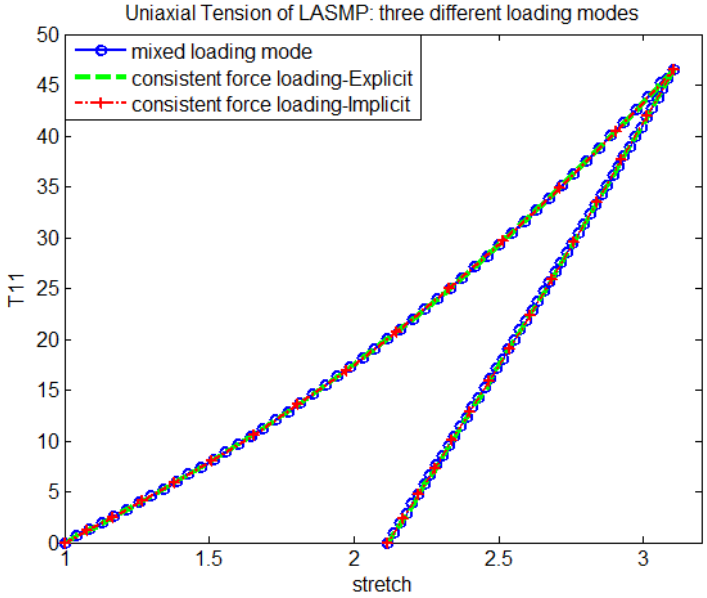

Fig. 6 Results of three different methods for uniaxial tension of LASMP

Case 2 Comparison between the neo-Hookean and Mooney-Rivlin models for the networks

As shown in literature, the Neo-Hookean model can describe the mechanical behavior of rubber-like materials at moderate deformations. When the deformations are larger, the Neo-Hookean model often fails to capture the overall response of the materials. The Mooney-Rivlin model captures the response better at slightly larger deformations.

So for the original network, the uniaxial stress is:

$$T_{11} = -p + \mu_a B_{Ka11} + \mu_{aa} B^{-1}_{Ka11} = \mu_a(\Lambda^2 - \frac{1}{\Lambda}) + \mu_{aa}(\frac{1}{\Lambda^2} - \Lambda) \tag{2.35}$$

and for the two networks, the stress can be expressed as,

$$\mathbf{T} = -p\mathbf{I} + \mu_a \mathbf{B}_{Ka} + \mu_{aa} \mathbf{B}^{-1}_{Ka} + \alpha\mu_b \mathbf{B}_{Kb} + \alpha\mu_{bb} \mathbf{B}^{-1}_{Kb} \tag{2.36}$$

The uniaxial stress becomes:

$$T_{11} = \mu_a(\Lambda^2 - \frac{1}{\Lambda}) + \mu_{aa}(\frac{1}{\Lambda^2} - \Lambda) + \alpha\mu_b((\frac{\Lambda}{\Lambda_1})^2 - \frac{\Lambda_1}{\Lambda}) + \alpha\mu_{bb}((\frac{\Lambda_1}{\Lambda})^2 - \frac{\Lambda}{\Lambda_1}) \tag{2.37}$$

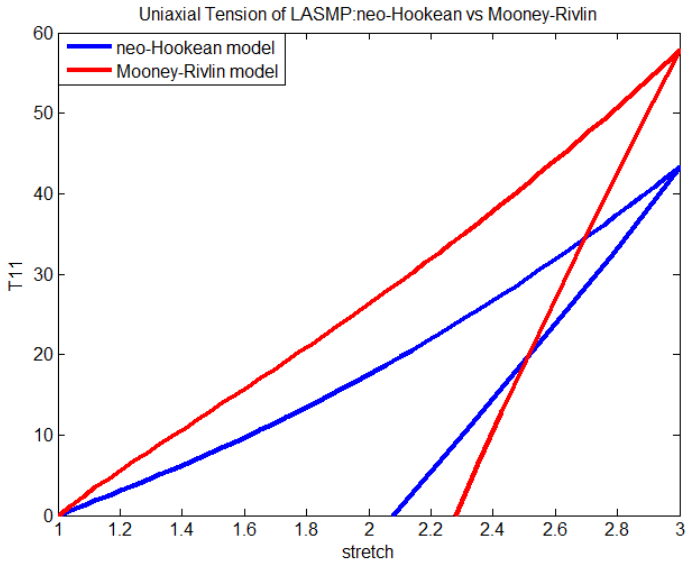

Fig. 7 neo-Hookean vs Mooney-Rivlin model for uniaxial tension of LASMP

Figure 7 shows the comparisons between neo-Hookean model and Mooney-Rivlin model with $\mu_a = 5$, $\mu_{aa} = -5$, $\mu_b = 20$, $\mu_{bb} = -20$ and $\alpha = 1$. At loading stage, $\frac{1}{\Lambda^2} - \Lambda < 0$, the extra negative modulus parameter μ_{aa} of the Mooney-Rivlin model causes a much faster increase than the neo-Hookean model. Similarly at loading phase, $(\frac{\Lambda_1}{\Lambda})^2 - \frac{\Lambda}{\Lambda_1} < 0$, a negative value of μ_{bb} contributes to lower decrease of stress.

Case 3 Comparison between three different loading histories

We now examine the responses under three different loading histories: In the first loading history the material is deformed to a specified stretch ratio (Λ=3), followed by light activation to initiate the second network till complete formation of the second

network is achieved, i.e., $\alpha = 1$, and the material is unloaded by removing the stress. In the second history, the material is deformed to a specific stretch ratio (Λ=3), followed by light activation with 60% formation of the new network, i.e., $\alpha = 0.6$, which we will refer to as the second network and then stress is removed completely, the material is then irradiated again until all the photosensitive particles are linked, that is, $\alpha = 1$. This however implies that a third network is formed which constitutes 40% of the body; this is followed by the body being stretched to Λ=3. In the third history, the material is first deformed to a stretch ratio Λ=1.5, and the second network is activated until $\alpha = 0.6$, and then the material is stretched so that Λ=3, followed by light activation until all the photosensitive particles are linked thereby leading to the formation of a third network that is 40% of the body, ensuring that $\alpha = 1$; then the loading is completely removed.

The response of the first loading history has been discussed above. For the second and third loading histories, there are totally three networks involved, and the relations between tension stress and axial stretch are obtained following the same method discussed above：

Original network: $T_{11} = \mu_a(\Lambda^2 - \frac{1}{\Lambda})$

Two networks: $T_{11} = \mu_a(\Lambda^2 - \frac{1}{\Lambda}) + \alpha_1\mu_b((\frac{\Lambda}{\Lambda_1})^2 - \frac{\Lambda_1}{\Lambda})$ (2.38)

Three networks: $T_{11} = \mu_a(\Lambda^2 - \frac{1}{\Lambda}) + \alpha_1\mu_b((\frac{\Lambda}{\Lambda_1})^2 - \frac{\Lambda_1}{\Lambda}) + \alpha_2\mu_c((\frac{\Lambda}{\Lambda_2})^2 - \frac{\Lambda_2}{\Lambda})$

where Λ_1 and Λ_2 are the stretch ratio when the second and third networks are formed respectively, μ_c is the modulus of the third network and in the calculation we take this to be the same value as μ_b. From the results shown in Fig 8., we can see that the first loading history can retain the highest stretch after unloading to the temporary shape configuration, followed by the second and third loading histories, which is to be expected. When all three networks are involved, the ability to retain shape is much higher. In the first loading history we can view the full activation of the second network as the second and third network are formed at the same time, the corresponding stress at the specified ratio is the smallest, so the least change of stretch is needed to relax the stress to zero, which results in largest residual stretch.

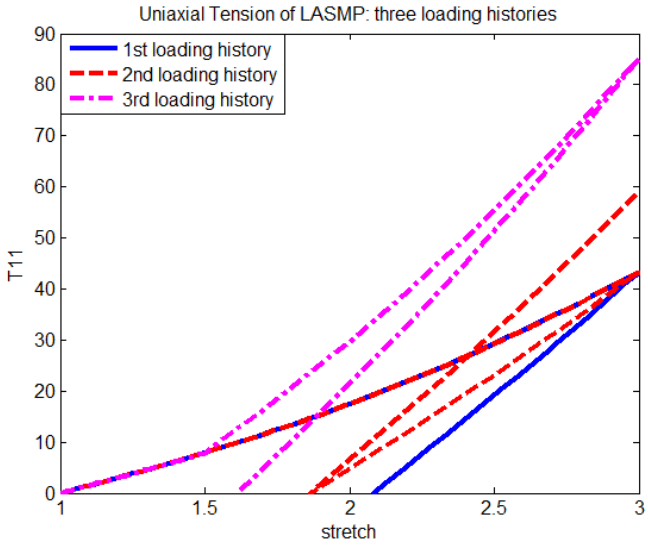

Fig. 8 Results of three different methods for uniaxial tension of LASMP

2.3.2.2 Inflation of a cylindrical annulus

Now, we analyze the response of a hollow cylindrical body made of LASMPs subjected to radial inflation (see Fig. 9). Consider a cylinder, in its reference configuration described by (R, Θ , Z) and in the deformed configuration is described in terms of (r, θ, z) . Suppose that the inner and outer radii of the cylinder in its reference configuration are R_i and R_o, respectively, and the length of the cylinder is L. The bottom surface of the cylinder is at Z=0 and the top surface is at Z=L. We assume that the motion of the body is described by:

$$r = r(R), \quad \theta = \Theta, \quad z = Z \tag{2.39}$$

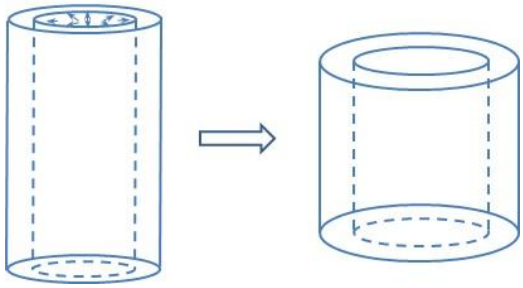

Fig. 9 Schematic of cylindrical inflation

The deformation gradient of the original network is:

$$\mathbf{F}_{Ka} = \begin{pmatrix} \frac{\partial r}{\partial R} & \frac{1}{R}\frac{\partial r}{\partial \Theta} & \frac{\partial r}{\partial Z} \\ r\frac{\partial \theta}{\partial R} & \frac{r}{R}\frac{\partial \theta}{\partial \Theta} & r\frac{\partial \theta}{\partial Z} \\ \frac{\partial z}{\partial R} & \frac{1}{R}\frac{\partial z}{\partial \Theta} & \frac{\partial z}{\partial Z} \end{pmatrix} = \begin{pmatrix} \frac{\partial r}{\partial R} & 0 & 0 \\ 0 & \frac{r}{R} & 0 \\ 0 & 0 & 1 \end{pmatrix} \tag{2.40}$$

Due to the constraint of incompressibility, the deformation gradient and stretch tensors reduce to:

$$\mathbf{F}_{Ka} = \begin{pmatrix} \frac{R}{r} & 0 & 0 \\ 0 & \frac{r}{R} & 0 \\ 0 & 0 & 1 \end{pmatrix} \qquad (2.41)$$

$$\mathbf{C}_{Ka} = \mathbf{B}_{Ka} = diag((\frac{R}{r})^2, (\frac{r}{R})^2, 1)$$

The governing equations are:

$$\begin{aligned} &\frac{\partial T_{rr}}{\partial r} + \frac{\partial (\frac{T_{\theta r}}{r})}{\partial \theta} + \frac{\partial T_{zr}}{\partial z} + \frac{T_{rr} - T_{\theta\theta}}{r} + \rho b_r = \rho a_r \\ \Rightarrow &\frac{\partial T_{rr}}{\partial r} + \frac{T_{rr} - T_{\theta\theta}}{r} = 0 \\ \Rightarrow &T_{rr}(r) - T_{rr}(r_1) = \int_{r_1}^{r} \frac{T_{\theta\theta} - T_{rr}}{r} dr \end{aligned} \qquad (2.42)$$

On satisfying the stress free condition at the outer surface of the cylinder, $T_{rr}(r_2) = 0$, we find that the inner pressure is given by:

$$P = \int_{r_1}^{r_2} \frac{T_{\theta\theta} - T_{rr}}{r} dr \qquad (2.43)$$

Here r_1 is the inner radius and r_2 is the outer radius in its current configuration. Using the neo-Hookean model, we obtain:

$$P = \int_{r_1}^{r_2} \mu(B_{\theta\theta} - B_{rr})/r dr = \int_{r_1}^{r_2} \mu[(\frac{r}{R})^2 - (\frac{R}{r})^2]/r dr \qquad (2.44)$$

From the balance of mass, we have

$$(r^2 - r_1^2) = (R^2 - R_1^2), \quad \frac{R}{r} = \sqrt{1 - (\frac{r_1}{r})^2 + (\frac{R_1}{r})^2}, \quad r_2 = \sqrt{R_2^2 - R_1^2 + r_1^2} \tag{2.45}$$

Substituting (4.28) into (4.27), the response of the original network under radial inflation is determined.

Now, the body is irradiated and the second network is formed. The radius of the cylinder when the second network is formed is $\bar{r}$; thus the stretch tensors in the two networks are:

$$\begin{aligned} \mathbf{F}_{Ka} &= diag(\frac{R}{r}, \frac{r}{R}, 1), \quad \mathbf{B}_{Ka} = diag((\frac{R}{r})^2, (\frac{r}{R})^2, 1) \\ \mathbf{F}_{Kb} &= diag(\frac{\bar{r}}{r}, \frac{r}{\bar{r}}, 1), \quad \mathbf{B}_{Kb} = diag((\frac{\bar{r}}{r})^2, (\frac{r}{\bar{r}})^2, 1) \end{aligned} \tag{2.46}$$

When the second network is assumed to be isotropic, the inner pressure at current state is

$$\begin{aligned} P &= \int_{r_1}^{r_2} [\mu_a (B_{Ka\theta\theta} - B_{Karr}) + \alpha\mu_b (B_{Kb\theta\theta} - B_{Kbrr})] / r dr \\ &= \int_{r_1}^{r_2} (\mu_a [(\frac{r}{R})^2 - (\frac{R}{r})^2] + \alpha\mu_b [(\frac{r}{\bar{r}})^2 - (\frac{\bar{r}}{r})^2]) / r dr \end{aligned} \tag{2.47}$$

It is also noted that the balance of mass leads to:

$$\begin{aligned} r_2 &= \sqrt{R_2^2 - R_1^2 + r_1^2}, & \frac{R}{r} &= \sqrt{1 - (\frac{r_1}{r})^2 + (\frac{R_1}{r})^2} \\ \frac{\bar{r}}{r} &= \sqrt{(\frac{\bar{r}_1}{r})^2 - (\frac{r_1}{r})^2 + 1}, & \bar{r}_2^2 &= R_2^2 - R_1^2 + \bar{r}_1^2 \end{aligned} \tag{2.48}$$

When the newly formed network is assumed to be an orthotropic body, the material directions are determined by obtaining the eigenvalues and eigenvectors of the deformation at which the light irradiation starts, which are:

$$\boldsymbol{n}_{Kb} = \begin{pmatrix} a \\ b \\ 0 \end{pmatrix} \qquad \boldsymbol{m}_{Kb} = \begin{pmatrix} c \\ d \\ 0 \end{pmatrix} \tag{2.49}$$

For the radial inflation problem, $a = 1$; $b = 0$; $c = 0$; $d = 1$, therefore:

$$J_1 = \boldsymbol{n}_{Kb} \cdot \mathbf{C}_{Kb} \boldsymbol{n}_{Kb} = (\frac{\overline{r}}{r})^2 \qquad K_1 = \boldsymbol{m}_{Kb} \cdot \mathbf{C}_{Kb} \boldsymbol{m}_{Kb} = (\frac{r}{\overline{r}})^2 \tag{2.50}$$

and

$$B1 = \begin{pmatrix} (\frac{\overline{r}}{r})^2 & 0 & 0 \\ 0 & 0 & 0 \\ 0 & 0 & 0 \end{pmatrix} \qquad B2 = \begin{pmatrix} 0 & 0 & 0 \\ 0 & (\frac{r}{\overline{r}})^2 & 0 \\ 0 & 0 & 0 \end{pmatrix} \tag{2.51}$$

where for the sake of ease of computations, we denote $\mathbf{B}1 = \mathbf{F}_{Kb} \boldsymbol{n}_{Kb} \otimes \boldsymbol{n}_{Kb} \mathbf{F}_{Kb}^{\ T}$,

$\mathbf{B}2 = \mathbf{F}_{Kb} \boldsymbol{m}_{Kb} \otimes \boldsymbol{m}_{Kb} \mathbf{F}_{Kb}^{\ T}$.

Then substituting the above equations into (2.17), the following stresses are determined $T_{\theta\theta}$, T_{rr}. Thus, for the anisotropic case, the pressure in the two networks is:

$$\begin{aligned} P &= \int_{r_1}^{r_2} [\mu_a (B_{Ka\theta\theta} - B_{Karr}) + \alpha\mu_b (B_{Kb\theta\theta} - B_{Kbrr}) + \alpha\mu_{c1} (B1_{\theta\theta} - B1_{rr}) + \alpha\mu_{c2} (B2_{\theta\theta} - B2_{rr})] / r dr \\ &= \int_{r_1}^{r_2} [\mu_a ((\frac{r}{R})^2 - (\frac{R}{r})^2) + \alpha\mu_b ((\frac{r}{\overline{r}})^2 - (\frac{\overline{r}}{r})^2) - \alpha\mu_{c1} (\frac{\overline{r}}{r})^2 + \alpha\mu_{c2} (\frac{r}{\overline{r}})^2] / r dr \end{aligned} \tag{2.52}$$

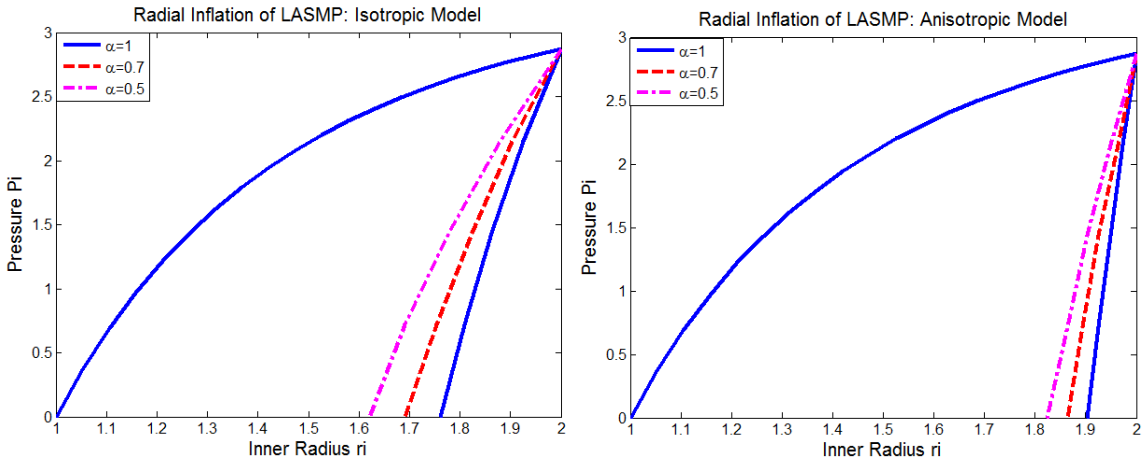

Fig. 10 Pressure vs. Inner Radius curve for cylindrical inflation of LASMP: Isotropic (Left) and Anisotropic (Right)

From the results depicted in Fig. 10, we can infer the influence of the anisotropy of the second network, wherein $\mu_a = 5$, $\mu_b = 20$, $\mu_{c1} = 40$, $\mu_{c2} = 40$ and three different values $\alpha = 1, \alpha = 0.7, \alpha = 0.5$ are considered. By comparing the unloading process, the material is much stiffer with higher percentage of second network. And the anisotropic response leads to a much larger stretch after unloading than the isotropic model due to an extra term in (2.52) $-\alpha\mu_{c1}(\frac{\bar{r}}{r})^2 + \alpha\mu_{c2}(\frac{r}{\bar{r}})^2 < 0$ that will contribute to a decrease of pressure when unloading.

2.3.2.3 Circumferential shear

The following example deals with a circumferential shear imposed on a LASMP hollow cylinder (see Fig. 11), whose motion is given through:

$$r = R, \qquad \theta = \Theta + f(R,t), \qquad z = Z \tag{2.53}$$

Fig. 11 Schematic of circumferential shear

To better understand the response to this problem, two responses are presented. The first considers the relationship between the circular shear deformation and moment, and the second is an investigation of how the rotation angle changes with the applied moment. Both isotropic and anisotropic constitutive models are considered.

Case 1. Relationship between the moment and circular shear deformation

It follows from (2.53) that the deformation gradient $\mathbf{F}_{Ka}$, and the Cauchy-Green tensor $\mathbf{B}_{Ka}$ of the original network take the form

$$\mathbf{F}_{Ka}=\begin{pmatrix}1 & 0 & 0\\ k(t,r) & 1 & 0\\ 0 & 0 & 1\end{pmatrix}\qquad \mathbf{B}_{Ka}=\begin{pmatrix}1 & k(t,r) & 0\\ k(t,r) & k^2(t,r) & 0\\ 0 & 0 & 1\end{pmatrix} \tag{2.54}$$

where $k=r\dfrac{\partial f}{\partial r}$, and $\det(\mathbf{F}_{Ka})=1$ which already satisfies the constraint of incompressibility. The balance of linear momentum yields

$$\begin{cases}\dfrac{\partial T_{rr}}{\partial r}+\dfrac{T_{rr}-T_{\theta\theta}}{r}=0\\ \dfrac{\partial T_{r\theta}}{\partial r}+2\dfrac{T_{r\theta}}{r}=0 \quad\Rightarrow\quad T_{r\theta}=\dfrac{C}{r^2}\end{cases} \tag{2.55}$$

C is a constant that is to be determined by the boundary condition at the outer surface on the lateral boundary:

$$\begin{aligned} & T_{r\theta} \cdot 2\pi R_o \cdot 1 = \bar{M} \cdot 1 \\ \Rightarrow & \frac{C}{R_o^{\,2}} \cdot 2\pi R_o = \bar{M} \\ \Rightarrow & C = \frac{\bar{M} R_o}{2\pi} = \frac{M}{2\pi} \end{aligned} \tag{2.56}$$

where $M = \bar{M} R_o$, $\bar{M}$ is the moment per unit length applied on the outer surface of the cylinder.

Substituting (2.56) into (2.55), we obtain

$$\begin{aligned} & T_{r\theta} = \frac{M}{2\pi r^2} = \mu_a B_{Kar\theta} = \mu_a k(t) \\ \Rightarrow & \frac{M}{2\pi r^2 \mu_a} = k(t) \end{aligned} \tag{2.57}$$

After the shear deformation or moment reaches certain magnitude, the cylinder is exposed to light in order to activate the second network. The stretch tensors for the two networks are:

$$\mathbf{F}_{Kb} = \begin{pmatrix} 1 & 0 & 0 \\ \Delta k & 1 & 0 \\ 0 & 0 & 1 \end{pmatrix} \quad \mathbf{B}_{Kb} = \begin{pmatrix} 1 & \Delta k & 0 \\ \Delta k & 1+\Delta k^2 & 0 \\ 0 & 0 & 1 \end{pmatrix} \quad \mathbf{C}_{Kb} = \begin{pmatrix} 1+\Delta k^2 & \Delta k & 0 \\ \Delta k & 1 & 0 \\ 0 & 0 & 1 \end{pmatrix} \tag{2.58}$$

where $\Delta k = k(t) - k(\tau)$.

We consider two constitutive models for the second network, i.e., isotropic and anisotropic models.

When the second network is assumed isotropic, the total shear stress is

$$T_{r\theta} = \mu_a B_{Kar\theta} + \alpha\mu_b B_{Kbr\theta} = \mu_a k + \alpha\mu_b \Delta k$$

$$\Rightarrow \frac{M}{2\pi r^2 \mu_a} = k + \alpha \frac{\mu_b}{\mu_a} \Delta k \tag{2.59}$$

If we assume that the second network is anisotropic, namely that the second network is orthotropic, the directions being determined by the eigenvectors (2.60) of the stretch tensor $\mathbf{B}_{Ka}(\tau)$

$$\boldsymbol{n}_{Kb} = \begin{pmatrix} a \\ b \\ 0 \end{pmatrix} \qquad \boldsymbol{m}_{Kb} = \begin{pmatrix} c \\ d \\ 0 \end{pmatrix} \tag{2.60}$$

Then it follows that

$$J_1 = \boldsymbol{n}_{Kb} \cdot \mathbf{C}_{Kb} \boldsymbol{n}_{Kb} = (1+\Delta k^2)a^2 + 2ab\Delta k + b^2$$
$$K_1 = \boldsymbol{m}_{Kb} \cdot \mathbf{C}_{Kb} \boldsymbol{m}_{Kb} = (1+\Delta k^2)c^2 + 2cd\Delta k + d^2$$

$$\mathbf{B}1 = \mathbf{F}_{Kb} \boldsymbol{n}_{Kb} \otimes \boldsymbol{n}_{Kb} \mathbf{F}_{Kb}{}^T = \begin{pmatrix} a^2 & \Delta k a^2 + ab & 0 \\ \Delta k a^2 + ab & \Delta k^2 a^2 + 2\Delta k ab + b^2 & 0 \\ 0 & 0 & 0 \end{pmatrix} \tag{2.61}$$

and $\mathbf{B}2 = \mathbf{F}_{Kb} \boldsymbol{m}_{Kb} \otimes \boldsymbol{m}_{Kb} \mathbf{F}_{Kb}{}^T$ has a similar structure. Substituting Eqs. (2.60) and (2.61) into Eq. (2.17), we can obtain the relation between the moment and the shear deformation for the anisotropic response:

$$\frac{M}{2\pi r^2 \mu_a} = B_{Kar\theta} + \alpha \frac{\mu_b}{\mu_a} B_{Kbr\theta} + \alpha \frac{\mu_{c1}}{\mu_a} (J_1 - 1) B1_{r\theta} + \alpha \frac{\mu_{c2}}{\mu_a} (K_1 - 1) B2_{r\theta} \tag{2.62}$$

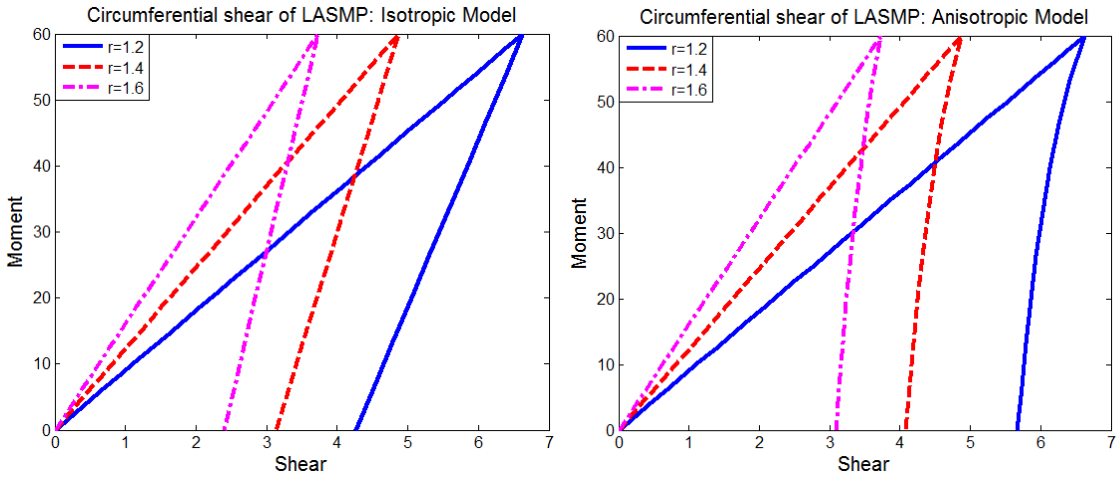

Fig. 12 Moment vs Circular shear curve for circumferential shear of LASMP: Isotropic (Left) and Anisotropic (Right)

Figure 12 shows the relationship between the moment and shear deformation at specific radius for both the isotropic and anisotropic models. At the location closer to the inner surface, the moment increases much faster during loading and decreases slower during unloading than the one at the location closer to the outer surface. In comparison, the anisotropic mixture can retain a much larger deformation than the isotropic model after unloading. In the above calculation, three different radii $r=1.2$, $r=1.4$, $r=1.6$ are considered and the material parameters are: $\frac{\mu_b}{\mu_a}=3$, $\frac{\mu_{c1}}{\mu_a}=5$, $\frac{\mu_{c2}}{\mu_a}=5$, $\alpha=0.6$.

Case 2. Relationship between the moment and rotation angle

Now we determine the rotation angle due to the circumferential moment. Instead of introducing another symbol k, we directly use rf' in all the expressions, where

$f' = \frac{\partial f}{\partial r}$. For the neo-Hookean constitutive model, the stress of the original network is written as

$$\mathbf{T} = -p\mathbf{I} + \mu_a \mathbf{B}_{Ka} = \begin{pmatrix} -p & 0 & 0 \\ 0 & -p & 0 \\ 0 & 0 & -p \end{pmatrix} + \mu_a \begin{pmatrix} 1 & rf' & 0 \\ rf' & 1+(rf')^2 & 0 \\ 0 & 0 & 1 \end{pmatrix}$$
$$= \begin{pmatrix} -p+\mu_a & \mu_a rf' & 0 \\ \mu_a rf' & -p+\mu_a[1+(rf')^2] & 0 \\ 0 & 0 & -p+\mu_a \end{pmatrix} \tag{2.63}$$

The balance of linear momentum leads to

$$\begin{cases} \frac{\partial p}{\partial r} + \mu_a rf' = 0 \\ 3f' + rf'' - \frac{\partial p}{r\partial \theta} = 0 \\ -\frac{\partial p}{\partial z} = 0 \end{cases} \tag{2.64}$$

From (2.64), it is easily to find that $p = p(r,\theta)$. Here we assume $p = p(r)$ that means p doesn't depend on θ but only on the radius r, and Eq. (2.64) reduces to:

$$\begin{cases} \frac{\partial p}{\partial r} + \mu_a rf' = 0 \\ 3f' + rf'' = 0 \end{cases} \tag{2.65}$$

The general solution of (2.65) is

$$f = -\frac{C_1}{2} r^{-2} + C_2 \tag{2.66}$$

where C_1, C_2 are constants which are determined by imposing the appropriate boundary conditions. Let's suppose that we specify the rotation angle at inner and outer lateral boundary surface:

$$f(R_i) = a, \quad f(R_o) = b \tag{2.67}$$

Then substituting Eq. (2.67) into Eq. (2.66), the constants C_1, C_2 are determined to be:

$$\begin{cases} f(R_i) = -\dfrac{C_1}{2} R_i^{-2} + C_2 = a \\ f(R_o) = -\dfrac{C_1}{2} R_o^{-2} + C_2 = b \end{cases}$$

$$\Rightarrow C_1 = \frac{2(b-a)}{R_i^{-2} - R_o^{-2}}, \quad C_2 = \frac{aR_o^{-2} - bR_i^{-2}}{R_o^{-2} - R_i^{-2}} \tag{2.68}$$

From (2.65.1) the solution for p is obtained:

$$\frac{\partial p}{\partial r} + \mu_a r (C_1 r^{-3})^2 = 0$$

$$\Rightarrow p = \frac{\mu_a C_1^{\,2}}{4} r^{-4} + d \tag{2.69}$$

where d is a constant determined by satisfying the resultant boundary conditions associated with the boundary conditions at the ends Z=0 and Z=L, and the lateral boundary.

Let us now consider the resultant force at the ends; we have

$$N = 0 = \int_0^{2\pi} \int_{R_i}^{R_o} T_{zz} r dr d\theta$$

$$\Rightarrow 2\pi \int_{R_i}^{R_o} (-\frac{\mu_a C_1^{\,2}}{4} r^{-4} - d + \mu_a) r dr = 0 \tag{2.70}$$

$$\Rightarrow d = \mu_a - \frac{\mu_a C_1^{\,2}}{4 R_o^{\,2} R_i^{\,2}}$$

We can easily find that for an axisymmetric problem, the resultant moment $M = 0$ at the ends and the resultant force $N = 0$ at the lateral boundary are satisfied automatically. In order to present the relations between the moment and rotation angle,

the boundary condition on the outer surface should be defined in terms of the specified moment. So we assume that the boundary conditions are:

$$f(R_i) = a = 0, \quad f(R_o) = M \tag{2.71}$$

The above boundary conditions imply that a rotation moment M is prescribed on the outer lateral surface and the inner surface is constrained due to the deformations. To ensure Eq. (2.71) has the same effect as the constraint imposed on the body as in Eq. (2.67), the relation between b and M is given as:

$$C_1 = \frac{2b}{R_i^{-2} - R_o^{-2}}, \quad C_2 = -\frac{bR_i^{-2}}{R_o^{-2} - R_i^{-2}} \tag{2.72}$$

and

$$\frac{M}{2\pi r^2 \mu_a} = k(t) = r\frac{\partial f}{\partial r} = C_1 r^{-2} = \frac{2b}{R_i^{-2} - R_o^{-2}} r^{-2}$$

$$\Rightarrow b = \frac{R_i^{-2} - R_o^{-2}}{4\pi\mu_a} M \tag{2.73}$$

Thus, the deformation function f in Eq. (2.66) is rewritten in terms of the relation between moment and rotation angle:

$$f = -\frac{C_1}{2} r^{-2} + C_2 = \frac{M}{4\pi\mu_a}\left(\frac{1}{R_i^2} - \frac{1}{r^2}\right) \tag{2.74}$$

Next, the cylinder is subjected to light irradiation and the material in the cylinder consists of two networks. The circular shear deformation at $t = \tau$ when the second network is formed is:

$$k(\tau) = C_1(\tau) r^{-2} = \frac{2b}{R_i^{-2} - R_o^{-2}} r^{-2} = \frac{M(\tau)}{2\pi r^2 \mu_a} \tag{2.75}$$

Substituting Eq. (2.59) into the equation of balance of linear momentum and replacing k by rf', we determine the governing equation for f:

$$\frac{\partial T_{r\theta}}{\partial r} + 2\frac{T_{r\theta}}{r} = 0$$

$$\Rightarrow \frac{\partial}{\partial r}[rf' + \alpha\frac{\mu_b}{\mu_a}(rf' - k(\tau))] + \frac{2}{r}[rf' + \alpha\frac{\mu_b}{\mu_a}(rf' - k(\tau))] = 0$$
$$\Rightarrow rf'' + 3f' = 0 \qquad (2.76)$$

Here it should be noted that $k(\tau)$ is also a function of r. Thus, two networks have the same governing equation for f as original network, so by the same procedure we should have the same forms of solution as in (2.66), and C_1, C_2 as in (2.68). By imposing the boundary conditions (2.71), we need to obtain the relation between b and M. From the expression of shear stress, we have

$$T_{r\theta} = \frac{M}{2\pi r^2} = \mu_a rf' + \alpha\mu_b(rf' - k(\tau))$$
$$\Rightarrow C_1 = \frac{1}{2\pi(\mu_a + \alpha\mu_b)}(M + \frac{\alpha\mu_b M(\tau)}{\mu_a}) \qquad (2.77)$$

On correlating (2.72) and (2.77), and replacing b by M in Eq. (2.66), the rotation angle can be expressed in terms of M as below:

$$f = \frac{1}{4\pi(\mu_a + \alpha\mu_b)}(M + \frac{\alpha\mu_b M(\tau)}{\mu_a})(\frac{1}{R_i^2} - \frac{1}{r^2}) \qquad (2.78)$$

The Lagrange multiplier p is determined as following:

$$\frac{\partial T_{rr}}{\partial r} + \frac{T_{rr} - T_{\theta\theta}}{r} = 0$$
$$\Rightarrow -\frac{\partial p}{\partial r} - \frac{\mu_a k^2 + \alpha\mu_b \Delta k^2}{r} = 0$$

$$\Rightarrow p = \frac{1}{4}[\mu_a C_1^{\,2} + \alpha\mu_b (C_1 - C_1(\tau))^2]\, r^{-4} + d \tag{2.79}$$

where d is determined by satisfying the resultant boundary conditions similar to the situation discussed previously:

$$d = (\mu_a + \alpha\mu_b) - \frac{\mu_a C_1^{\,2} + \alpha\mu_b (C_1 - C_1(\tau))^2}{4R_o^{\,2} R_i^{\,2}} \tag{2.80}$$

By comparing the results shown in Figs. 12 and 13, we see that the relationship between the moment-rotational angle is opposite to the relationship between the moment and the shear in how it changes with the radius. At small radius, the same amount of moment produces a smaller rotational angle but a larger shear deformation, which is expected from the solutions presented above.

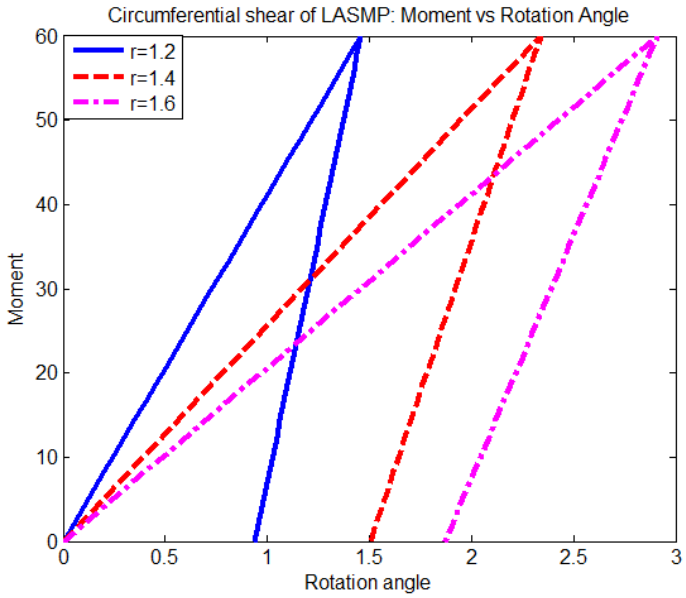

Fig. 13 Moment vs Rotation angle curve for circumferential shear of LASMP

2.3.2.4 Telescopic shear

Next we discuss another classical BVP, namely that of telescopic shear, shown in Fig. 14, in which a hollow cylinder of LASMP is subjected to a motion described by

$$r = r(R), \quad \theta = \Theta, \quad z = Z + f(R) \tag{2.81}$$

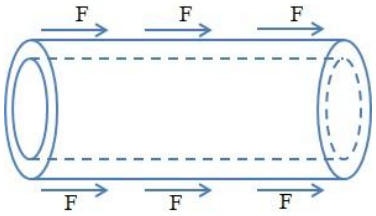

Fig. 14 Schematic of telescopic shear

Similar to the circumferential shear problem, two responses are discussed, which are the relation between the shear force and telescopic shear deformation, and the relation between the shear force and displacement.

Case 1. Force vs Telescopic shear

It follows from (2.81) that the deformation gradient $\mathbf{F}_{Ka}$ and the Cauchy-Green tensor $\mathbf{B}_{Ka}$ of the original network are given by

$$\mathbf{F}_{Ka} = \begin{pmatrix} 1 & 0 & 0 \\ 0 & 1 & 0 \\ k(t,r) & 0 & 1 \end{pmatrix} \qquad \mathbf{B}_{Ka} = \begin{pmatrix} 1 & 0 & k(t,r) \\ 0 & 1 & 0 \\ k(t,r) & 0 & k^2(t,r)+1 \end{pmatrix} \tag{2.82}$$

where $k = \dfrac{\partial f}{\partial r}$, and $\det(\mathbf{F}_{Ka}) = 1$. The balance of linear momentum leads to

$$\frac{\partial T_{rr}}{\partial r}+\frac{T_{rr}-T_{\theta\theta}}{r}=0$$
$$\frac{\partial T_{rz}}{\partial r}+\frac{T_{rz}}{r}=0 \tag{2.83}$$

From (2.83.2) the solution of T_{rz} is determined by applying the boundary condition:

$$T_{rz}=\frac{F}{2\pi r} \tag{2.84}$$

In the case of the neo-Hookean constitutive model, the relationship between shear force and telescopic shear is

$$T_{rz}=\frac{F}{2\pi r}=\mu_a k(t)$$
$$\Rightarrow \frac{F}{2\pi r\mu_a}=k(t) \tag{2.85}$$

After light irradiation, the stretch tensors for two networks take the following form

$$\mathbf{F}_{Kb}=\begin{pmatrix}1&0&0\\0&1&0\\\Delta k&0&1\end{pmatrix}\quad \mathbf{B}_{Kb}=\begin{pmatrix}1&0&\Delta k\\0&1&0\\\Delta k&0&1+\Delta k^2\end{pmatrix}\quad \mathbf{C}_{Kb}=\begin{pmatrix}1+\Delta k^2&0&\Delta k\\0&1&0\\\Delta k&0&1\end{pmatrix} \tag{2.86}$$

When we assume the second network is isotropic, the total shear stress is written as

$$T_{rz}=\mu_a B_{Karz}+\alpha\mu_b B_{Kbrz}=\mu_a k+\alpha\mu_b\Delta k \tag{2.87}$$

Substituting (2.84) into (2.87), we have:

$$\frac{F}{2\pi r\mu_a}=k+\alpha\frac{\mu_b}{\mu_a}\Delta k \tag{2.88}$$

When the anisotropy of the second network is taken into account, the shear deformation and shear force is

$$\frac{F}{2\pi r\mu_a} = B_{Karz} + \alpha\frac{\mu_b}{\mu_a}B_{Kbrz} + \alpha\frac{\mu_{c1}}{\mu_a}(J_1 - 1)B1_{rz} + \alpha\frac{\mu_{c2}}{\mu_a}(K_1 - 1)B2_{rz} \qquad (2.89)$$

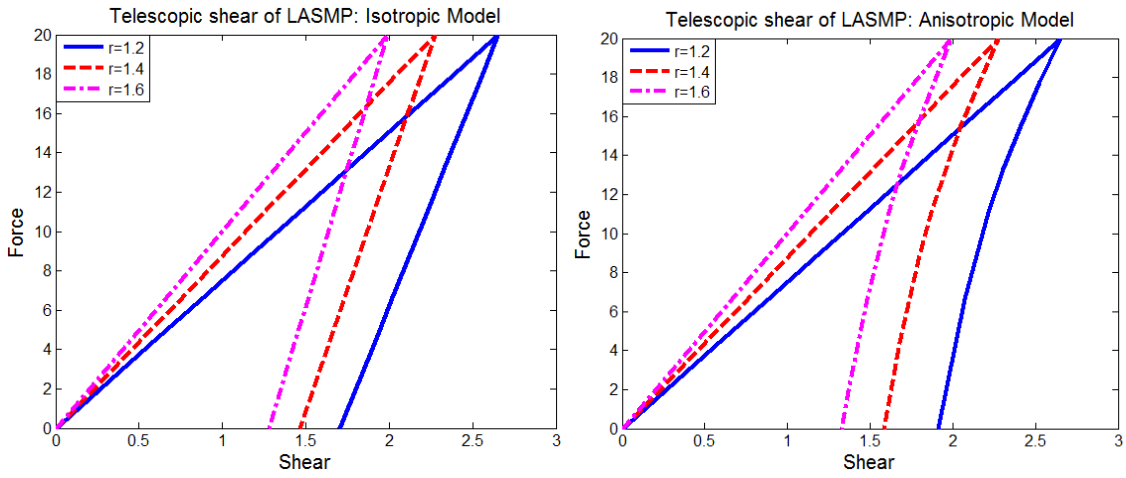

Fig. 15 Force vs telescopic shear curve for telescopic shear of LASMP: Isotropic (Left) and Anisotropic (Right)

Fig. 15 illustrates the relationship between shear force and telescopic shear at a specific radius for both isotropic and anisotropic models. Close to the inner surface, the force increases much faster during loading and decreases slower during unloading than the one close to the outer surface. It is also seen that the anisotropic model retains a much larger deformation than the isotropic model after unloading. Three different radii $r = 1.2$, $r = 1.4$, $r = 1.6$ are considered and the material parameters are: $\frac{\mu_b}{\mu_a} = 3$, $\frac{\mu_{c1}}{\mu_a} = 5$, $\frac{\mu_{c2}}{\mu_a} = 5$, $\alpha = 0.6$.

Case 2. Force vs Displacement

In order to study the relation between shear force and displacement, we use f' directly instead of extra variable k, where $f' = \frac{\partial f}{\partial r}$. The stress tensor of the original network is:

$$\mathbf{T} = -p\mathbf{I} + \mu_a \mathbf{B}_{Ka} = \begin{pmatrix} -p+\mu_a & 0 & \mu_a f' \\ 0 & -p+\mu_a & 0 \\ \mu_a f' & 0 & -p+\mu_a(1+f'^2) \end{pmatrix} \tag{2.90}$$

Substituting the stress components into the balance of linear momentum leads to

$$\begin{cases} -\frac{\partial p}{\partial r} = 0 \\ -\frac{\partial p}{r\partial \theta} = 0 \\ \frac{\mu_a \partial f'}{\partial r} - \frac{\partial p}{\partial z} + \frac{\mu_a f'}{r} = 0 \end{cases} \tag{2.91}$$

From (2.91) we can see p is in general a function of z. Here we assume $p = constant$, so (2.91.3) is simplified and we can derive the solution of f through:

$$\begin{aligned} &\frac{\partial f'}{\partial r} + \frac{f'}{r} = 0 \\ \Rightarrow\ & f = C_1 \ln r + C_2 \end{aligned} \tag{2.92}$$

where C_1, C_2 are constants which are determined by the following boundary conditions

$$\begin{aligned} &\begin{cases} f(R_i) = C_1 \ln R_i + C_2 = a \\ f(R_o) = C_1 \ln R_o + C_2 = b \end{cases} \\ \Rightarrow\ & C_1 = \frac{a-b}{\ln R_i - \ln R_o}, \quad C_2 = \frac{-a\ln R_o + b \ln R_i}{\ln R_i - \ln R_o} \end{aligned} \tag{2.93}$$

Let $a = 0$. Then C_1, C_2 are

$$C_1 = \frac{-b}{\ln R_i - \ln R_o}, \quad C_2 = \frac{b \ln R_i}{\ln R_i - \ln R_o} \tag{2.94}$$

To determine the relationship between the shear force and displacement, we need to correlate b and F

$$T_{rz} = \frac{F}{2\pi r} = \mu_a f' = \mu_a \frac{C_1}{r} = \frac{\mu_a}{r} \frac{-b}{\ln R_i - \ln R_o}$$
$$\Rightarrow b = -\frac{F(\ln R_i - \ln R_o)}{2\pi\mu_a} \tag{2.95}$$

So (2.92) can be rewritten as

$$f = \frac{F}{2\pi\mu_a}(\ln r - \ln R_i) \tag{2.96}$$

Similarly p is determined by the resultant boundary conditions at the end boundary surfaces and lateral boundary surface,

$$N = \int_0^{2\pi} \int_{R_i}^{R_o} T_{zz} r dr d\theta = 0$$
$$\Rightarrow p = \frac{2\mu_a C_1^{\,2}(\ln R_o - \ln R_i)}{R_o^{\,2} - R_i^{\,2}} + \mu_a \tag{2.97}$$

Next we assume at time $t = \tau$, the second network is formed, the corresponding shear is

$$k(\tau) = \frac{C_1(\tau)}{r} = \frac{F(\tau)}{2\pi\mu_a r} \tag{2.98}$$

By substituting the shear stress component of two networks into (2.83.2), we obtain the governing equation of f

$$\frac{\partial T_{rz}}{\partial r}+\frac{T_{rz}}{r}=0$$
$$\Rightarrow \frac{\partial}{\partial r}[\mu_a f'+\alpha\mu_b(f'-k(\tau))]+\frac{1}{r}[\mu_a f'+\alpha\mu_b(f'-k(\tau))]=0$$
$$\Rightarrow f''+\frac{f'}{r}=0 \tag{2.99}$$

We notice that the governing equation for f for two networks is the same as that of original network, so we can directly adopt the solution (2.92) and C_1, C_2 in (2.93). By applying the boundary conditions $f(R_i)=a=0$ and $f(R_o)=F$, we can derive the relations between b and F through shear stress in the following manner:

$$\begin{aligned} T_{r\theta} &= \frac{F}{2\pi r}=\mu_a f'+\alpha\mu_b(f'-k(\tau)) \\ \Rightarrow C_1 &= \frac{1}{2\pi(\mu_a+\alpha\mu_b)}(F+\frac{\alpha\mu_b F(\tau)}{\mu_a}) \end{aligned} \tag{2.100}$$

Then by correlating (2.94) and (2.100), and replacing b by F in Eq. (2.92), the displacement can be expressed in terms of F as below:

$$f=\frac{1}{2\pi(\mu_a+\alpha\mu_b)}(F+\frac{\alpha\mu_b F(\tau)}{\mu_a})(\ln r-\ln R_i) \tag{2.101}$$

Similarly, the parameter p is determined by satisfying the resultant forces at the boundaries,

$$N=\int_0^{2\pi}\int_{R_i}^{R_o} T_{zz} r dr d\theta=0$$
$$\Rightarrow p=(\mu_a+\alpha\mu_b)+\frac{2[\mu_a C_1^{\,2}+\alpha\mu_b(C_1-C_1(\tau))^2]}{R_o^{\,2}-R_i^{\,2}}(\ln R_o-\ln R_i) \tag{2.102}$$

Figures 15 and 16 also show a similar phenomenon as circumferential shear problem. At small radius, the same amount of force produces a smaller telescopic displacement but a larger shear which is because of the term $1/r$ in the derivation of the shear displacement.

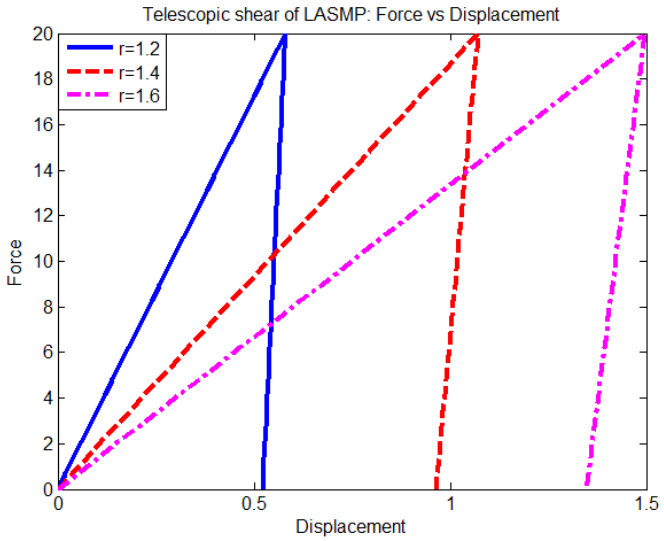

Fig. 16 Force vs Displacement curve for telescopic shear of LASMP

2.4 Viscoelastic model

2.4.1 Viscoelastic constitutive model

In the above model, we described the response of the LASMPs based on the assumption that the LASMPs have multiple natural configurations within the context of elastic response. However, although limited, there have been experimental studies on LASMPs from which we can gain some idea concerning the stress relaxations that is exhibited by such materials. Lendlein et al. [30] carried out cyclic photomechanical experiments on LASMPs under both stress control and strain control conditions; we cannot see strong stress relaxation behavior. But it is still worthwhile to model a

viscoelastic response by reconsidering the coarse fluctuated curve and experimental data on strain-fixity rate and strain-recovery rate. The stress relaxation behavior can be clearly observed in the research [33] where three control experiments were carried out. Several publications on TASMPs [62-64] consider the viscous response of the materials, and one can observe that temperature can significantly change the mechanical behavior of polymers. Most of existing models for LASMPs are based on hyperelasticity and do not consider the time dependent response of polymers [42, 38, 41]. Therefore, to investigate such a response we adopt the quasi-linear viscoelasticity framework to model the behavior of LASMPs.

2.4.1.1 Quasi-linear viscoelasticity

A quasi-linear viscoelastic (QLV) model was proposed by Fung [56] to describe the uniaxial elongation of biological soft tissue like muscles, ligaments and tendons. In that study, he assumed the relaxation rate is independent of the instantaneous local strain. The quasi-linear viscoelastic model is widely used today, because it seems to be the simplest way to incorporate both nonlinearity (dependence of properties on load or strain) and time dependence (viscoelasticity) in a simplified integral model. Besides the biomedical applications [65, 66], the QLV model has also been used to model materials like elastomeric polymers, rubbers or composites [67,68].

The response of QLV bodies can be defined by separating the reduced time function and the nonlinear elastic measure in the manner described below. In terms of strain tensors, the constitutive relation is expressed as:

$$\mathbf{S}(t) = \int_{0^-}^{t} \mathbf{G}(t-s) \frac{d\mathbf{g}^e(\mathbf{E}(s))}{ds} ds \tag{2.103}$$

where $\mathbf{S}$ is the second Piola Kirchhoff stress, $\mathbf{G}$ is the reduced relaxation tensor that depends on time history, $\mathbf{g}^e(\mathbf{E})$ is the nonlinear elastic function expressed in terms of Green-St. Venant strain tensor, and *t* is current time. Here it should be noted that we have used 2nd Piola-Kirchhoff stress and not the Cauchy stress. The nonlinear elastic function $\mathbf{g}^e(\mathbf{E})$ is derived from the strain energy $W(\mathbf{E})$, which is given as $\mathbf{S}^e = \mathbf{g}^e(\mathbf{E}) = \frac{\partial W(\mathbf{E})}{\partial \mathbf{E}}$.

In the QLV model, it is assumed that the stress depends linearly on the time history, and the relaxation function does not depend on the deformation state, and response at current time can be approximated by a linear combination of responses of multiple deformation inputs applied at different time histories. Further discussion on the reappraisal of QLV can be found in the reference (De et al., 2014). The objectivity, in which physical quantities should be independent of observer transformations, is satisfied by using the 2nd Piola-Kirchhoff stress measure, which is expressed as

$$\mathbf{S} = \mathbf{S}_D + \mathbf{S}_H = \int_{-\infty}^{t} \mathbf{D}(t-s) \frac{\partial}{\partial s} \mathbf{S}_D^e(s) ds + \int_{-\infty}^{t} \mathbf{H}(t-s) \frac{\partial}{\partial s} \mathbf{S}_H^e(s) ds \tag{2.104}$$

where $\mathbf{S}_D^e$, $\mathbf{S}_H^e$ are the corresponding terms of Cauchy stress to the 2nd Piola-Kirchoff stress, which are given by the following relations $\mathbf{S}_D^e = \mathrm{J}\mathbf{F}^{-1}\mathbf{T}_D^e\mathbf{F}^{-\mathrm{T}}$ and $\mathbf{S}_H^e = \mathrm{J}\mathbf{F}^{-1}\mathbf{T}_H^e\mathbf{F}^{-\mathrm{T}}$ where $\mathbf{T}_D^e = \mathbf{T}^e - \frac{1}{3} tr(\mathbf{T}^e)\mathbf{I}$, $\mathbf{T}_H^e = \frac{1}{3} tr(\mathbf{T}^e)\mathbf{I}$ are the deviatoric and hydrostatic Cauchy

stress components, respectively. $\mathbf{D}(t)$ and $\mathbf{H}(t)$ are the associated reduced tensorial relaxation operators, J is the det(**F**). Then by converting the 2nd Piola-Kirchhoff stress to Cauchy stress via $\mathbf{S} = J\mathbf{F}^{-1}\mathbf{T}\mathbf{F}^{-T}$ and integrating by parts, we can obtain the Cauchy stress as:

$$\begin{aligned}\mathbf{T}(t) = J^{-1}\mathbf{F}(t)(\mathbf{S}_D^e(t) + \int_0^t \frac{d\mathbf{D}(t-s)}{d(t-s)}\mathbf{S}_D^e(s)ds)\mathbf{F}^{\mathbf{T}}(t) \\ + J^{-1}\mathbf{F}(t)(\mathbf{S}_H^e(t) + \int_0^t \frac{d\mathbf{H}(t-s)}{d(t-s)}\mathbf{S}_H^e(s)ds)\mathbf{F}^{\mathbf{T}}(t)\end{aligned} \tag{2.105}$$

By virtue of the constraint of incompressibility, we have J=1 and the second term of (2.105) only contains the hydrostatic term which can represent the compressible deformation of the body, so we can reduce

$$J^{-1}\mathbf{F}(t)(\mathbf{S}_H^e(t) + \int_0^t \frac{d\mathbf{H}(t-s)}{d(t-s)}\mathbf{S}_H^e(s)ds)\mathbf{F}^{\mathbf{T}}(t) \rightarrow -p(t)\mathbf{I} \tag{2.106}$$

Where $p\mathbf{I}$ refers to the indeterminate part of the stress due to incompressibility. Therefore, (2.105) can be rewritten as

$$\mathbf{T}(t) = -p\mathbf{I} + \mathbf{F}(t)(\mathbf{S}_D^e(t) + \int_0^t \frac{d\mathbf{D}(t-s)}{d(t-s)}\mathbf{S}_D^e(s)ds)\mathbf{F}^{\mathbf{T}}(t) \tag{2.107}$$

For a general discussion of three dimensional QLV models, the readers can refer to [57, 68].

2.4.1.2 Loading of the original network

LASMPs can undergo large deformations due to the twist and stretch of the polymeric chains. We assume the LASMP bodies considered in this study are

incompressible, initially stress free and isotropic. Before the second network is formed, only the original network is present in the body in its original natural configuration, which for both PMC and PNR LASMPs can be expressed as:

$$\mathbf{T}(t) = -p\mathbf{I} + \mathbf{F}_{Ka}(t)(\mathbf{S}_D^e(t) + \int_0^t \frac{d\mathbf{D}_a(t-s)}{d(t-s)}\mathbf{S}_D^e(s)ds)\mathbf{F}_{Ka}^T(t) \qquad (2.108)$$

The subscript K_a refers to the original natural configuration and the subscript a is associated with the original network.

2.4.1.3 Formation of the second network at constant stretch or strain

After the body is elongated to a particular length at time t_1, light is irradiated to start the formation of the second network, then the body is a mixture of two networks. Based on the theory of multiple natural configurations, the mechanical response of each network can be expressed using Eq. (2.107). By applying the theory of constrained mixtures [58], we assume that the two networks have the same displacement, so the stress would be the summation of the partial stresses in the two networks, that is

$$\mathbf{T} = -p\mathbf{I} + \mathbf{T_a} + \mathbf{T_b} \qquad (2.109)$$

where $\mathbf{T_a}$ denotes the Cauchy stress in the original network, which is given as

$$\mathbf{T}_a(t) = \mathbf{F}_{Ka}(t)(\mathbf{S}_{Da}^e(t) + \int_0^t \frac{d\mathbf{D}_a(t-s)}{d(t-s)}\mathbf{S}_{Da}^e(s)ds)\mathbf{F}_{Ka}^T(t) \qquad (2.110)$$

and $\mathbf{T_b}$ denotes the Cauchy stresses in the newly formed networks, which is given by the constitutive expression

$$\mathbf{T}_b(t) = \mathbf{F}_{Kb}(t)(\mathbf{S}_{Db}^e(t) + \int_{t_1}^t \frac{d\mathbf{D}_b(t-s)}{d(t-s)}\mathbf{S}_{Db}^e(s)ds)\mathbf{F}_{Kb}^T(t) \qquad (2.111)$$

where $\mathbf{S}_{Da}^{e}$ and $\mathbf{S}_{Db}^{e}$ are the elastic parts of the 2nd Piola-Kirchoff stress associated with the two networks, t_1 is the starting time when the second network is formed, t is the current time ($t \geq t_1$), K_b refers to the new natural configuration and the subscript b is associated with the new network. In Eq. (2.110) different histories of $\mathbf{S}_{Da}^{e}$ occur during time intervals $[0, t_1]$ and $[t_1, t]$. which will be considered later in Section 2.2.2.1.

In a typical application of LASMPs, the formation process of the second network is achieved by fixing the deformation during light irradiation. Therefore, in this study we just consider the case of the formation of the second network under constant strain or stretch, while the case of constant stress will not be discussed in this paper wherein the constitutive model will be more complicated since the newly formed network has an evolving natural configuration. The deformation gradients of the two networks are related through:

$$\mathbf{F}(t) = \mathbf{F}_{Kb}(t)\mathbf{F}_{Ka}(t_1) \tag{2.112}$$

In the constant stretch situation, $\mathbf{F}_{Kb}(t) = \mathbf{I}$ and $\mathbf{F}(t) = \mathbf{F}_{Ka}(t) = \mathbf{F}_{Ka}(t_1), t \geq t_1$, which means that the second network does not undergo deformation, so the stress from second network during this period will be zero and the total stress-stretch/strain relationship will be the same as equation (2.107). In our previous study [51], we modeled the thin PMC LASMPs under the assumption that both networks are elastic but with two different stress free configurations, where we have $\frac{d\mathbf{D}_a(t-s)}{d(t-s)} = \mathbf{0}$, so $\mathbf{T}(t) = -p\mathbf{I} + \mathbf{F}_{Ka}(t)\mathbf{S}_{Da}^{e}(t)\mathbf{F}_{Ka}^{T}(t)$. By keeping the stretch or strain constant while radiating

the polymer to activate the second network, the stresses in elastic LASMPs will not change. However, if we consider the viscoelastic behavior of LASMPs when $\frac{d\mathbf{D}_a(t-s)}{d(t-s)} \neq \mathbf{0}$, they can exhibit stress relaxation, and during light irradiation, the stress is no longer constant but relaxing with time. So within the context of the viscoelastic model, the constitutive relation of LASMPs during light irradiation, when the deformation is fixed, reduces to:

$$\mathbf{T}(t) = -p\mathbf{I} + \mathbf{F}_{Ka}(t)(\mathbf{S}_D^e(t) + \int_0^t \frac{d\mathbf{D}_a(t-s)}{d(t-s)} \mathbf{S}_D^e(s)ds)\mathbf{F}_{Ka}^T(t) \qquad (2.113)$$

During the irradiation process $t \in [t_1, t]$, the elastic stress part $\mathbf{S}_D^e$ is constant due to keeping the stretch fixed. We consider solid like isotropic viscoelastic behavior for both networks, and the tensorial reduced relaxation function can be expressed by its component with the following form:

$$D_i(t) = \frac{\mu_{\infty i}}{\mu_{oi}} + (1 - \frac{\mu_{\infty i}}{\mu_{oi}})e^{-t/\tau_i} \qquad (i = a, b) \qquad (2.114)$$

where μ_{oi} and $\mu_{\infty i}$ are the shear modulus and long-time shear modulus, respectively, for the network *i*, τ_i is their characteristic relaxation time.

The properties of LASMPs, such as the shear modulus μ_{oi} and relaxation characteristic time τ_i, can also change because of the formation of the second network. In this study, we assume the shear modulus of each network is a function of the current volume ratio of the second network α, which can be expressed as: $\tilde{\mu}_i = \tilde{\mu}_i(\alpha)$, where $\tilde{\mu}_i$ is the new modulus of each network, and we keep relaxation time τ_i same.

For PMC LASMPs, the property of the original network will not change since it has no conversion or transformation to the second network, and only the properties of the second network will change by the formation process. However, tracking the phases formed at different times will be computationally very expensive, and also there is limited experimental data for us to corroborate the model during such a process. Therefore, we simplify this process by assuming the shear modulus $\tilde{\mu}_b = \alpha\mu_b$, where α is the volume ratio of the second network and μ_b is the shear modulus when the second network is formed completely at $\alpha = 1$.

For PNR LASMPs, the formation mechanism of the second network is different from PMC LASMPs. PNR LASMPs transform some parts of the original network into a new network under light irradiation, so we have to take the formation process of the new network into consideration since the cleavage of the original network affects its mechanical property such as the shear modulus and/or the relaxation characteristic time. If the volume ratio of the second network is α, the remaining volume fraction of the original network is (1-α). Based on this, we modify the constitutive equation in Eq. (2.113) for PNR LASMPs. We still assume the shear modulus of the second network is $\tilde{\mu}_b = \tilde{\mu}_b(\alpha)$, the shear modulus of the original network is $\tilde{\mu}_a = \tilde{\mu}_a(1-\alpha) = \tilde{\mu}_a(\alpha)$. When there is no decrease of the original network α=0, then $\tilde{\mu}_a = \mu_a$. As a consequence of the network rearrangement, the shear modulus of the original network appears to decline which causes the body to experience more significant stress relaxation behavior, and the modulus of the newly formed (second) network will increase. This effect can be

incorporated by choosing proper functions for $\tilde{\mu}_i = \tilde{\mu}_i(\alpha)$. With regard to how the formation process of the new network is modeled, we will adopt the methodology developed by Long et al. [42] which is discussed in Section 2.2.2.2.

By holding the stretch constant, we can determine the corresponding stress by analytical or numerical calculations. The classical trapezoid integration algorithm and recursive method are implemented to get the approximate solution.

2.4.1.4 Unloading of the two-network mixtures

As a consequence of the formation of the second network, the body will not go back to the original configuration by unloading the force but comes to a temporary shape because there are two networks in the body to support the stress. The original network tends to recover the entire deformation, while the new network tends to hold the deformation upon removing the force. The response of the mixture of the two networks is in the form of equation (2.109), the total stress is the summation of the partial stresses of two networks, which are

$$\mathbf{T}_a(t) = \mathbf{F}_{Ka}(t)(\mathbf{S}^e_{Da}(t) + \int_0^t \frac{d\mathbf{D}_a(t-s)}{d(t-s)}\mathbf{S}^e_{Da}(s)ds)\mathbf{F}^T_{Ka}(t) \tag{2.115}$$

$$\mathbf{T}_b(t) = \mathbf{F}_{Kb}(t)(\mathbf{S}^e_{Db}(t) + \int_{t_2}^t \frac{d\mathbf{D}_b(t-s)}{d(t-s)}\mathbf{S}^e_{Db}(s)ds)\mathbf{F}^T_{Kb}(t) \tag{2.116}$$

where t_2 is the final time of the formation of the second network and the starting time for the unloading and the current time $t \geq t_2$. It is noted that the stress from the second network is not zero because the second network is also deformed $\mathbf{F}_{Kb}(t) \neq \mathbf{I}$.

Equations (2.109), (2.115), (2.116) are valid for both PMC and PNR LASMPs, but the shear modulus of PNR LASMPs should be obtained by the function $\tilde{u}_i = \tilde{u}_i(a)$ as discussed above. So the total stress of the two-network mixture leads to

$$\mathbf{T}(t) = -p\mathbf{I} + \mathbf{F}_{Ka}(t)(\mathbf{S}^e_{Da}(t) + \int_0^t \frac{d\mathbf{D}_a(t-s)}{d(t-s)}\mathbf{S}^e_{Da}(s)ds)\mathbf{F}^T_{Ka}(t) + \mathbf{F}_{Kb}(t)(\mathbf{S}^e_{Db}(t) + \int_{t_2}^t \frac{d\mathbf{D}_b(t-s)}{d(t-s)}\mathbf{S}^e_{Db}(s)ds)\mathbf{F}^T_{Kb}(t) \tag{2.117}$$

During unloading, we release the force gradually and investigate how the stretch of the body changes with stress. However, from eqn. (2.117) we can see that the stress is given in terms of the integral of the history of the strain or stretch with a kernel representing the fading memory of the material. To determine the stretch from known stresses is challenging because of the necessity of carrying information about the history of the material response over time that makes it difficult or impossible to obtain the form $\mathbf{E} = f(\mathbf{T})$ analytically. To solve this problem, De Pascalis et al. [57] adopted a discrete numerical method. In this article, we use a combination of classical trapezoidal algorithm, recursive method, and Newton–Raphson scheme which seem much easier to implement. The detailed numerical procedure is outlined in Appendix 2.

2.4.2 Boundary-initial value problems

In this section we study the viscoelastic responses of thin PMC LASMPs within the context of several boundary value problems. Parametric studies are carried out in order to understand the qualitative behavior of the model. The neo-Hookean model is considered for the elastic instantaneous behavior, so that we can compare the response of

our viscoelastic LASMP with the ones in our previous study. For the relaxation function, we take the values $\mu_a = 5$, $\mu_a = 20$, α=0.6 for our particular calculation. Then in section ‘‘PNR LASMPs’’ , we will show how to use our viscoelastic model to fit the experimental data reported in the literature [33] and capture the stress relaxation behavior of PNR LASMPs.

2.4.2.1 PMC LASMPs

1. Uniaxial tension

In the case of uniaxial tension, during the loading period, only the original network is carrying the load and Eq. (2.105) leads to,

$$T_{11}(t) = T(t) = -p + \Lambda^2(t)(S^e_{D11}(t) + \int_0^t \frac{dD_a(t-s)}{d(t-s)} S^e_{D11}(s)ds) \qquad (2.118)$$

and

$$T_{22}(t) = T_{33}(t) = -p + \Lambda^{-1}(t)(S^e_{D22}(t) + \int_0^t \frac{dD_a(t-s)}{d(t-s)} S^e_{D22}(s)ds) = 0 \quad (2.119)$$

So we have

$$T(t) = \Lambda^2(t)S^e_{D11}(t) - \Lambda^{-1}(t)S^e_{D22}(t) + \int_0^t \frac{dD_a(t-s)}{d(t-s)} (\Lambda^2(t)S^e_{D11}(s) - \Lambda^{-1}(t)S^e_{D22}(s))ds \quad (2.120)$$

where

$$S^e_{D11} = 2[\frac{2}{3}(W_1 + \frac{W_2}{\Lambda})(1 - \frac{1}{\Lambda^3})], \quad S^e_{D22} = 2[\frac{1}{3}(W_1 + \frac{W_2}{\Lambda})(1 - \Lambda^3)] \qquad (2.121)$$

Here W_1, W_2 are the derivatives of strain energy function W with respect to the principal invariants of the left Cauchy-Green tensor $\mathbf{B}$ denoted by I_1 and I_2. In the case of the purely elastic neo-Hookean response, (2.120) is rewritten as

$$\frac{T(t)}{\mu_a} = \Lambda^2(t) - \Lambda^{-1}(t) + \int_0^t \frac{dD_a(t-s)}{d(t-s)} (\Lambda^2(t)[\frac{2}{3}(1-\Lambda^{-3}(s))] - \Lambda^{-1}(t)[\frac{1}{3}(1-\Lambda^3(s))])ds \quad (2.122)$$

After prescribing mechanical loads to the body to a specified stretch ratio $\bar{\Lambda}$ at time t_1, we expose the material to the light to form the second network. During the formation, we keep the stretch constant till time t_2, the stress will be relaxing due to the viscoelasticity of the polymer. The stress-stretch relation can be determined as following:

$$\begin{aligned}\frac{T(t)}{\mu_a} =& \Lambda^2(t) - \Lambda^{-1}(t) + \int_0^{t_1} \frac{dD_a(t-s)}{d(t-s)} (\Lambda^2(t)[\frac{2}{3}(1-\Lambda^{-3}(s))] - \Lambda^{-1}(t)[\frac{1}{3}(1-\Lambda^3(s))])ds \\ &+ \int_{t_1}^t \frac{dD_a(t-s)}{d(t-s)} (\bar{\Lambda}^2 - \bar{\Lambda}^{-1})ds\end{aligned} \quad (2.123)$$

We see that there are three terms, each of which can be associated with different physical mechanisms. The first term is related to the instantaneous elastic response, the second is due to the relaxation of the stress from purely mechanical loading from time 0 to t_1, and the third term represents the effect of time evolution due to viscoelasticity during light radiation from time t_1 to t.

When the required percentage of the second network is formed, we then unload the force gradually to zero at time t_3. Now the two networks carry the load, which would cause some amount of stretch to be retained by the material. Each network exhibits the

mechanical response described by the constitutive equation (2.120), and the total stress of two-network mixture in the tension direction is:

$$\begin{aligned} T_{11} = T(t) &= T_{a11} + T_{b11} \\ &= \mu_a(\Lambda^2(t) - \Lambda^{-1}(t) + \int_0^{t_1} \frac{dD_a(t-s)}{d(t-s)}(\Lambda^2(t)[\frac{2}{3}(1-\Lambda^{-3}(s))] - \Lambda^{-1}(t)[\frac{1}{3}(1-\Lambda^3(s))])ds \\ &+ \int_{t_1}^{t_2} \frac{dD_a(t-s)}{d(t-s)}(\Lambda^2(t)[\frac{2}{3}(1-\bar{\Lambda}^{-3})] - \Lambda^{-1}(t)[\frac{1}{3}(1-\bar{\Lambda}^3)])ds \\ &+ \int_{t_2}^{t} \frac{dD_a(t-s)}{d(t-s)}(\Lambda^2(t)[\frac{2}{3}(1-\Lambda^{-3}(s))] - \Lambda^{-1}(t)[\frac{1}{3}(1-\Lambda^3(s))])ds) \\ &+ \alpha\mu_b((\frac{\Lambda(t)}{\bar{\Lambda}})^2 - \frac{\bar{\Lambda}}{\Lambda(t)} + \int_{t_2}^{t} \frac{dD_b(t-s)}{d(t-s)}((\frac{\Lambda(t)}{\bar{\Lambda}})^2[\frac{2}{3}(1-(\frac{\bar{\Lambda}}{\Lambda(s)})^3)] - \frac{\bar{\Lambda}}{\Lambda(t)}[\frac{1}{3}(1-(\frac{\Lambda(s)}{\bar{\Lambda}})^3)])ds) \end{aligned} \tag{2.124}$$

Even after the stress is totally released, LASMPs will still exhibit stretch changes due to the viscoelasticity which is reflected in our calculations. Several calculations are carried out to investigate the effects of the various parameters and differences between the quasi-linear viscoelastic model and neo-Hookean model. Figures 17 show how the value of μ_∞ / μ_a can influence the relations between stress, stretch and time. From the results, we can see that larger μ_∞ / μ_a leads to stiffer materials, which are seen from the loading and unloading paths, and the amount of stress relaxation is smaller during light irradiation. In other words, the body with larger μ_∞ / μ_a responds much more like an elastic body and exhibits less viscoelastic behavior.

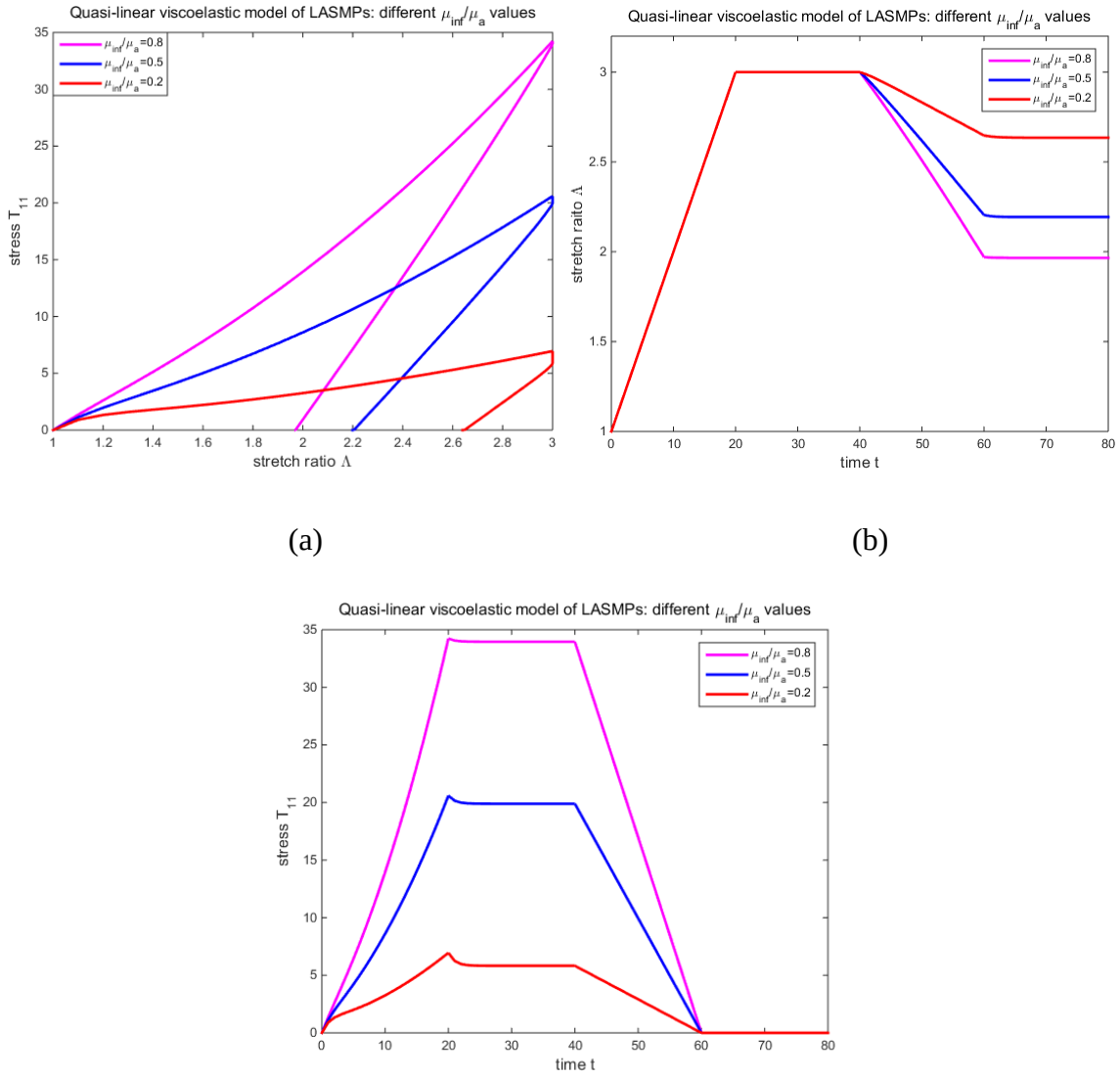

Fig. 17 (a) Stress-stretch plot of LASMPs for different values. (b) Stretch-time plot of LASMPs for different values. (c) Stress-time plot of LASMPs for different values

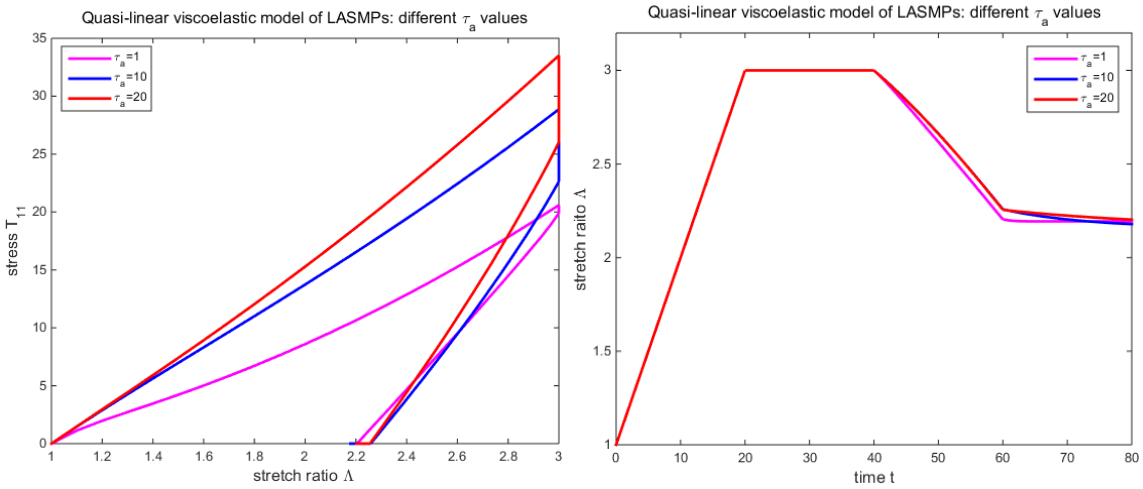

(a) (b)

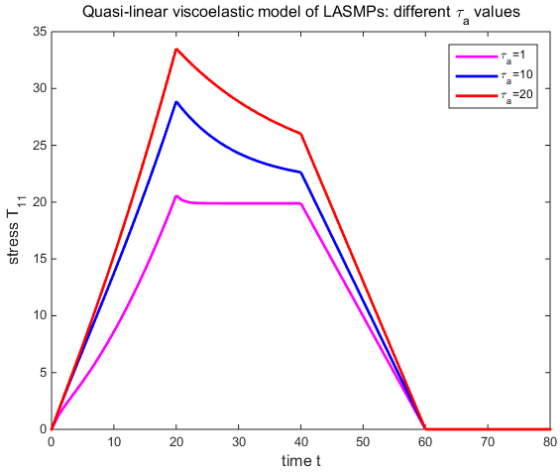

(c)

Fig. 18 (a) The corresponding stress-stretch plot of LASMPs for different values. (b) Stretch-time plot of LASMPs for different values. (c) Stress-time plot of LASMPs for different values

Figures 18 depict the effect of the characteristic time τ_a with regard to the stress response and stretch with respect to time. It is noted that if τ_a is larger, the stress will

increase much faster when loading, and relax faster under light irradiation. During and after the unloading period, the stretch decreases at a much slower rate.

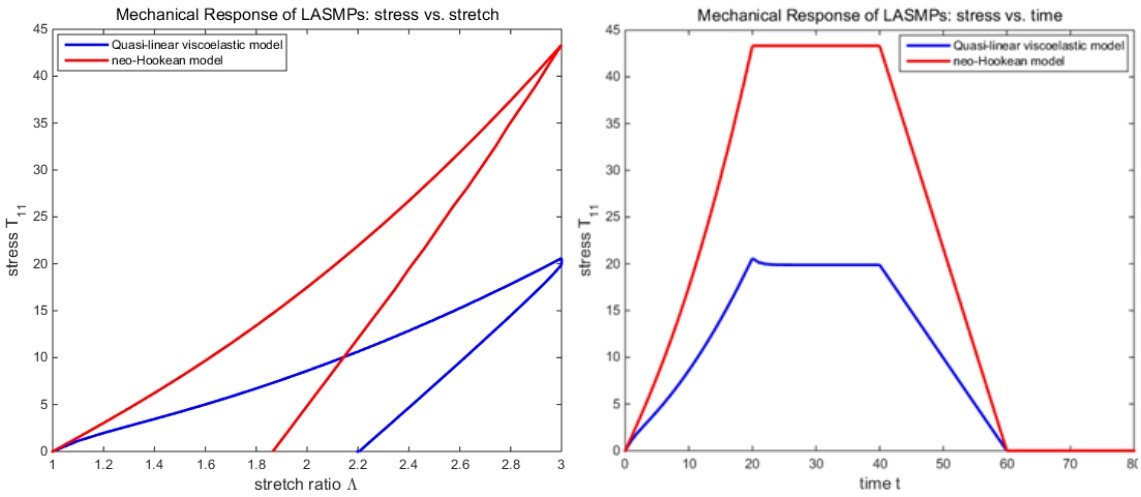

Fig. 19 Comparison between the responses of the quasi-linear viscoelastic and neo-Hookean model: Stress versus stretch (Left) and Stress versus time (Right)

A comparison of the mechanical response of the quasi-linear viscoelastic model and the neo-Hookean elastic model can be carried out by referring to Fig 19. We note that the viscoelastic body, with the same instantaneous elastic response of the elastic body undergoes a far larger deformation when subjected to identical loading histories.

2. Biaxial tension

Biaxial tension which is also a common deformation can be described as:

$$x = \Lambda_1 X, \quad y = \Lambda_2 Y, \quad z = \frac{1}{\Lambda_1 \Lambda_2} Z \tag{2.125}$$

where Λ_1, Λ_2 are the stretch ratios in the x, y directions respectively, and Λ_1 can be equal or different from Λ_2. Similarly we can have

$$T_{11}(t)=\mu_a\{\Lambda_1^2(t)\frac{1}{3}(2-\frac{\Lambda_2^2(t)}{\Lambda_1^2(t)}-\frac{1}{\Lambda_1^4(t)\Lambda_2^2(t)})-\frac{1}{\Lambda_1^2(t)\Lambda_2^2(t)}\frac{1}{3}(2-\Lambda_1^4(t)\Lambda_2^2(t)-\Lambda_1^2(t)\Lambda_2^4(t))$$
$$+\int_0^t\frac{dD_a(t-s)}{d(t-s)}[\Lambda_1^2(t)\frac{1}{3}(2-\frac{\Lambda_2^2(s)}{\Lambda_1^2(s)}-\frac{1}{\Lambda_1^4(s)\Lambda_2^2(s)})-\frac{1}{\Lambda_1^2(t)\Lambda_2^2(t)}\frac{1}{3}(2-\Lambda_1^4(s)\Lambda_2^2(s)$$
$$-\Lambda_1^2(s)\Lambda_2^4(s))]ds\}$$

and

$$T_{22}(t)=\mu_a\{\Lambda_2^2(t)\frac{1}{3}(2-\frac{\Lambda_1^2(t)}{\Lambda_2^2(t)}-\frac{1}{\Lambda_1^2(t)\Lambda_2^4(t)})-\frac{1}{\Lambda_1^2(t)\Lambda_2^2(t)}\frac{1}{3}(2-\Lambda_1^4(t)\Lambda_2^2(t)-\Lambda_1^2(t)\Lambda_2^4(t))$$
$$+\int_0^t\frac{dD_a(t-s)}{d(t-s)}[\Lambda_2^2(t)\frac{1}{3}(2-\frac{\Lambda_1^2(s)}{\Lambda_2^2(s)}-\frac{1}{\Lambda_1^2(s)\Lambda_2^4(s)})-\frac{1}{\Lambda_1^2(t)\Lambda_2^2(t)}\frac{1}{3}(2-\Lambda_1^4(s)\Lambda_2^2(s)$$
$$-\Lambda_1^2(s)\Lambda_2^4(s))]ds\} \tag{2.126}$$

We assume that the stretch Λ_1 and Λ_2 are given through:

$$\Lambda_1=1+k_1t,\ \Lambda_2=1+k_2t \tag{2.127}$$

At $t=t_1$, we keep the stretch ratio constant and expose the stretched body to irradiation by light, whereby the second network starts forming. During this time period, we assume the second network makes no contribution to the total stress, and therefore the stress components at the two tensile directions should have the same form as before. When the amount of the second network reaches the volume fraction α at $t=t_2$ we start unloading. During this time period, both networks carry the total stress and together. The stress $\mathbf{T_b}$ carried by the second network can be derived using the same procedure above and is given by

$$T_{b11}(t)=\mu_b\{\frac{\Lambda_1^2(t)}{\Lambda_1^2(\tau)}\frac{1}{3}(2-\frac{\Lambda_2^2(t)\Lambda_1^2(\tau)}{\Lambda_2^2(\tau)\Lambda_1^2(t)}-\frac{\Lambda_1^4(\tau)\Lambda_2^2(\tau)}{\Lambda_1^4(t)\Lambda_2^2(t)})-\frac{\Lambda_1^2(\tau)\Lambda_2^2(\tau)}{\Lambda_1^2(t)\Lambda_2^2(t)}\frac{1}{3}(2-\frac{\Lambda_1^4(t)\Lambda_2^2(t)}{\Lambda_1^4(\tau)\Lambda_2^2(\tau)}-\frac{\Lambda_1^2(t)\Lambda_2^4(t)}{\Lambda_1^2(\tau)\Lambda_2^4(\tau)})$$
$$+\int_{t_2}^{t}\frac{dD_b(t-s)}{d(t-s)}[\frac{\Lambda_1^2(t)}{\Lambda_1^2(\tau)}\frac{1}{3}(2-\frac{\Lambda_2^2(s)\Lambda_1^2(\tau)}{\Lambda_2^2(\tau)\Lambda_1^2(s)}-\frac{\Lambda_1^4(\tau)\Lambda_2^2(\tau)}{\Lambda_1^4(s)\Lambda_2^2(s)})-\frac{\Lambda_1^2(\tau)\Lambda_2^2(\tau)}{\Lambda_1^2(t)\Lambda_2^2(t)}\frac{1}{3}(2-\frac{\Lambda_1^4(s)\Lambda_2^2(s)}{\Lambda_1^4(\tau)\Lambda_2^2(\tau)}$$
$$-\frac{\Lambda_1^2(s)\Lambda_2^4(s)}{\Lambda_1^2(\tau)\Lambda_2^4(\tau)})]ds\}$$

$$T_{b22}(t)=\mu_b\{\frac{\Lambda_2^2(t)}{\Lambda_2^2(\tau)}\frac{1}{3}(2-\frac{\Lambda_1^2(t)\Lambda_2^2(\tau)}{\Lambda_1^2(\tau)\Lambda_2^2(t)}-\frac{\Lambda_1^2(\tau)\Lambda_2^4(\tau)}{\Lambda_1^2(t)\Lambda_2^4(t)})-\frac{\Lambda_1^2(\tau)\Lambda_2^2(\tau)}{\Lambda_1^2(t)\Lambda_2^2(t)}\frac{1}{3}(2-\frac{\Lambda_1^4(t)\Lambda_2^2(t)}{\Lambda_1^4(\tau)\Lambda_2^2(\tau)}-\frac{\Lambda_1^2(t)\Lambda_2^4(t)}{\Lambda_1^2(\tau)\Lambda_2^4(\tau)})$$
$$+\int_{t_2}^{t}\frac{dD_b(t-s)}{d(t-s)}[\frac{\Lambda_2^2(t)}{\Lambda_2^2(\tau)}\frac{1}{3}(2-\frac{\Lambda_1^2(s)\Lambda_2^2(\tau)}{\Lambda_1^2(\tau)\Lambda_2^2(s)}-\frac{\Lambda_1^2(\tau)\Lambda_2^4(\tau)}{\Lambda_1^2(s)\Lambda_2^4(s)})-\frac{\Lambda_1^2(\tau)\Lambda_2^2(\tau)}{\Lambda_1^2(t)\Lambda_2^2(t)}\frac{1}{3}(2-\frac{\Lambda_1^4(s)\Lambda_2^2(s)}{\Lambda_1^4(\tau)\Lambda_2^2(\tau)}$$
$$-\frac{\Lambda_1^2(s)\Lambda_2^4(s)}{\Lambda_1^2(\tau)\Lambda_2^4(\tau)})]ds\}$$

(2.128)

Although the procedure to obtain the constitutive relation is similar to that for the uniaxial tension problem, obtaining the solution is more challenging as there are two variables involved which are of high order and the equations are coupled.

3. Equal biaxial tension

We first calculate the equal biaxial tension case by setting the values of the loading rate and unloading rate $k_1 = k_2 = 0.1$. Fig.20 portrays that two tensile stresses T_{11}, T_{22} exhibit the same response and this makes sense since we assume that the body is isotropic.

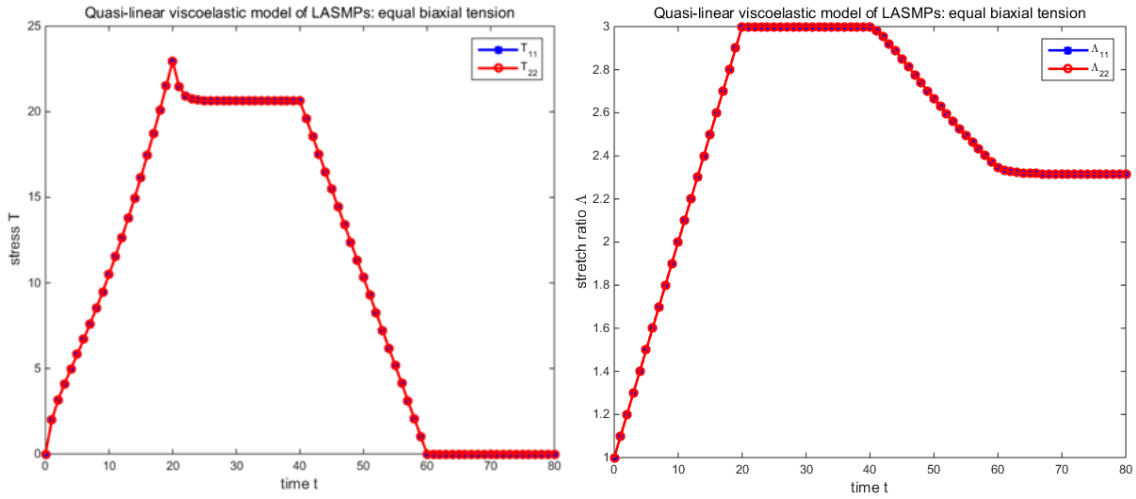

Fig. 20 Equal biaxial tension of LASMPs: Stress versus time (Left) and Stretch versus time (Right)

4. Unequal biaxial tension

For the case of unequal biaxial tension, we find an interesting response characteristic when we have different values for the loading or unloading rate. When we keep the loading/unloading rate in the y direction to be $k_2 = 0.1$, and increase the loading/unloading rate at x direction to $k_1 = 0.15$, we obtain the responses that are depicted in Fig. 21, and this is to be expected. During the loading period, T_{11} increases much faster than T_{22} because of higher loading rate, and the unloading period is the same in both directions. During the unloading period, the stretches in the two directions are reduced as is to be expected. When we increase the loading rate in the x-direction further and set $k_1 = 0.2$, nothing new is observed with regard to the stress response (see Fig.22), however the stretch in the y direction during the loading period appears to show some increase initially but then decreases, a consequence of the incompressibility of the body.

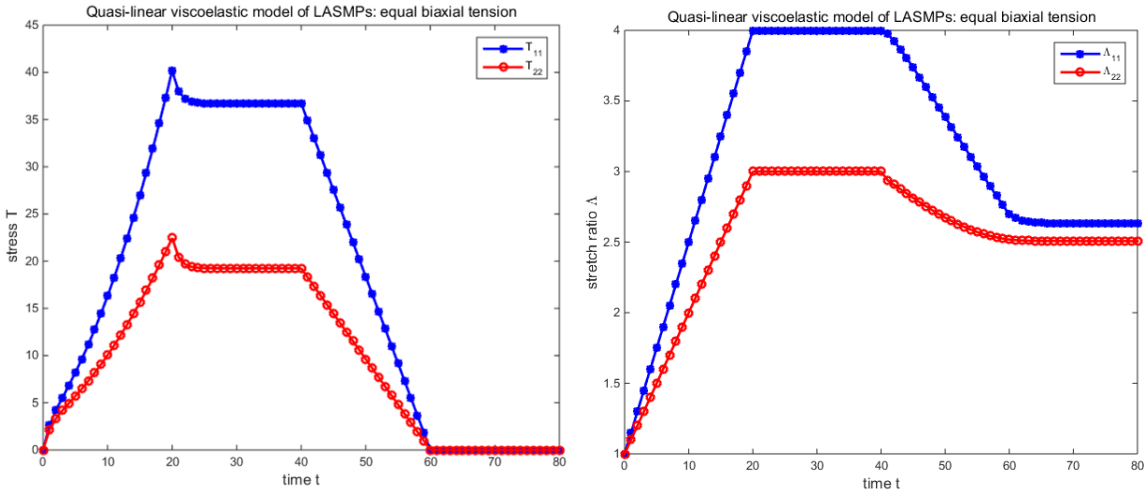

Fig. 21 Unequal biaxial tension of LASMPs: Stress versus time (Left) and Stretch versus time (Right)

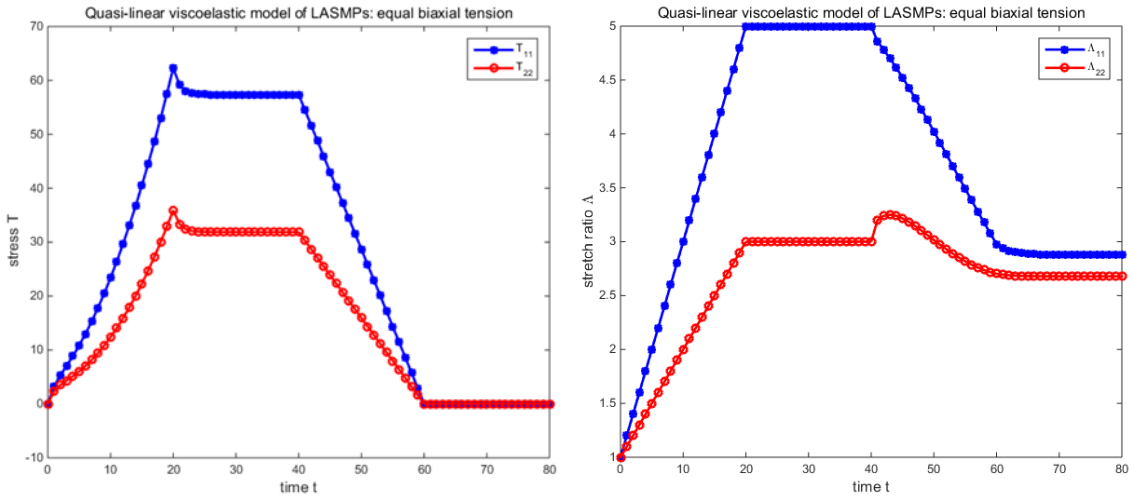

Fig. 22 Unequal biaxial tension of LASMPs: Stress versus time (Left) and Stretch versus time (Right)

2.4.2.2 PNR LASMPs

In this section we show how our model can capture the behavior of PNR LASMPs. As discussed earlier, the mechanism of PNR LASMPs is slightly different from the one of PMC LASMPs. The multi-network configuration approach is adopted to capture the microstructural changes of polymers due to the external stimuli, so the constitutive equations can be the same form of PMC LASMPs as in Eqs. (2.108)-(2.112) but need to take into consideration the changes of the mechanical properties of the different networks due to the cleavage and formation. The shear modulus and relaxation characteristic time can change because of the network rearrangement, and in this study we assume that the shear modulus is a function of the current volume ratio of the new network which can be expressed as: $\tilde{u}_i = \tilde{u}_i(\alpha)$, where $\tilde{u}_i$ is the new modulus and α is the volume ratio of the new network, and keep the relaxation time τ same. The remaining volume fraction of the original network is given by (1-α).

Long et al. [42] have described the formation process of PNR LASMPs from the viewpoint of photochemistry and given the local time evolution of the volume ratios of the original and new networks as shown below, which is adopted in this study.

$$\begin{aligned} &\frac{df_{original}}{dt} = -k_1 C_R f_{original}^{\,p} \\ &f_{original} + \alpha = 1 \\ &f_{original}(t=0) = 1,\ \ \alpha(t=0) = 0 \end{aligned} \tag{2.129}$$

Here $f_{original}$ is the volume ratio of the original network, α is volume ratio of the new network, k_1 and p are material parameters, C_R is the concentration field of the

free radicals. The evolution of the free radicals and photo initiator concentration can be described by:

$$\frac{\partial C_R(\mathbf{y},t)}{\partial t} = m\frac{[\alpha_i\phi_i C_I(\mathbf{y},t)I(\mathbf{y},t)]}{N_A h\nu} + D_R\nabla^2 C_R(\mathbf{y},t) - k_{term}(C_R(\mathbf{y},t))^n \quad (2.130)$$

$$\frac{\partial C_I(\mathbf{y},t)}{\partial t} = -\frac{[\alpha_i\phi_i C_I(\mathbf{y},t)I(\mathbf{y},t)]}{N_A h\nu} + D_I\nabla^2 C_I(\mathbf{y},t) \quad (2.131)$$

where C_I is the concentration field of initiators, α_i is photo initiator molar absorptivity, ϕ_i is quantum efficiency of the photo initiation, I is the light intensity, N_A, h, ν are Avogadro's number, Planck's constant, and light frequency, D_R, D_I are radical and initiator diffusivity, *m* is the parameter to describe the number of free radicals produced by each photo initiator, k_{term}, n are the radical termination constants. For a thin sample studied here, C_R, C_I are assumed to be the same at every point in the material, then we can simplify (80)(81) by ignoring the terms with $\nabla^2 C_R(\mathbf{y},t)$ and $\nabla^2 C_I(\mathbf{y},t)$ which means C_R C_I only depend on time. By using the same values as in [43] and solving the equations (2.129) to (2.131), we obtain the volume ratio of the original network $f_{original}$ which is:

$$\begin{aligned} f_{original} = \exp\{&\frac{k_1 C_{R0}}{k_{term}}(-1+e^{-k_{term}t}) + \frac{mk_1 C_{I0}}{k_{term}-\beta}(-1+e^{-\beta t}) \\ &+ \frac{mk_1\beta C_{I0}}{k_{term}(k_{term}-\beta)}(1-e^{-k_{term}t})\} \end{aligned} \quad (2.132)$$

where $\beta = \frac{\alpha_i\phi_i I}{N_A h\nu}$. Then for our application we choose the following form for the shear modulus:

$$\tilde{u}_i = u_i e^{-c\alpha} = u_i e^{-c(1-f_{original})} \tag{2.133}$$

where c is a positive constant.

Table 1. The parameter values of the model used in the calculation

Parameters	Values	Description
α_i ($Lmol^{-1}cm^{-1}$)	118	photo initiator molar absorptivity
ϕ_i (Dimensionless)	0.5	quantum efficiency of the photo initiation
I ($mWcm^{-2}$)	40	the light intensity
N_A (mol^{-1})	6.02214129e23	Avogadro's number
h (J·s)	6.62607004e-34	Planck's constant
ν (Hz)	8.213e14	light frequency
m (dimensionless)	2	parameter to describe the number of free radicals produced by each photo initiator
k_{term} ($(L\ mol^{-1})n^{-1}\ s^{-1}$)	1.0e4	the radical termination constants
n (dimensionless)	1	
k_1 ($m^3\ mol^{-1}\ s^{-1}$)	300	material parameters
p (dimensionless)	1.0	

Three experimental tests were carried out by Long et al. [33] to investigate the relaxation response of PNR LASMPs. The three experiments differ either in the weight percentage of Irgacure 184 or in the irradiation treatment, but the same

loading history is maintained in all of them, namely extension for 12 minutes at the rate of 0.5% strain per minute and then keeping the strain constant for around one hour. The first specimen is not a standard PNR LASMPs because it had no Irgacure 184 which is a kind of photo initiator although subjected to light irradiation, so it is impossible to form a new network which is out of our study scope here. The second specimen received both light irradiation and consists of 3 wt% Irgacure 184 which is the standard setting of PNR LASMPs. The third specimen contained 3 wt% Irgacure 184 but didn't receive light irradiation, but it can be used for capturing the viscoelastic behavior of the PNR LASMPs before light activation. Hence we will consider the second and third experiments for our parameter calibration. We consider the following steps in calibrating the four parameters μ_a, $\frac{\mu_\infty}{\mu_a}$, τ_a, c. The first step is to calibrate μ_a, $\frac{\mu_\infty}{\mu_a}$, τ_a by using the experimental data in the absence of light irradiation, which is mainly the original network. The initial values are determined by observing the characteristics of the experiment data. During loading, we can see the stress-strain history relation is quasi-linear, so we can get the approximate instantaneous modulus $E_{a0} = \frac{0.57}{0.06} = 9.5MPa$ and then the shear modulus is $\mu_{a0} = \frac{E_{a0}}{2(1+0.5)} = 3.2MPa$. During light irradiation, we estimate the characteristic relaxation time from the inflection point of the curve which is close to $\tau_{a0} = 16$ and set the initial value of $\frac{\mu_\infty}{\mu_a}$=0.5. In the second step, we determine the

parameter c . The software OriginPro 2015 is used to digitize the experimental data and find the optimal parameter values. The calibrated material parameters are $\mu_a = 3.3, \frac{\mu_\infty}{\mu_a} = 0.39$, $\tau_a = 15$, $c = 255$. Figure 23 shows a comparison of the response the model and experimental data. We note that our model can capture the behavior of PNR LASMPs quite well.

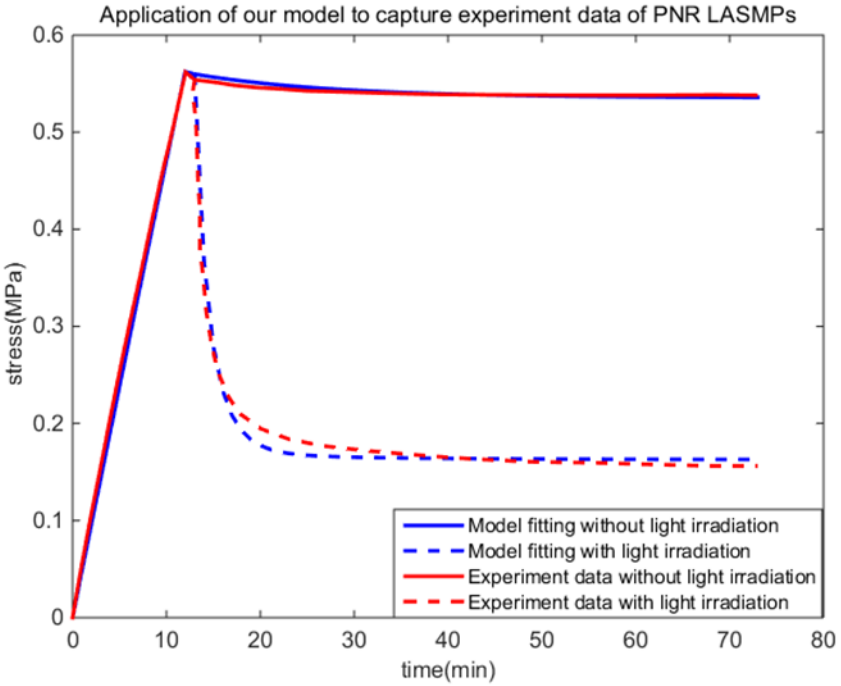

Fig. 23 Application of viscoelastic model on PNR LASMPs compared with experimental data from reference [33]

CHAPTER III

FINITE ELEMENT IMPLEMENTATION OF CONSTITUTIVE MODELS OF LIGHT-ACTIVATED SHAPE MEMORY POLYMERS

Light-activated shape memory polymer (LASMP) is a new generation of active materials that undergoes multiple phase transformations upon light irradiation at different wavelength and intensities. This type of materials has potential applications in adaptive and shape reconfiguration structures in biomedical and aerospace engineering. In many engineering applications the adaptive structures are often in the form of rather complex geometries and subjected to various boundary conditions, in which obtaining exact analytical solutions in predicting the response of such adaptive structures becomes impossible. In such situation, numerical methods are usually considered which give approximate solutions. In this chapter, the constitutive models developed for elastic and viscoelastic LASMPs in Chapter II are implemented within ABAQUS finite element (FE) through the use of user-material subroutines (UMAT). Both isotropic and deformation induced anisotropic cases are presented. For the anisotropic hyperelastic model, a modified model is developed to define the Cauchy stress and tangent stiffness at the material integration points within finite elements. The common method has been based on the volumetric-deviatoric separation form of the strain energy, which for some cases do not give reasonable physical results. The numerical results obtained from the UMAT ABAQUS FE are first compared with the results obtained from the analytical or semi-

analytical solutions and standard ABAQUS FE solutions for several simple boundary value problems. The purpose is to verify the UMAT implementation.

3.1 Introduction

LASMPs have many potential applications. For example, they can be used as a scaffold for minimally invasive surgery or stents to remove the thrombus which obstructs the blood circulation; they can be designed as a damper in an automobile by changing the frequency of the systems; they are potentially being used in morphing structures in aircraft to reduce the effect of drag force due to fluid flow; they can also be incorporated as self-healing materials in structural components; and so on. In the previous chapter, also published in these references [51, 55] several constitutive models were developed to capture the mechanical behavior of light-activated shape memory polymers (LASMPs), and the solutions of some simple boundary value problems are also shown to investigate how the material responses. The general governing equations for adaptive structures using active materials are usually in the form of partial differential equations whose analytical solutions are often difficult or impossible to obtain. Thus, numerical methods, such as finite difference, finite element, and finite volume, are considered in such situation. Finite element method has shown great successes in solving multi-field problems. In this work, ABAQUS commercial FE code is used. Since there is not any constitutive model for LASMPs in ABAQUS standard library, a user material subroutine (UMAT) which is written in Fortran language is considered.

Table 2. Variables in UMAT

STATEV	An array containing the solution-dependent state variables
TIME(1)	Value of step time at the beginning of the current increment or frequency
TIME(2)	Value of total time at the beginning of the current increment
DTIME	Time increment.
NDI	Number of direct stress components at this point
NSHR	Number of engineering shear stress components at this point
NTENS	Size of the stress or strain component array (NDI + NSHR)
NSTATEV	Number of solution-dependent state variables that are associated with this material type
NPROPS	User-defined number of material constants associated with this user material
DFGRD0	Array containing the deformation gradient at the beginning of the increment
DFGRD1	Array containing the deformation gradient at the end of the increment
PROPS	User-specified array of material constants associated with this user material
KSTEP	Step number
KINC	Increment number

During the analysis, the user subroutine UMAT is called at each material integration point within elements at every time increment. Table 2 lists some variables that are passed to UMAT from the global structural elements [79].

The following variables should be defined and updated in UMAT:

(1) STRESS. Here the measure of stress used is the Cauchy stress or true stress, and all six components should be defined and updated at the end of the increment.

(2) STATEV: Solution-dependent state variables. These are variables that will be used for the next time increment within the incremental formulation. For example, the volume ratio of the second network of LASMPs will evolve based on the stimuli prescribed to them and the deformation gradient at the time of the formation of the second network is needed to calculate the current deformation gradient of the second network.

(3) DDSDDE: Material Jacobian tensor. It represents the stress increment for each strain increment which is also referred to as the material stiffness tensor, tangent modulus tensor or elasticity tensor in the case of elastic materials.

The detailed numerical implementations are discussed below.

3.2 Preliminaries

Let $\mathbf{F}$ describe the kinematics of deformation locally in terms of deformation gradient tensor relative to some reference configuration, $\mathbf{B}$ and $\mathbf{C}$ be the left and right Cauchy-Green tensors, respectively, defined by $\mathbf{B} = \mathbf{F}\mathbf{F}^{\mathbf{T}}$, $\mathbf{C} = \mathbf{F}^{\mathbf{T}}\mathbf{F}$.

In the constitutive models of LASMPs [51, 55], hyperelastic models are employed to describe the mechanical behavior of LASMPs. A hyperelastic material is defined as an elastic material which possesses a stored elastic energy function W. From the principles of conservation of energy and conservation of angular momentum, the time derivative of the stored energy potential can be expressed as:

$$\dot{W} = \mathbf{S} \cdot \dot{\mathbf{E}} = \frac{1}{2}\mathbf{S} \cdot \dot{\mathbf{C}} \tag{3.1}$$

where $\mathbf{S}$ is the second Piola-Kirchhoff stress tensor, $\mathbf{E}$ is the Green strain tensor related with $\mathbf{C}$ by $\mathbf{E} = \frac{1}{2}(\mathbf{C} - \mathbf{1})$. Assuming the stored strain energy W is a function of $\mathbf{C}$ and applying the chain rule, we have the following relation:

$$\dot{W} = \frac{\partial W}{\partial \mathbf{C}} \cdot \dot{\mathbf{C}} = \frac{1}{2}\mathbf{S} \cdot \dot{\mathbf{C}} \tag{3.2}$$

The stress is then obtained as:

$$\mathbf{S} = 2\frac{\partial W}{\partial \mathbf{C}} \text{ for arbitrary } \dot{\mathbf{C}} \tag{3.3}$$

By taking further material time derivative of the above equation, the stress rate is:

$$\dot{\mathbf{S}} = 2\frac{\partial^2 W}{\partial \mathbf{C}\partial \mathbf{C}} \cdot \dot{\mathbf{C}} = \mathbb{C} \cdot \frac{1}{2}\dot{\mathbf{C}} \tag{3.4}$$

where $\mathbb{C}$ is the material stiffness tensor expressed by Lagrangian variables:

$$\mathbb{C}=2\frac{\partial \mathbf{S}}{\partial \mathbf{C}}=4\frac{\partial^2 W}{\partial \mathbf{C}\partial \mathbf{C}} \tag{3.5}$$

Here it should be noted that the above quantities of stress and stiffness tensor are not the one we need for UMAT in which the quantities should be expressed by the Eulerian description at the current configuration. Therefore, by substituting the relations $\mathbf{S}=\mathbf{F}^{-1}\boldsymbol{\tau}\mathbf{F}^{-T}$ and $\mathbf{C}=\mathbf{F}^{\mathbf{T}}\mathbf{F}$ into the rate form, it is found that:

$$\dot{\mathbf{F}}^{\mathbf{-1}}\boldsymbol{\tau}\mathbf{F}^{\mathbf{-T}}+\mathbf{F}^{\mathbf{-1}}\dot{\boldsymbol{\tau}}\mathbf{F}^{\mathbf{-T}}+\mathbf{F}^{\mathbf{-1}}\boldsymbol{\tau}\dot{\mathbf{F}}^{\mathbf{-T}}=\mathbb{C}\cdot\frac{1}{2}(\dot{\mathbf{F}}^{\mathbf{T}}\mathbf{F}+\mathbf{F}^{\mathbf{T}}\dot{\mathbf{F}}) \tag{3.6}$$

where $\boldsymbol{\tau}$ is Kirchhoff stress. Further it can be transformed,

$$\dot{\boldsymbol{\tau}}+\mathbf{F}\dot{\mathbf{F}}^{\mathbf{-1}}\boldsymbol{\tau}+\boldsymbol{\tau}\dot{\mathbf{F}}^{\mathbf{-T}}\mathbf{F}^{\mathbf{T}}=\mathbf{F}[\mathbb{C}\cdot\frac{1}{2}(\dot{\mathbf{F}}^{\mathbf{T}}\mathbf{F}+\mathbf{F}^{\mathbf{T}}\dot{\mathbf{F}})]\mathbf{F}^{\mathbf{T}} \tag{3.7}$$

Thus the rate form in the current configuration by Oldroyd or Lie rate of Kirchhoff stress is deduced as

$$\mathcal{L}_v\boldsymbol{\tau}=\dot{\boldsymbol{\tau}}-\mathbf{L}\boldsymbol{\tau}+\boldsymbol{\tau}\mathbf{L}^{\mathbf{T}}=\mathbf{F}[\mathbb{C}\cdot(\mathbf{F}^{\mathbf{T}}\mathbf{D}\mathbf{F})]\mathbf{F}^{\mathbf{T}}=\mathbb{C}^{\tau c}\cdot\mathbf{D} \tag{3.8}$$

where $\mathbf{L}=\dot{\mathbf{F}}\mathbf{F}^{\mathbf{-1}}=-\mathbf{F}\dot{\mathbf{F}}^{\mathbf{-1}}$, $\mathbf{D}=\frac{1}{2}(\mathbf{L}^{\mathbf{T}}+\mathbf{L})$, and $\mathbb{C}^{\tau c}$ is the transformed elasticity tensor related to $\mathbb{C}$ by $\mathbb{C}^{\tau c}_{ijkl}=\mathbb{C}_{pqrs}F_{ip}F_{jq}F_{kr}F_{ls}$. It is noted that $\mathbb{C}^{\tau c}$ is used in the older version of ABAQUS, while the form of the Zaremba-Jaumann objective rate of the Kirchhoff stress is

$$\boldsymbol{\tau}^{\nabla}=\dot{\boldsymbol{\tau}}-\mathbf{W}\boldsymbol{\tau}-\boldsymbol{\tau}\mathbf{W}^{T}=\mathbb{C}^{\tau Z-J}\cdot\mathbf{D} \tag{3.9}$$

where $\mathbf{W}=\frac{1}{2}(\mathbf{L}-\mathbf{L}^{\mathbf{T}})$, and $\mathbb{C}^{\tau Z-J}$ is related to $\mathbb{C}^{\tau c}$ by

$$\mathbb{C}^{\tau Z-J}=\mathbb{C}^{\tau c}+\frac{1}{2}(\delta_{\mathrm{ik}}\tau_{jl}+\tau_{ik}\delta_{\mathrm{jl}}+\delta_{\mathrm{il}}\tau_{jk}+\tau_{il}\delta_{\mathrm{jk}})\ \mathbf{e}_i\otimes\mathbf{e}_j\otimes\mathbf{e}_k\otimes\mathbf{e}_l \tag{3.10}$$

The form of the material Jacobian tensor used in UMAT code is

$$\mathbb{C}^{MZ-J}=\frac{1}{J}\mathbb{C}^{\tau Z-J} \tag{3.11}$$

and finally, the Cauchy stress is:

$$\boldsymbol{\sigma}=J^{-1}\boldsymbol{\tau}\ \text{ or }\ \boldsymbol{\sigma}=J^{-1}\mathbf{F}\mathbf{S}\mathbf{F}^{\mathbf{T}} \tag{3.12}$$

where $J=\det(\mathbf{F})$ which can reflect the volume change of the body.

The strain energy W of the hyperelastic materials may be expressed as a function of the corresponding principal strain invariants of $\mathbf{C}$ which is a proper form to satisfy the frame indifference and the description requirements of material symmetry. For isotropic hyperelastic materials, W may be expressed as follow:

$$W(\mathbf{C})=W(I_1,I_2,I_3) \tag{3.13}$$

The three invariants of the right Cauchy-Green tensor $\mathbf{C}$ are defined by

$$I_1=tr\mathbf{C},I_2=\frac{1}{2}((tr\mathbf{C})^2-tr\mathbf{C}^2),I_3=J^2=\det\mathbf{C} \tag{3.14}$$

and for the anisotropic hyperelastic materials, there are two more invariants added in order to describe the anisotropic characteristics which are mentioned in the model developed in Chapter II, which are:

$$J_1=\boldsymbol{n}_0\cdot\mathbf{C}\,\boldsymbol{n}_0\ ,K_1=\boldsymbol{m}_0\cdot\mathbf{C}\,\boldsymbol{m}_0 \tag{3.15}$$

where $\boldsymbol{n}_0,\boldsymbol{m}_0$ are the anisotropic direction in the reference configuration. Then, the strain energy of the anisotropic hyperelastic material is:

$$W(\mathbf{C}) = W(I_1, I_2, I_3, J_1, K_1) \tag{3.16}$$

3.3 Implementation of the LASMP models in UMAT

Since the constitutive models for LASMPs are developed based on the theory of multiple natural configurations and the assumption of the mixture theory wherein the two networks have the same displacement, the total stress and elasticity tensor of the LASMP body are treated as the summation of the partial parts from the two networks. Three constitutive models for LASMPs have been developed in Chapter II which are isotropic elastic, anisotropic elastic, and quasi-linear viscoelastic models. These models are implemented in ABAQUS FE analysis.

3.3.1 Isotropic elastic model of LASMPs

This model assumes each network in LASMPs shows a rubber-like property, so a hyperelasticity model is employed to describe its behavior and the classical neo-Hookean model is used for demonstrations. The total stress for is:

$$\boldsymbol{\sigma} = \boldsymbol{\sigma}_1 + \alpha\boldsymbol{\sigma}_2 \tag{3.17}$$

and the total elasticity tensor is:

$$\mathbb{C}^{MZ-J} = \mathbb{C}_1^{MZ-J} + \alpha\mathbb{C}_2^{MZ-J} \tag{3.18}$$

where the subscripts 1, 2 represent the 1st and 2nd network respectively, α is the volume ratio of the second network. However, care must be taken on the deformation gradient of

the second network in $\boldsymbol{\sigma}_2$ and $\mathbb{C}_2^{MZ-J}$ because the second network has a different natural configuration from the original network, and the relationship below needs to be used:

$$\mathbf{F}_2 = \mathbf{F}_1\mathbf{F}_0^{-1} \tag{3.19}$$

where $\mathbf{F}_1$ is the total deformation gradient of the body or the deformation gradient of the first/original network, $\mathbf{F}_0$ is the deformation gradient of the first network at time τ when the second network starts to form.

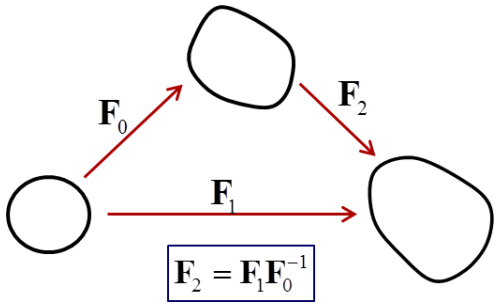

Fig. 24 Relationship of deformation gradient among different configurations

3.3.1.1 Isotropic neo-Hookean model

In order to implement the hyperelastic model in UMAT, it is assumed that the strain energy function for a slight compressible material is expressed by the summation of volumetric and isochoric components, which is

$$W(\mathbf{C}) = U(J) + \bar{W}(\bar{\mathbf{C}}) \tag{3.20}$$

where U , $\bar{W}$ are the volumetric and isochoric stored-energy potentials, respectively. This decoupled form can facilitate the derivation of the stress and elasticity tensor in a reduced form, and also the derived formulations in FE analysis can eliminate the element

locking issues due to the incompressibility of the materials. Here the incompressibility constraint can be simply achieved for this uncoupled form of the strain energy, by assuming a properly high value of the bulk modulus. For an isotropic neo-Hookean solid, the strain energy is in the form of:

$$W = \frac{\mu}{2}(\bar{I}_1 - 3) + \frac{1}{D_1}(J-1)^2 \tag{3.21}$$

the volumetric component is

$$U = \frac{1}{D_1}(J-1)^2 \tag{3.22}$$

and the isochoric component is

$$\bar{W} = \frac{\mu}{2}(\bar{I}_1 - 3) \tag{3.23}$$

From this strain energy, the Cauchy stress and Jacobian matrix are:

$$\boldsymbol{\sigma} = J^{-1}\boldsymbol{\tau} = \frac{2}{D_1}(J-1)\mathbf{I} + \frac{\mu}{J}(\bar{\mathbf{B}} - \frac{1}{3}\bar{I}_1\mathbf{I}) \tag{3.24}$$

$$\mathbb{C}_{ijkl}^{MZ-J} = \frac{\mu}{J}[\frac{1}{2}(\delta_{ik}\bar{B}_{jl} + \bar{B}_{ik}\delta_{jl} + \delta_{il}\bar{B}_{jk} + \bar{B}_{il}\delta_{jk}) + \frac{2}{3}(\frac{1}{3}\bar{I}_1\delta_{ij}\delta_{kl} - \bar{B}_{ij}\delta_{kl} - \delta_{ij}\bar{B}_{kl})] + \frac{2}{D_1}(2J-1)\delta_{ij}\delta_{kl} \tag{3.25}$$

Detailed derivations can be found in the Appendix B.

Two simple boundary value problems, uniaxial and biaxial tension, are first considered to evaluate the UMAT code for the isotropic neo-Hookean model by comparing with the results obtained from Abaqus built-in neo-Hookean model.

1. Uniaxial tension

As shown in Fig.25, a cubic block with dimension of 20mmx20mmx20mm is stretched by a force of 4KN on the right side along x direction and the roller constraints are imposed on the left, bottom and front faces of the body respectively. This case is a simulation of the uniaxial tension experiment and just one eighth of the experimental sample is taken out for analysis due to symmetry.

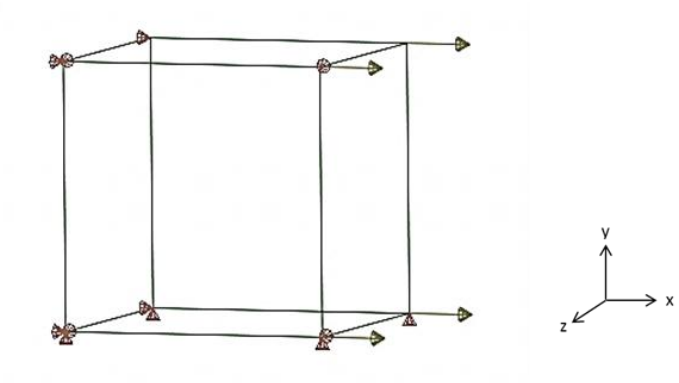

Fig. 25 Uniaxial tension of single element

The entire body is meshed as one single element and modeled as a homogeneous isotropic neo-Hookean material. By comparing the responses from the UMAT and ABAQUS built-in neo-Hookean model, Fig.26 to Fig 30, the developed UMAT subroutine is first validated. Fig. 30 showed the relations between stress and stretch from UMAT and ABAQUS built-in model. The values of shear modulus $\mu = 20MPa$ and constant $D_1 = 3e-8$ are used in the calculation.

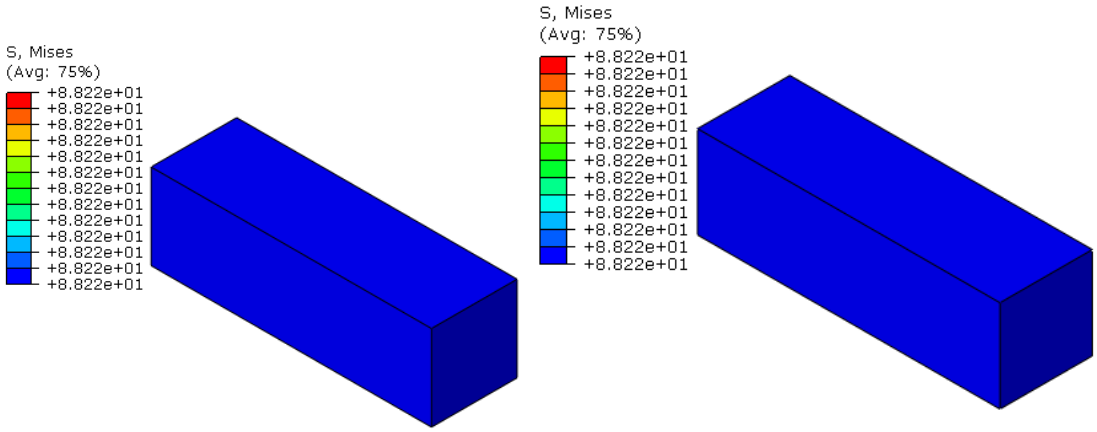

Fig. 26 Stress under uniaxial tension: UMAT (Left) and Abaqus Built-in Model (Right)

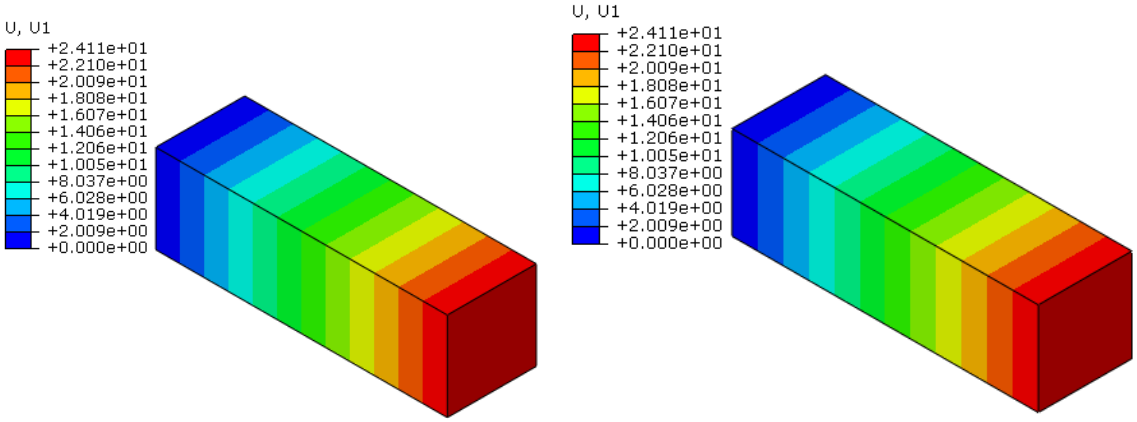

Fig. 27 x- direction displacement under uniaxial tension: UMAT (Left) and Abaqus Built-in Model (Right)

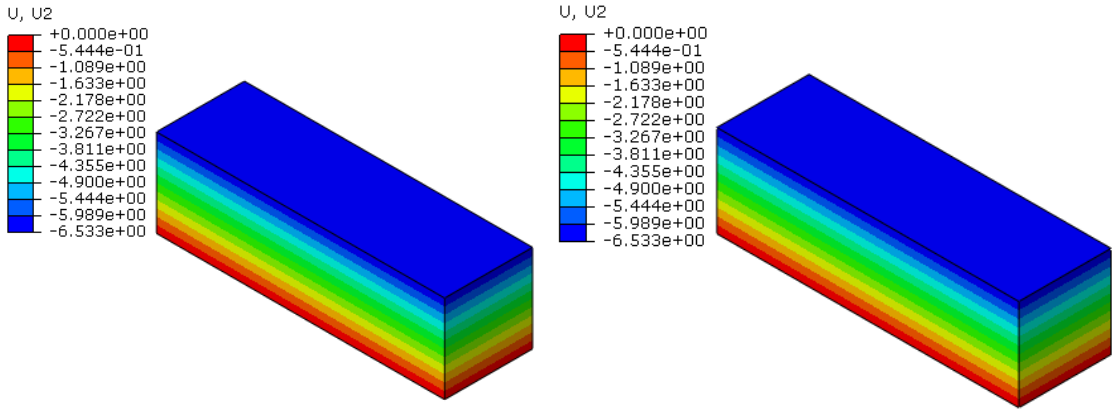

Fig. 28 y- direction displacement under uniaxial tension: UMAT (Left) and Abaqus Built-in Model (Right)

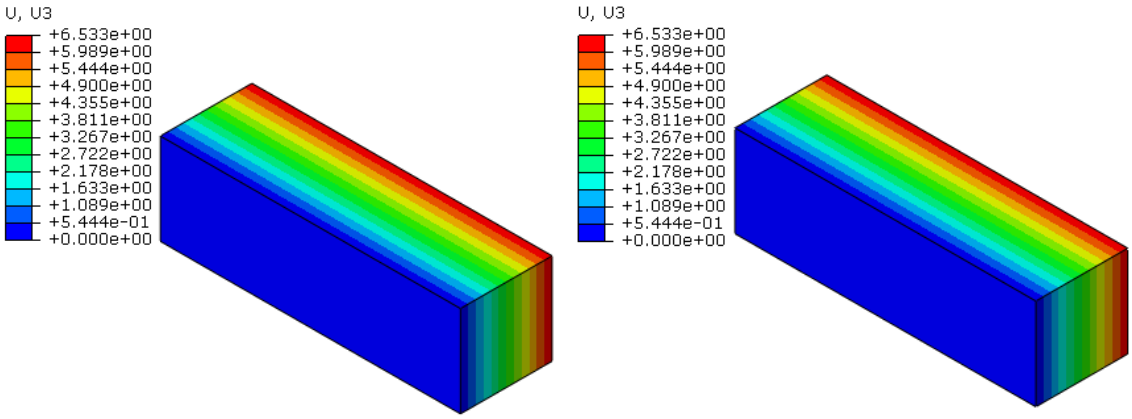

Fig. 29 z- direction displacement under uniaxial tension: UMAT (Left) and Abaqus Built-in Model (Right)

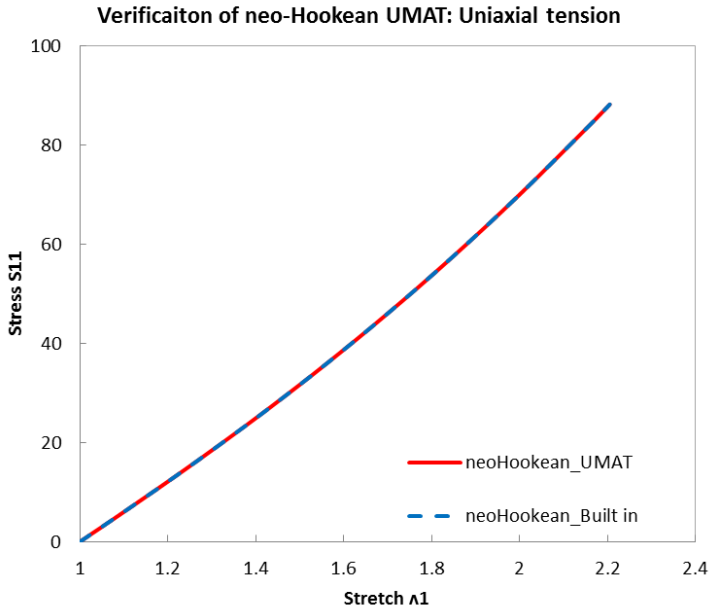

Fig. 30 Comparison of stress vs stretch between UMAT and Abaqus Built-in Model under uniaxial tension

2. Biaxial tension

Now based on the above uniaxial tension problem, we consider the case of biaxial tension by exerting a traction force of 2KN along x, y direction and keeping the

boundary constraints the same. Similarly, two groups of the results obtained from the UMAT and ABAQUS built-in model are in good agreements.

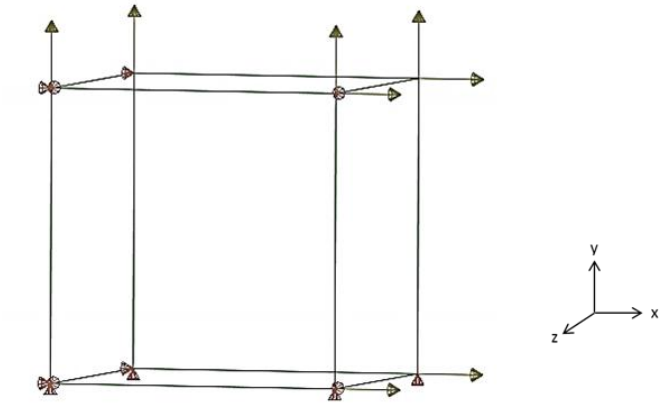

Fig. 31 Biaxial tension of single element

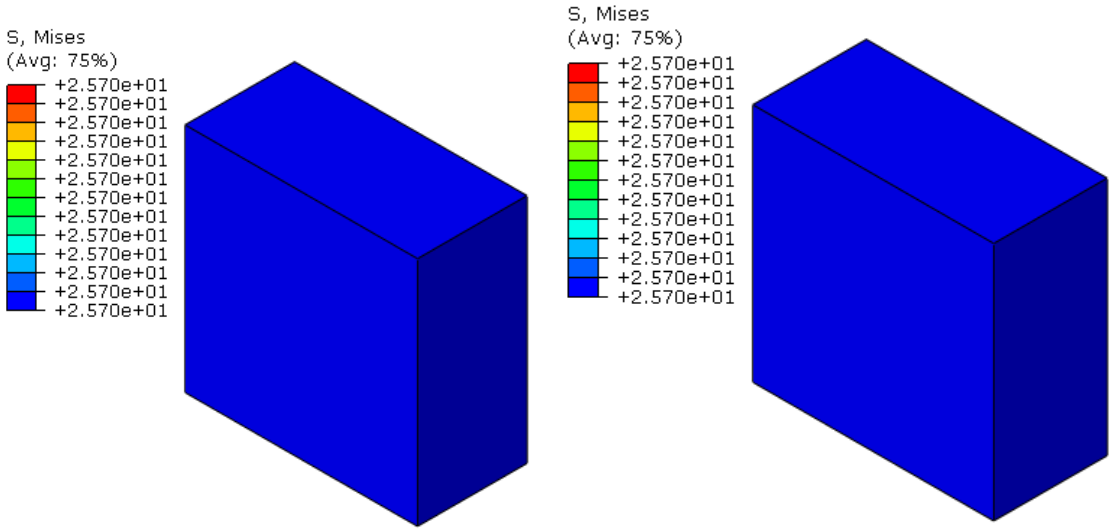

Fig. 32 Stress under biaxial tension: UMAT (Left) and Abaqus Built-in Model (Right)

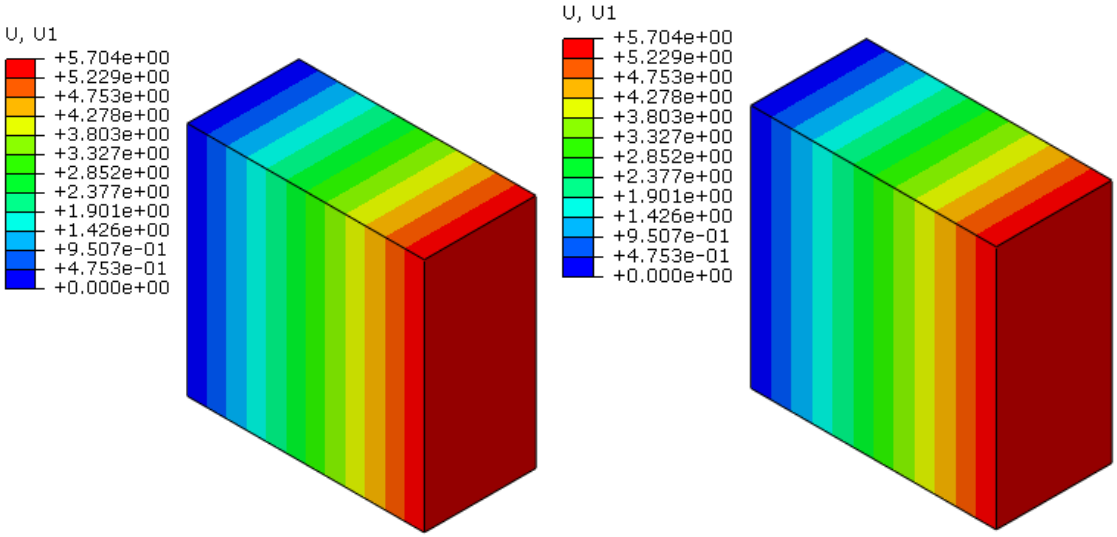

Fig. 33 x- direction displacement under biaxial tension: UMAT (Left) and Abaqus Built-in Model (Right)

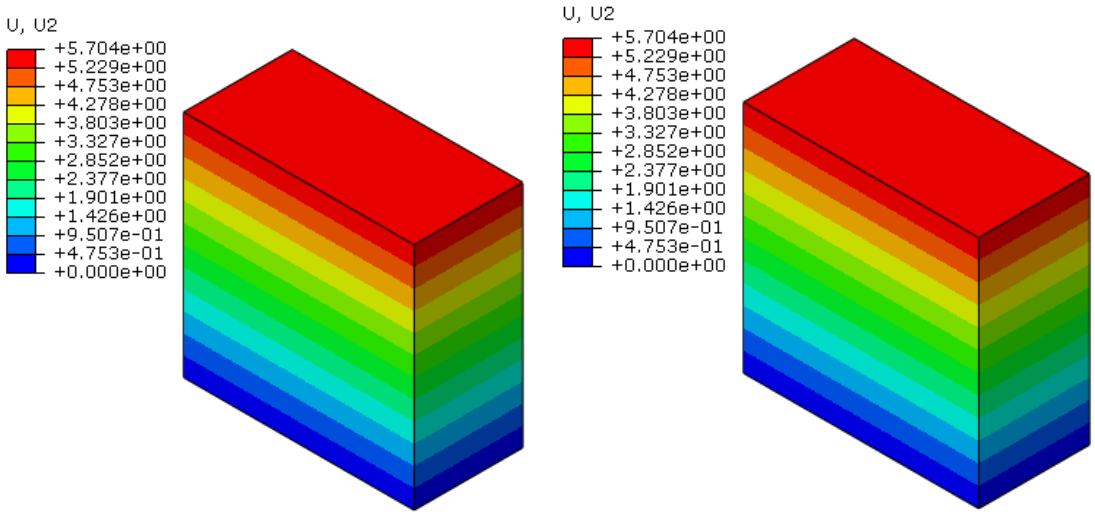

Fig. 34 y- direction displacement under biaxial tension: UMAT (Left) and Abaqus Built-in Model (Right)

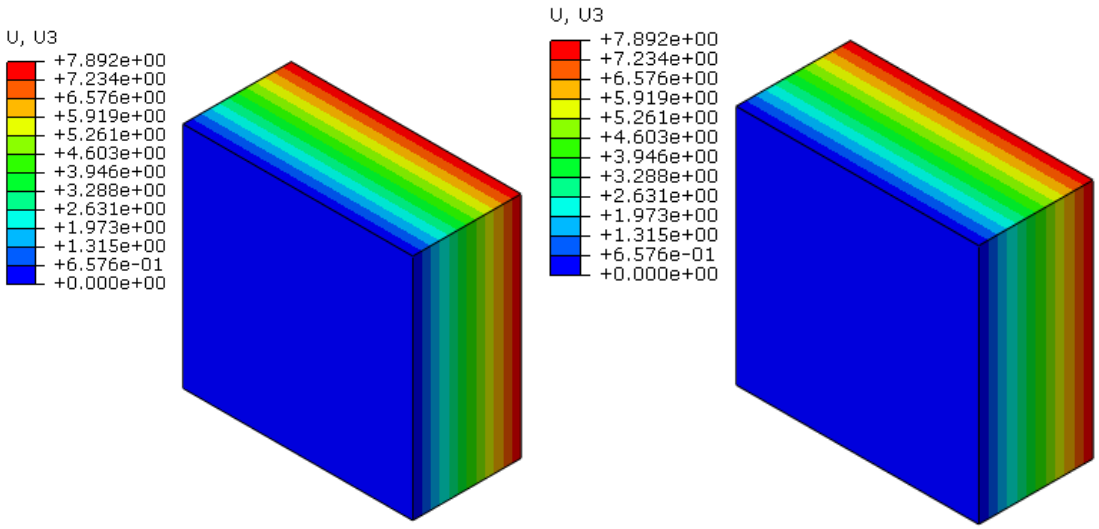

Fig. 35 z- direction displacement under biaxial tension: UMAT (Left) and Abaqus Built-in Model (Right)

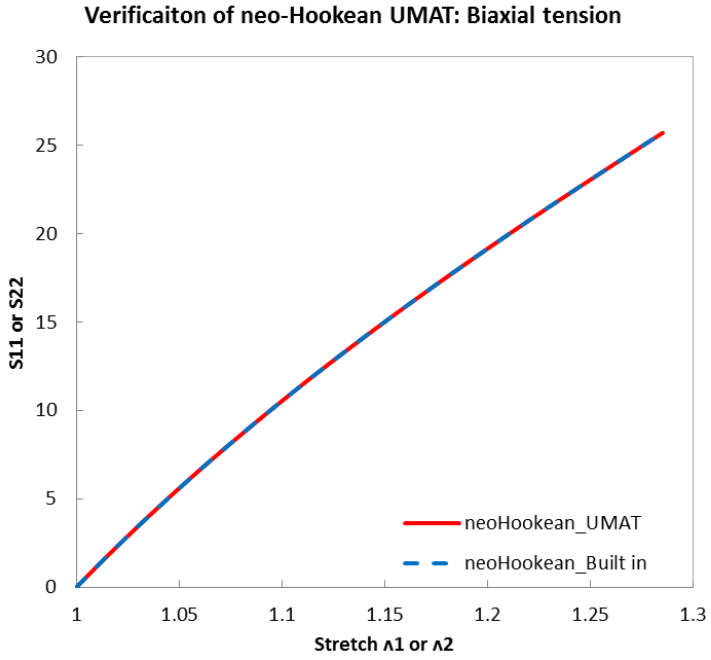

Fig. 36 Comparison of stress vs stretch between UMAT and Abaqus Built-in Model under biaxial tension

The UMAT code up to this point has been validated for rather simple cases and will be used in the elastic constitutive model of LASMPs.

3.3.1.2 Isotropic elastic model of LASMPs

This model assumes that both networks are isotropic elastic. The constitutive equations have been described above. The Cauchy stress and Jacobian tensor for each network are calculated separately and then added together. However, each network has its own reference configuration, while the deformation gradient provided by ABAQUS interface via UMAT is the total deformation gradient of the body, which is also the deformation gradient of the original network. To obtain the deformation gradient associated with the second network, we need to store the values of the deformation gradient at the moment of the new network starting to form as solution dependent variables (SDV) and its determinant. In addition, we need to set as SDV is the volume ratio of the second network. Two cases are used here to test the UMAT code for isotropic elastic model of LASMPs.

1. Uniaxial tension

Using the same single element model, the following steps are considered in order to simulate the full cycle of the mechanisms of LASMPs:

(1) Step1: stretch the body to the stretch ratio of 3.

(2) Step 2: keep the stretch constant for the formation of the new network.

(3) Step 3: release the load to the stress of zero.

(4) Step 4: keep the stress free state but decrease the volume ratio of the second network to be zero.

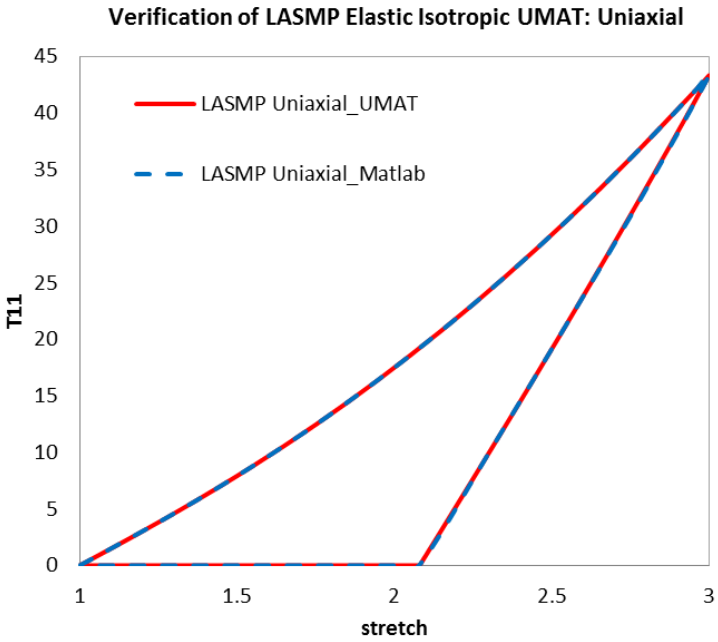

Fig. 37 Comparison of stress vs stretch between UMAT and Matlab under uniaxial tension for LASMP isotropic elastic model

From Fig.37, we can see that the response from the isotropic elastic UMAT code for LASMPs matches very well with the one obtained from analytical solution, obtained in Matlab code.

2. Radial inflation

For comparison with the results calculated from the analytical or semi-analytical solutions (solved in Matlab), the radial inflation is carried out by imposing a radial displacement of ratio of 2 as shown in Fig.38. From the results after loading and

unloading in Fig. 39, all the material points at the same radius have the same displacements due to isotropy, and from the relation between pressure and inner radius in Fig. 40 it is seen that UMAT code gives correct solutions.

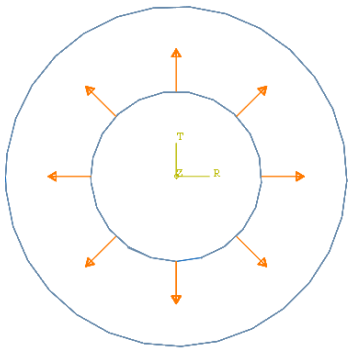

Fig. 38 FEM model of cylinder annulus under inner pressure

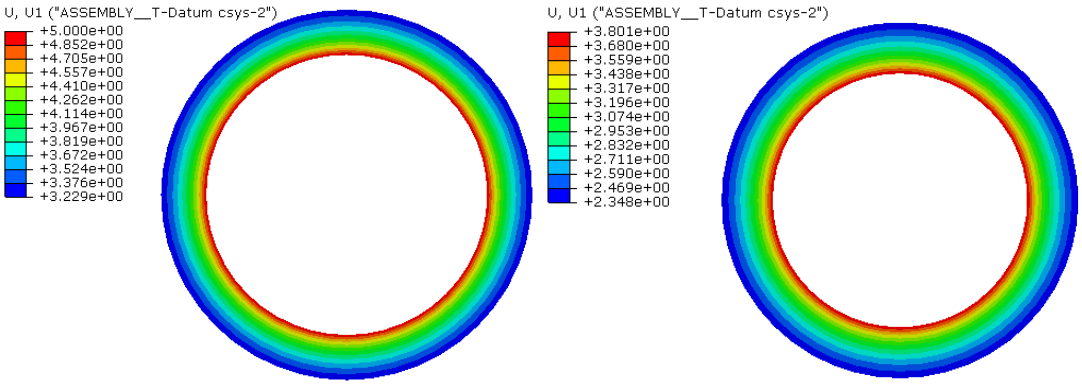

Fig. 39 Radial displacement of LASMPs under cylindrical inflation: Before unloading (Left) and After unloading (Right)

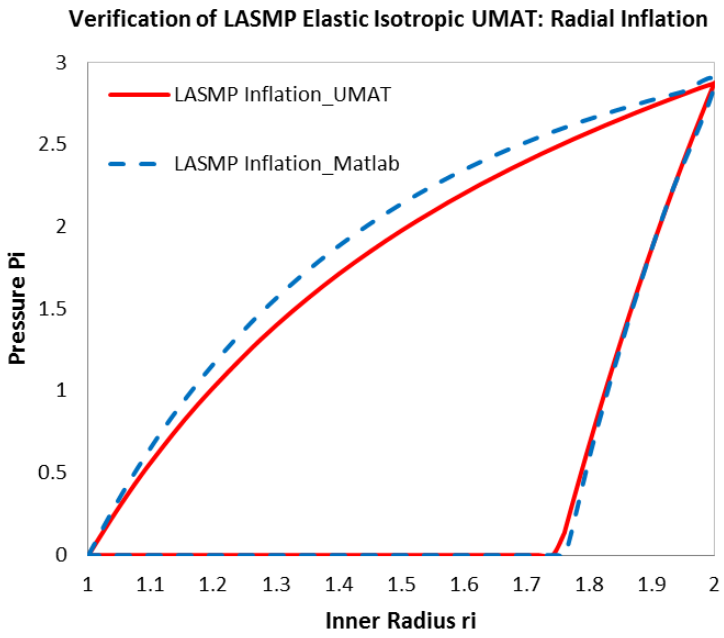

Fig. 40 Comparison of stress vs stretch between UMAT and Matlab under cylindrical inflation for LASMP isotropic elastic model

3.3.2 Anisotropic elastic model of LASMPs

Since the second network is formed based on a deformed shape, it may have some preferred orientations which can lead to anisotropic property. So hereby based on the isotropic elastic model, we take the possible anisotropy for consideration. The total stress and elasticity are in the same form as above except the part from the second network which is based on the anisotropic neo-Hookean model and the part from the first network still preserve the isotropic neo-Hookean form.

3.3.2.1 Anisotropic neo-Hookean model

The incompressible anisotropic hyperelastic constitutive model proposed by Holzapfel et al. is originally based upon the previous transversely isotropic constitutive

models [70], and widely used to model collagen fiber reinforced biological materials by taking into account the anisotropic contributions from the reinforced fiber families. Similar as above, for FE implementation the Lagrange multiplier penalty term is modified to a dilatation term which can approximate the incompressibility by a large value of bulk modulus. This compressible anisotropic hyperelastic model (HGO-C model) is widely used to describe the anisotropic soft tissues of incompressibility or some level of compressibility. However, several recent papers presented that the original form of the HGO-C model was shown to inaccurately capture the physical characteristics in some boundary conditions. For example, Vergori et al. [71] showed that a sphere described by HGO-C model was deformed into a larger sphere under a hydrostatic pressure, but this result is obviously not correct since that obtained response is actually an isotropic response without showing any anisotropic behavior and the realistic deformation shape of the body with anisotropic property should be an ellipsoid. Gilchrist et al. [72, 75] also showed that a transversely isotropic cube under hydrostatic tension deformed into another cube instead of a rectangular cuboid.

In order to address this issue and improve the model accuracy, several researchers have addressed the mathematical issue involved and proposed different methods. For instance, Nolan et al. [73] gave a modified model wherein the anisotropic component used the full anisotropic invariants instead of the previous isochoric anisotropic invariants. Gilchris et al. [72] proposed a different form for the strain energy function in which the isochoric part remained unchanged while the volumetric part not only depended on J or I_3 but also depended on I_4 (equivalent to the above J_1 and K_1).

Here, both the original method and the modified method are considered and examined in order to capture the anisotropic behavior.

a. The original method (HGO-C)

The original HGO-C method splits the local deformation into volumetric and isochoric parts, and accordingly the strain energy function is expressed in the uncoupled form as follows:

$$W = U(J) + \bar{W}(\bar{\mathbf{C}}, \mathbf{n}_0, \mathbf{m}_0) \tag{3.26}$$

If based on the neo-Hookean model, the specific form of an orthotropic neo-Hookean solid is:

$$\begin{aligned} W &= W(J, \bar{I}_1, \bar{J}_1, \bar{K}_1) = \frac{\mu}{2}(\bar{I}_1 - 3) + \frac{1}{D}(J-1)^2 + C_{201}(\bar{J}_1\text{-}1)^2 + C_{202}(\bar{K}_1\text{-}1)^2 \\ &= \frac{1}{D}(I_3^{1/2} - 1)^2 + \frac{\mu}{2}(\bar{I}_1 - 3) + C_{201}(\bar{J}_1\text{-}1)^2 + C_{202}(\bar{K}_1\text{-}1)^2 \\ &= W_{vol}(I_3) + W_{iso}(\bar{I}_1, \bar{J}_1, \bar{K}_1) \end{aligned} \tag{3.27}$$

In the above form, the first term is the volumetric part of the strain energy $W_{vol} = \frac{1}{D}(I_3^{1/2} - 1)^2$, the second term is the isochoric part of the strain energy $W_{iso} = \frac{\mu}{2}(\bar{I}_1 - 3) + C_{201}(\bar{J}_1\text{-}1)^2 + C_{202}(\bar{K}_1\text{-}1)^2$ which due to both isotropic and anisotropic deformation, and $\bar{I}_1 = J^{-2/3} I_1$, $\bar{J}_1 = J^{-2/3} J_1$, $\bar{K}_1 = J^{-2/3} K_1$.

For convenience, we will drop off the subscript and use w and w to represent the two parts of energy, and I_4, I_5 to represent J_1, K_1. Therefore,

$$W = W(I_3) + w(\bar{I}_1, \bar{I}_4, \bar{I}_5) \tag{3.28}$$

Before taking the neo-Hookean model into the derivation process of the Cauchy stress and elasticity tensor, we present a general form of the strain energy function as in Eq. (3.28). By the similar procedure (see Appendix C or literature [77,78]), we can obtain the forms of the Cauchy stress and elasticity tensor which are:

$$\begin{aligned}\boldsymbol{\sigma} = {} & \frac{\mu}{J}\bar{\mathbf{B}} + [\frac{2}{D}(J-1) - \frac{2}{3J}(\frac{\mu}{2}\bar{I}_1 + 2C_{201}(\bar{I}_4 - 1)\,\bar{I}_4 + 2C_{202}(\bar{I}_5 - 1)\bar{I}_5)]\mathbf{1} \\ & + \frac{4C_{201}}{J}(\bar{I}_4 - 1)\,\bar{I}_4\mathbf{n}\otimes\mathbf{n} + \frac{4C_{202}}{J}(\bar{I}_5 - 1)\bar{I}_5\mathbf{m}\otimes\mathbf{m}\end{aligned} \tag{3.29}$$

$$\begin{aligned}\frac{1}{4}\mathbb{C}^{\tau c} = {} & I_3^{-2/3}w_{11}\mathbf{B}\otimes\mathbf{B} \\ & + (-\frac{1}{3}I_3^{-1/3}\bar{I}_1 w_{11} - \frac{1}{3}I_3^{-1/3}w_1 - \frac{1}{3}I_3^{-1/3}\bar{I}_4 w_{14} - \frac{1}{3}I_3^{-1/3}\bar{I}_5 w_{15})(\mathbf{B}\otimes\mathbf{1} + \mathbf{1}\otimes\mathbf{B}) \\ & + [I_3^2 W_{33} + I_3 W_3 + \frac{1}{9}(\bar{I}_1 w_1 + \bar{I}_4 w_4 + \bar{I}_5 w_5 + \bar{I}_1^2 w_{11} + \bar{I}_4^2 w_{44} + \bar{I}_5^2 w_{55} + 2\bar{I}_1\bar{I}_4 w_{14} \\ & + 2\bar{I}_1\bar{I}_5 w_{15} + 2\bar{I}_4\bar{I}_5 w_{45})]\mathbf{1}\otimes\mathbf{1} \\ & + I_3^{-2/3}w_{14}(\mathbf{B}\otimes I_4\mathbf{n}\otimes\mathbf{n} + I_4\mathbf{n}\otimes\mathbf{n}\otimes\mathbf{B}) + I_3^{-2/3}w_{15}(\mathbf{B}\otimes I_5\mathbf{m}\otimes\mathbf{m} + I_5\mathbf{m}\otimes\mathbf{m}\otimes\mathbf{B}) \\ & + (-\frac{1}{3}I_3^{-1/3}\bar{I}_1 w_{14} - \frac{1}{3}I_3^{-1/3}\bar{I}_4 w_{44} - \frac{1}{3}I_3^{-1/3}w_4 - \frac{1}{3}I_3^{-1/3}\bar{I}_5 w_{45})(\mathbf{1}\otimes I_4\mathbf{n}\otimes\mathbf{n} + I_4\mathbf{n}\otimes\mathbf{n}\otimes\mathbf{1}) \\ & + (-\frac{1}{3}I_3^{-1/3}\bar{I}_1 w_{15} - \frac{1}{3}I_3^{-1/3}\bar{I}_5 w_{55} - \frac{1}{3}I_3^{-1/3}w_5 - \frac{1}{3}I_3^{-1/3}\bar{I}_4 w_{45})(\mathbf{1}\otimes I_5\mathbf{m}\otimes\mathbf{m} + I_5\mathbf{m}\otimes\mathbf{m}\otimes\mathbf{1}) \\ & + I_3^{-2/3}w_{44}I_4^2\mathbf{n}\otimes\mathbf{n}\otimes\mathbf{n}\otimes\mathbf{n} + I_3^{-2/3}w_{55}I_5^2\mathbf{m}\otimes\mathbf{m}\otimes\mathbf{m}\otimes\mathbf{m} \\ & + I_3^{-2/3}w_{45}I_4 I_5(\mathbf{n}\otimes\mathbf{n}\otimes\mathbf{m}\otimes\mathbf{m} + \mathbf{m}\otimes\mathbf{m}\otimes\mathbf{n}\otimes\mathbf{n}) \\ & + [W_3 I_3 - \frac{1}{3}(\bar{I}_1 w_1 + \bar{I}_4 w_4 + \bar{I}_5 w_5)](-\frac{1}{2})(\delta_{ik}\delta_{jl} + \delta_{il}\delta_{jk})\mathbf{e}_i\otimes\mathbf{e}_j\otimes\mathbf{e}_k\otimes\mathbf{e}_l\end{aligned} \tag{3.30}$$

$$\mathbb{C}^{MZ-J} = \frac{1}{J}\mathbb{C}^{\tau c} + \frac{1}{2}(\delta_{ik}\sigma_{jl} + \sigma_{ik}\delta_{jl} + \delta_{il}\sigma_{jk} + \sigma_{il}\delta_{jk})\mathbf{e}_i\otimes\mathbf{e}_j\otimes\mathbf{e}_k\otimes\mathbf{e}_l \tag{3.31}$$

where $\mathbf{n}=\lambda_n^{-1}\mathbf{F}\mathbf{n}_0$, $\mathbf{m}=\lambda_m^{-1}\mathbf{F}\mathbf{m}_0$ and λ_n, λ_m are the stretch quantities along the $\mathbf{n}_0$, $\mathbf{m}_0$ directions， $W_i=\dfrac{\partial W}{\partial I_i}, i\in\{3\}$ and $w_i=\dfrac{\partial w}{\partial \bar{I}_i}, i\in\{1,4,5\}$

Now turn back to the neo-Hookean model and substitute the specific form of $W=\dfrac{1}{D}(I_3^{1/2}-1)^2$ and $w=\dfrac{\mu}{2}(\bar{I}_1-3)+C_{201}(\bar{I}_4\text{-}1)^2+C_{202}(\bar{I}_5\text{-}1)^2$ into the above relations， we have

$$\begin{aligned}\boldsymbol{\sigma}=&\frac{\mu}{J}\bar{\mathbf{B}}+[\frac{2}{D}(J-1)-\frac{2}{3J}(\frac{\mu}{2}\bar{I}_1+2C_{201}(\bar{I}_4-1)\,\bar{I}_4+2C_{202}(\bar{I}_5-1)\bar{I}_5)]\mathbf{1}\\&+\frac{4C_{201}}{J}(\bar{I}_4-1)\,\bar{I}_4\mathbf{n}\otimes\mathbf{n}+\frac{4C_{202}}{J}(\bar{I}_5-1)\bar{I}_5\mathbf{m}\otimes\mathbf{m}\end{aligned}\tag{3.32}$$

and

$$\begin{aligned}\mathbb{C}^{MZ-J}=&\frac{1}{J}\mathbb{C}^{\tau c}+\frac{1}{2}(\delta_{ik}\sigma_{jl}+\sigma_{ik}\delta_{jl}+\delta_{il}\sigma_{jk}+\sigma_{il}\delta_{jk})\mathbf{e}_i\otimes\mathbf{e}_j\otimes\mathbf{e}_k\otimes\mathbf{e}_l\\&=-\frac{2\mu}{3J}(\bar{\mathbf{B}}\otimes\mathbf{1}+\mathbf{1}\otimes\bar{\mathbf{B}})\\&+[\frac{2}{D}(2J-1)+\frac{4}{9J}(\frac{\mu}{2}\bar{I}_1+2C_{201}(\bar{I}_4-1)\,\bar{I}_4+2C_{202}(\bar{I}_5-1)\bar{I}_5+2C_{201}\bar{I}_4^2+2C_{202}\bar{I}_5^2)]\mathbf{1}\otimes\mathbf{1}\\&-\frac{8}{3J}C_{201}(2\bar{I}_4-1)\bar{I}_4(\mathbf{1}\otimes\mathbf{n}\otimes\mathbf{n}+\mathbf{n}\otimes\mathbf{n}\otimes\mathbf{1})\\&-\frac{8}{3J}C_{202}(2\bar{I}_5-1)\bar{I}_5(\mathbf{1}\otimes\mathbf{m}\otimes\mathbf{m}+\mathbf{m}\otimes\mathbf{m}\otimes\mathbf{1})\\&+\frac{8}{J}C_{201}\bar{I}_4^2\mathbf{n}\otimes\mathbf{n}\otimes\mathbf{n}\otimes\mathbf{n}+\frac{8}{J}C_{202}\bar{I}_5^2\mathbf{m}\otimes\mathbf{m}\otimes\mathbf{m}\otimes\mathbf{m}\\&+[\frac{4}{D}(J-1)-\frac{4}{3J}(\frac{\mu}{2}\bar{I}_1+2C_{201}(\bar{I}_4-1)\,\bar{I}_4+2C_{202}(\bar{I}_5-1)\,\bar{I}_5)](-\frac{1}{2})(\delta_{ik}\delta_{jl}+\delta_{il}\delta_{jk})\mathbf{e}_i\otimes\mathbf{e}_j\otimes\mathbf{e}_k\otimes\mathbf{e}_l\\&+\frac{1}{2}(\delta_{ik}\sigma_{jl}+\sigma_{ik}\delta_{jl}+\delta_{il}\sigma_{jk}+\sigma_{il}\delta_{jk})\mathbf{e}_i\otimes\mathbf{e}_j\otimes\mathbf{e}_k\otimes\mathbf{e}_l\end{aligned}\tag{3.33}$$

By reconstructing the above formulation, we can obtain that the stress and elasticity tensor are comprised of two parts, the isotropic and anisotropic parts:

$$\boldsymbol{\sigma} = \boldsymbol{\sigma}_{iso} + \boldsymbol{\sigma}_{aniso} \tag{3.34}$$

$$\mathbb{C}^{MZ-J} = \mathbb{C}^{MZ-J}_{\text{iso}} + \mathbb{C}^{MZ-J}_{aniso} \tag{3.35}$$

The isotropic part is nothing but same as the equations (3.24)(3.25), and the anisotropic parts are:

$$\boldsymbol{\sigma}_{aniso} = -A_1\mathbf{I} + A_2\tilde{\mathbf{n}}\otimes\tilde{\mathbf{n}} + A_3\tilde{\mathbf{m}}\otimes\tilde{\mathbf{m}} \tag{3.36}$$

$$\begin{aligned}
\mathbb{C}^{MZ-J}_{aniso} = {} & A_4\mathbf{I}\otimes\mathbf{I} + A_5(\mathbf{I}\otimes\tilde{\mathbf{n}}\otimes\tilde{\mathbf{n}} + \tilde{\mathbf{n}}\otimes\tilde{\mathbf{n}}\otimes\mathbf{I}) + A_6(\mathbf{I}\otimes\tilde{\mathbf{m}}\otimes\tilde{\mathbf{m}} + \tilde{\mathbf{m}}\otimes\tilde{\mathbf{m}}\otimes\mathbf{I}) \\
& + A_7\tilde{\mathbf{n}}\otimes\tilde{\mathbf{n}}\otimes\tilde{\mathbf{n}}\otimes\tilde{\mathbf{n}} + A_8\tilde{\mathbf{m}}\otimes\tilde{\mathbf{m}}\otimes\tilde{\mathbf{m}}\otimes\tilde{\mathbf{m}} \\
& + \frac{1}{2}\delta_{ik}(A_2\tilde{\mathbf{n}}\otimes\tilde{\mathbf{n}} + A_3\tilde{\mathbf{m}}\otimes\tilde{\mathbf{m}})_{jl}\ \mathbf{e}_i\otimes\mathbf{e}_j\otimes\mathbf{e}_k\otimes\mathbf{e}_l \\
& + \frac{1}{2}\delta_{jl}(A_2\tilde{\mathbf{n}}\otimes\tilde{\mathbf{n}} + A_3\tilde{\mathbf{m}}\otimes\tilde{\mathbf{m}})_{ik}\ \mathbf{e}_i\otimes\mathbf{e}_j\otimes\mathbf{e}_k\otimes\mathbf{e}_l \\
& + \frac{1}{2}\delta_{il}(A_2\tilde{\mathbf{n}}\otimes\tilde{\mathbf{n}} + A_3\tilde{\mathbf{m}}\otimes\tilde{\mathbf{m}})_{jk}\ \mathbf{e}_i\otimes\mathbf{e}_j\otimes\mathbf{e}_k\otimes\mathbf{e}_l \\
& + \frac{1}{2}\delta_{jk}(A_2\tilde{\mathbf{n}}\otimes\tilde{\mathbf{n}} + A_3\tilde{\mathbf{m}}\otimes\tilde{\mathbf{m}})_{il}\ \mathbf{e}_i\otimes\mathbf{e}_j\otimes\mathbf{e}_k\otimes\mathbf{e}_l
\end{aligned} \tag{3.37}$$

where $A_1 = \frac{4}{3J}[C_{201}(\bar{I}_4 - 1)\bar{I}_4 + C_{202}(\bar{I}_5 - 1)\bar{I}_5]$, $A_2 = \frac{4}{J}C_{201}(\bar{I}_4 - 1)$, $A_3 = \frac{4}{J}C_{202}(\bar{I}_5 - 1)$

$A_4 = \frac{8}{9J}[C_{201}(\bar{I}_4 - 1)\bar{I}_4 + C_{202}(\bar{I}_5 - 1)\bar{I}_5 + C_{201}\bar{I}_4^2 + C_{202}\bar{I}_5^2]$, $A_5 = -\frac{8}{3J}C_{201}(2\bar{I}_4 - 1)$,

$A_6 = -\frac{8}{3J}C_{202}(2\bar{I}_5 - 1)$, $A_7 = \frac{8}{J}C_{201}$, $A_8 = \frac{8}{J}C_{202}$, $\tilde{\mathbf{n}} = \bar{\mathbf{F}}\mathbf{n}_0$, $\tilde{\mathbf{m}} = \bar{\mathbf{F}}\mathbf{m}_0$

b. A modified anisotropic model

To address the issue pertinent to reasonable anisotropic deformations, we modify the strain energy into the following form:

$$W = W(J, \bar{I}_1, J_1, K_1) = \frac{1}{D_1}(J-1)^2 + \frac{\mu}{2}(\bar{I}_1 - 3) + C_{201}(J_1\text{-}1)^2 + C_{202}(K_1\text{-}1)^2 \tag{3.38}$$

Using the same notation, we have

$$W = W(I_3) = \frac{1}{D_1}(J-1)^2 = \frac{1}{D_1}(I_3^{1/2} - 1)^2 \tag{3.39}$$

and

$$w = w(\bar{I}_1, I_4, I_5) = \frac{\mu}{2}(\bar{I}_1 - 3) + C_{201}(J_1\text{-}1)^2 + C_{202}(K_1\text{-}1)^2 \tag{3.40}$$

Then,

$$W_3 = \frac{1}{D}(1 - I_3^{-1/2}), \quad W_{33} = \frac{1}{2D} I_3^{-3/2}$$

$$w_1 = \frac{\mu}{2}, \quad w_{11} = 0, \; w_{14} = 0, \; w_{15} = 0$$
$$w_4 = 2C_{201}(I_4 - 1), \; w_{41} = 0, \; w_{44} = 2C_{201}, \; w_{45} = 0$$
$$w_5 = 2C_{202}(I_5 - 1), \; w_{51} = 0, \; w_{54} = 0, \; w_{55} = 2C_{202}$$

It should be noted that here the differentiation of w with the subscript 4 and 5 are different than the original HGO-C method, where $w_4 = \frac{\partial w}{\partial I_4} = \frac{\partial w}{\partial J_1}$, $w_5 = \frac{\partial w}{\partial I_5} = \frac{\partial w}{\partial K_1}$

$$\begin{aligned}\frac{1}{4}\mathbb{C}^{\tau c} = &-\frac{\mu}{6} I_3^{-1/3}(\mathbf{B}\otimes\mathbf{1} + \mathbf{1}\otimes\mathbf{B}) \\ &+ [\frac{1}{2D} I_3^{1/2} + \frac{1}{D}(I_3 - I_3^{1/2}) + \frac{1}{9}\frac{\mu}{2}\bar{I}_1]\mathbf{1}\otimes\mathbf{1} \\ &+ 2C_{201}\mathbf{Fn}_0\otimes\mathbf{Fn}_0\otimes\mathbf{Fn}_0\otimes\mathbf{Fn}_0 + 2C_{202}\mathbf{Fm}_0\otimes\mathbf{Fm}_0\otimes\mathbf{Fm}_0\otimes\mathbf{Fm}_0 \\ &+ [\frac{1}{D}(1 - I_3^{-1/2})I_3 - \frac{1}{3}\frac{\mu}{2}\bar{I}_1](-\frac{1}{2})(\delta_{ik}\delta_{jl} + \delta_{il}\delta_{jk})\mathbf{e}_i\otimes\mathbf{e}_j\otimes\mathbf{e}_k\otimes\mathbf{e}_l\end{aligned} \tag{3.41}$$

$$\mathbb{C}^{MZ-J} = \frac{1}{J}\mathbb{C}^{\tau c} + \frac{1}{2}(\delta_{ik}\sigma_{jl} + \sigma_{ik}\delta_{jl} + \delta_{il}\sigma_{jk} + \sigma_{il}\delta_{jk})\mathbf{e}_i\otimes\mathbf{e}_j\otimes\mathbf{e}_k\otimes\mathbf{e}_l \tag{3.42}$$

By comparing the expressions, we can write the elasticity tensor as follow,

$$\mathbb{C}^{MZ-J} = \mathbb{C}_{\text{iso}}^{MZ-J} + \mathbb{C}_{aniso}^{MZ-J} \tag{3.43}$$

where $\mathbb{C}_{\text{iso}}^{MZ-J}$ is the same as the neo-Hookean model, and $\mathbb{C}_{aniso}^{MZ-J}$ is the added elasticity tensor due to anisotropy.

$$\begin{aligned}
(\mathbb{C}_{aniso}^{MZ-J})_{ijkl} = {} & \frac{8C_{201}}{J}(Fn_0)_i(Fn_0)_j(Fn_0)_k(Fn_0)_l + \frac{8C_{202}}{J}(Fm_0)_i(Fm_0)_j(Fm_0)_k(Fm_0)_l \\
& + \frac{1}{2}\delta_{ik}[\frac{4C_{201}}{J}(J_1-1)(Fn_0)_j(Fn_0)_l + \frac{4C_{202}}{J}(K_1-1)(Fm_0)_j(Fm_0)_l] \\
& + \frac{1}{2}\delta_{jl}[\frac{4C_{201}}{J}(J_1-1)(Fn_0)_i(Fn_0)_k + \frac{4C_{202}}{J}(K_1-1)(Fm_0)_i(Fm_0)_k] \\
& + \frac{1}{2}\delta_{il}[\frac{4C_{201}}{J}(J_1-1)(Fn_0)_j(Fn_0)_k + \frac{4C_{202}}{J}(K_1-1)(Fm_0)_j(Fm_0)_k] \\
& + \frac{1}{2}\delta_{jk}[\frac{4C_{201}}{J}(J_1-1)(Fn_0)_i(Fn_0)_l + \frac{4C_{202}}{J}(K_1-1)(Fm_0)_i(Fm_0)_l]
\end{aligned} \tag{3.44}$$

Similarly, we can have $\boldsymbol{\sigma} = \boldsymbol{\sigma}_{iso} + \boldsymbol{\sigma}_{aniso}$ where $\boldsymbol{\sigma}_{iso}$ is same as the Cauchy stress of the neo-Hookean model, and $\boldsymbol{\sigma}_{aniso}$ is the stress due to the anisotropic response.

$$(\boldsymbol{\sigma}_{aniso})_{ij} = \frac{4C_{201}}{J}(J_1-1)(Fn_0)_i(Fn_0)_j + \frac{4C_{202}}{J}(K_1-1)(Fm_0)_i(Fm_0)_j \tag{3.45}$$

In order to evaluate the UMAT subroutine of the anisotropic neo-Hookean model, we also investigate the three rather simple problems.

1. Pure dilatation

The first case is the pure dilatation problem as depicted in Fig. 41. The body is stretched along three principal directions with the same displacement, so the deformation gradient is $\mathbf{F} = \lambda\mathbf{I}$. In our simulation, the body is a cube of dimension 20x20x20 and the

stretched displacement in three directions is 20. The material parameter considered are $\mu = 5, D_1 = 0.2, C_{201} = 1, C_{202} = 10$, and the anisotropic directions are $\mathbf{n}_0 = (0.866, -0.5, 0)^{'}$, $\mathbf{m}_0 = (0.5, 0.866, 0)^{'}$. It should be noticed that we give a comparatively large value of D_1 to ensure the body have the ability to change its volume.

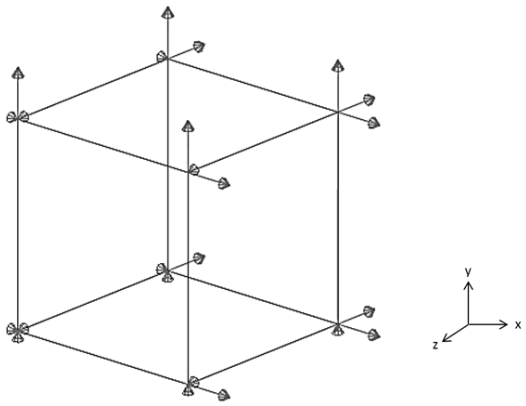

Fig. 41 Pure dilatation of single element

From the contour plots as shown in Fig. 42, we can see that the von Mises stress obtained from the original method is nearly zero, and in contrast there is 57.2 MPa for the modified model. According to the formula of von Mises stress which is

$$\sigma_{\mathrm{v}} = \sqrt{\frac{(\sigma_{11} - \sigma_{22})^2 + (\sigma_{22} - \sigma_{33})^2 + (\sigma_{33} - \sigma_{11})^2 + (\sigma_{12}^2 + \sigma_{23}^2 + \sigma_{31}^2)}{2}} \tag{3.46}$$

it is only valid that the von mises stress is zero under the condition of $\sigma_{11} = \sigma_{22} = \sigma_{33}$ and $\sigma_{12} = \sigma_{23} = \sigma_{31} = 0$. Thus the traditional way cannot produce an anisotropic response as expected. The reason owing to this problem has already been explained by [74] mathematically. For pure dilation problem, the stretch tensor $\mathbf{C} = \lambda^2 \mathbf{I}$, $J = \lambda^3$, the

invariants in anisotropic terms are $J_1 = I_4 = \lambda^2$, $K_1 = J_5 = \lambda^2$ and the corresponding deviatoric parts are $\bar{J}_1 = \bar{I}_4 = J^{-2/3} J_1 = 1$, $\bar{K}_1 = \bar{J}_5 = J^{-2/3} K_1 = 1$. By substituting these values into the equation (3.45), we can get $\boldsymbol{\sigma}_{aniso} = \mathbf{0}$ which results in an isotropic response for the traditional way, while the modified method can give a nonzero anisotropic stress because of J1≠1 and K1≠1.

To clearly observe this issue, the relationships between the principal stresses S11, S22, S33 and stretch are plotted in Fig. 43. We can see the three principal stress components exactly coincide for the traditional way, while for the modified method they are different, which should be expected.

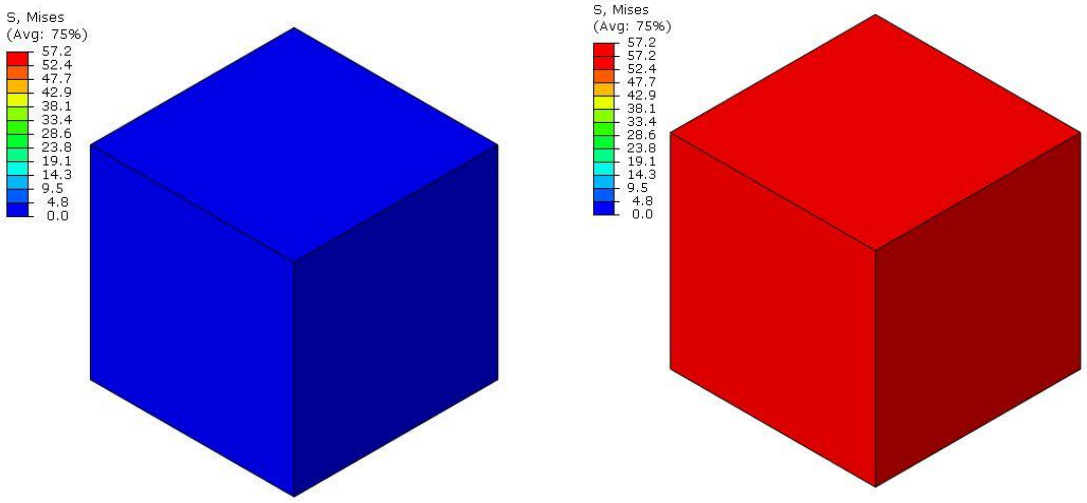

Fig. 42 Stress under pure dilatation: Original method (Left) and Modified method (Right)

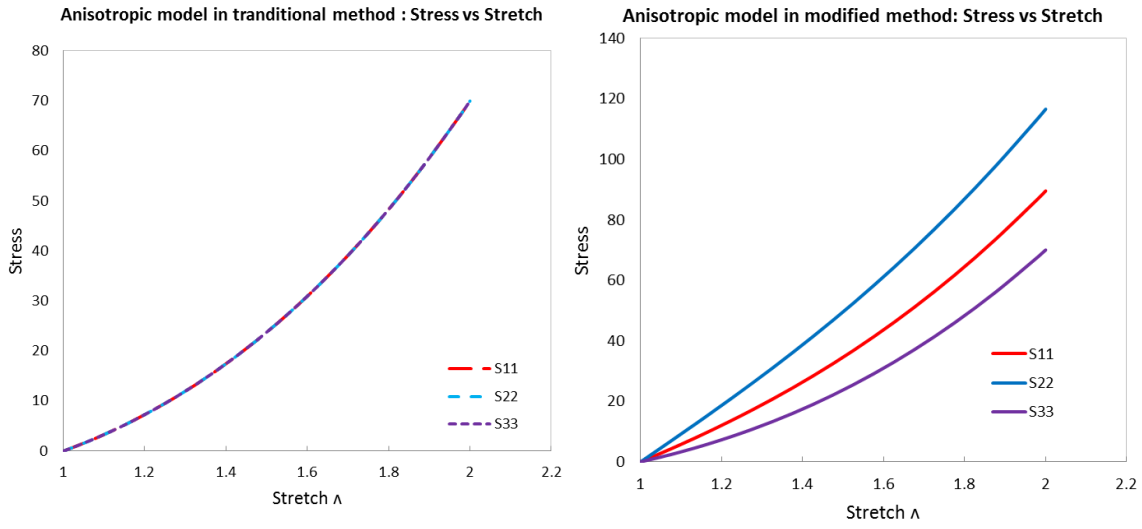

Fig. 43 Stress vs stretch of anisotropic model under pure dilation: Original method (Left) and Modified method (Right)

2. Sphere inflation under hydrostatic stress

Now we consider the sphere, of an anisotropic material, inflation problem under hydrostatic stress. By imposing a pressure of 0.45 MPa at the inner surface of the sphere, we can see the similar results to the pure dilation problem shown below in Fig. 44: the displacement magnitudes all over the outer surface in the left picture are almost the same within the range of 6.4-6.8mm, that means the original method deforms the sphere into another sphere which is an isotropic response; the right picture showed that the modified model deformed the sphere into an ellipsoid. Therefore, the modified model can produce realistic results wherein the stretches along x, y, z direction are different under the same stress. The values of $\mu = 5, D_1 = 0.2,\ C_{201} = 5,\ C_{202} = 5$, $\mathbf{n}_0 = (0.866, -0.5, 0)^{'}$, $\mathbf{m}_0 = (0.5, 0.866, 0)^{'}$ are used in the calculations.

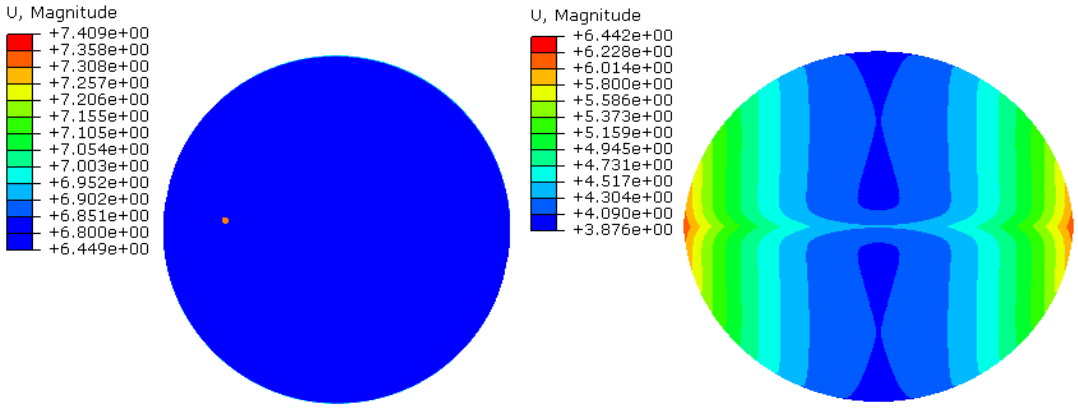

Fig. 44 Displacement magnitude under spherical inflation: Original method (Left) and Modified method (Right)

3. Reduction to isotropic neo-Hookean model : Uniaxial tension

Now we further verify the anisotropic model by setting the values of $C_{201} = 0$ and $C_{202} = 0$, and compare the results with isotropic model. The uniaxial tension is taken here for our test. From the results we can see that the degenerated anisotropic model have a same exact with isotropic model.

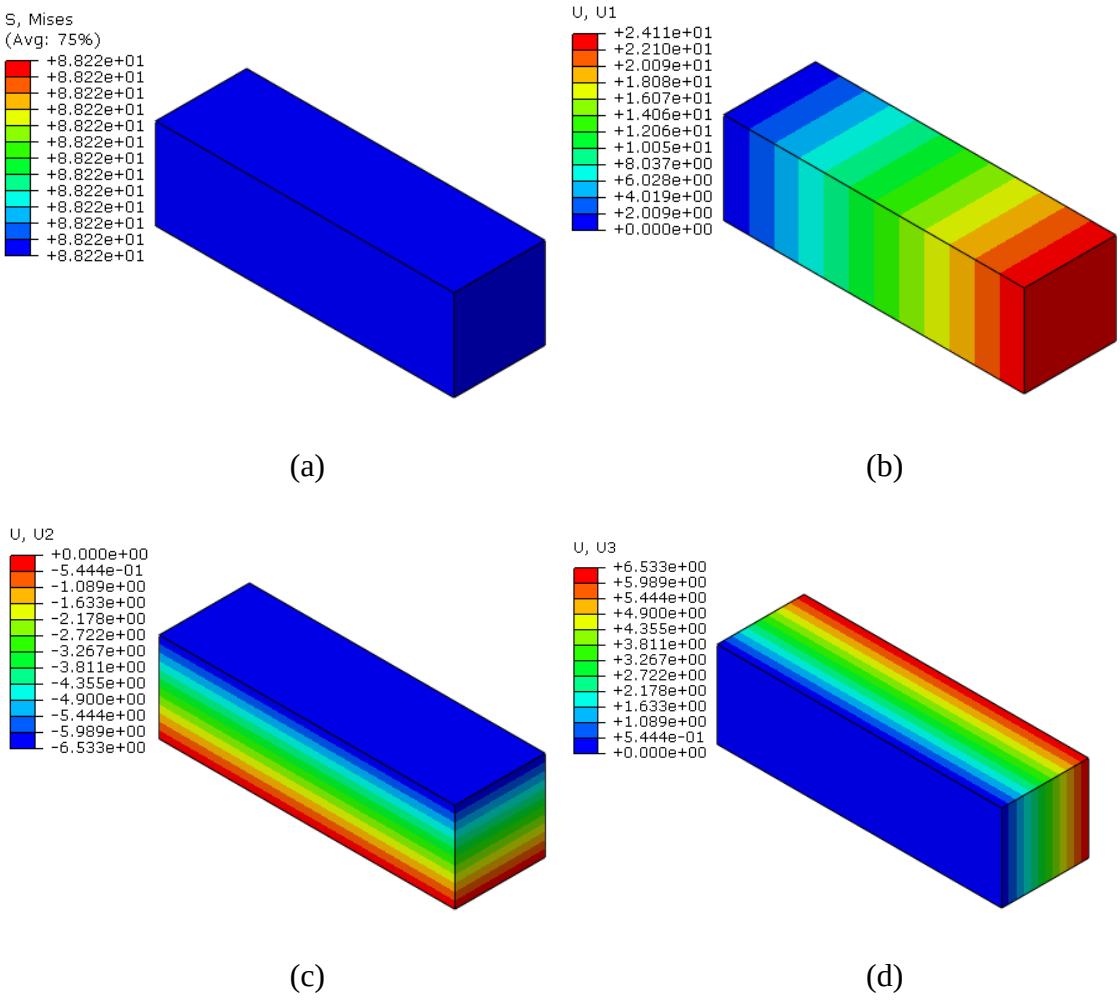

Fig. 45 Results of degenerated anisotropic model under uniaxial tension: (a) Von Mises stress (b) x-direction displacement (c) y-direction displacement (d) z-direction displacement

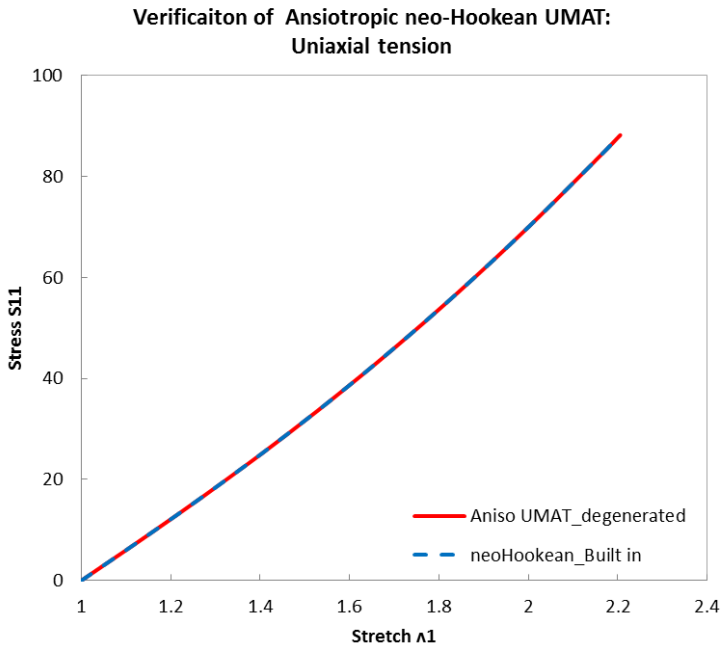

Fig. 46 Stress vs Stretch under uniaxial tension between degenerated anisotropic model (UMAT) and Abaqus built-in neo-Hookean model

3.3.2.2 Anisotropic elastic model of LASMPs

Two cases of uniaxial tension and radial inflation are used to test the anisotropic elastic model of LASMPs.

1. Uniaxial tension

Fig. 47 showed the displacement outputs before unloading and after unloading. From the results we can see when the body is released from the same amount of stretching as the isotropic model, the body can keep a much larger length. By comparison with the result from the analytical solution (implemented in Matlab), discussed in Chapter II the relationship between the stress and stretch from the UMAT agrees very well as plotted in Fig. 48.

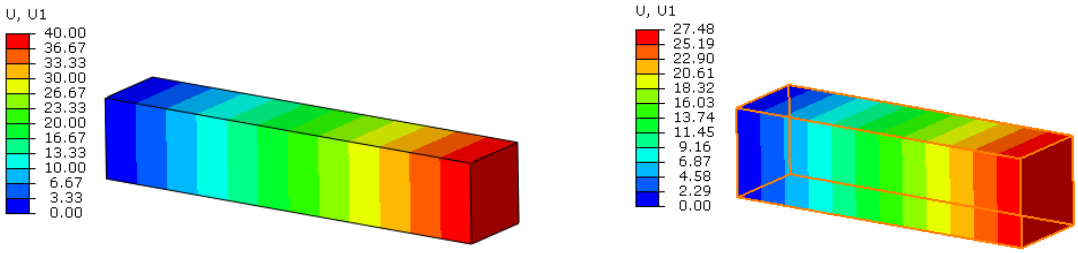

(a) (b)

Fig. 47 Results of LASMP anisotropic model under uniaxial tension: (a) x-direction displacement before unloading; (b) x-direction displacement after unloading

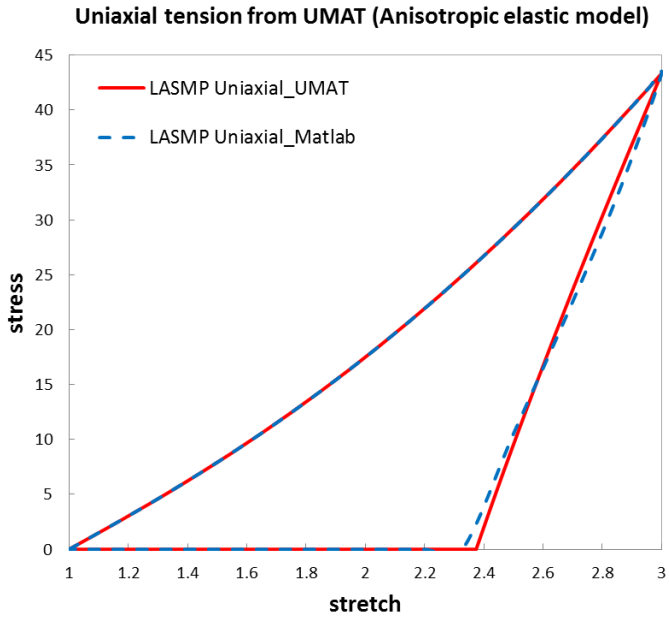

Fig. 48 Comparison of stress vs. stretch between UMAT and Matlab under uniaxial tension for LASMP anisotropic elastic model

2. Radial inflation

Fig. 49 showed the contour plots of displacement before unloading and after unloading. A similar result can be concluded: when there are two networks involved and the second network is described to be anisotropic elastic, the cylinder has a larger radius comparing with the response of isotropic model after stress is released. From the relationship between the inner radius and imposed pressure, UMAT code can keep a good agreement with semi-analytical solution in Chapter II.

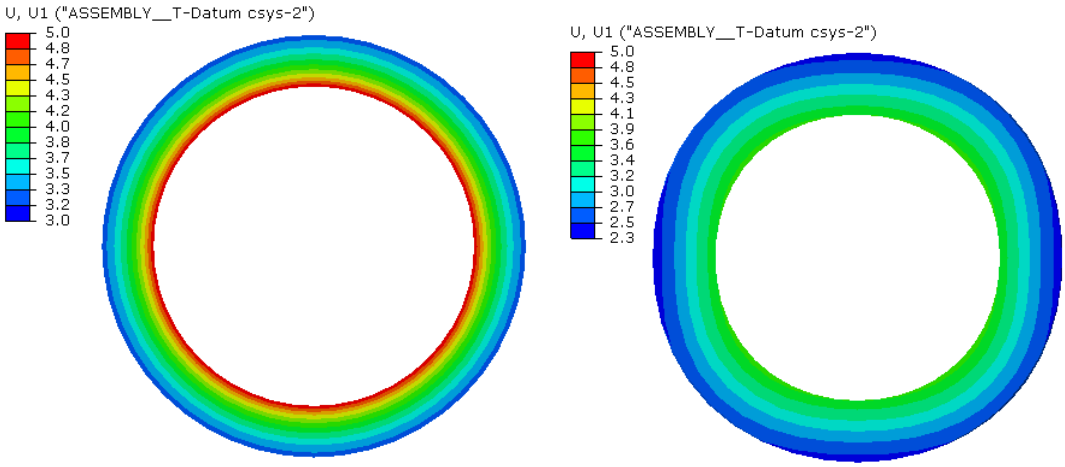

(a) (b)

Fig. 49 Cylindrical inflation output for LASMP anisotropic model: (a) radial displacement before unloading; (b) radial displacement after unloading

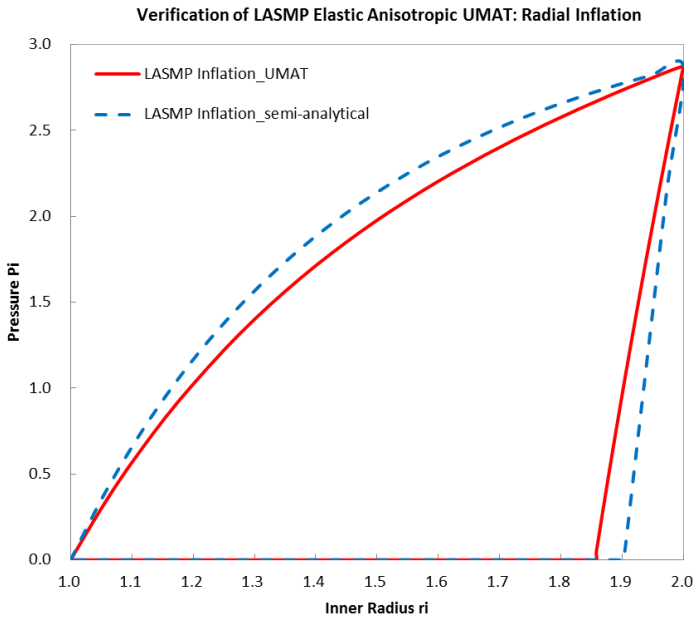

Fig. 50 Comparison of pressure vs inner radius between UMAT and Matlab under cylindrical inflation for LASMP anisotropic elastic model

3.3.3 Quasi-linear viscoelastic model of LASMPs

For the quasi-linear viscoelastic model, the form of the total stress and elasticity tensor are different from the elastic LASMPs. The formation process of the second network must be taken into calculation even under constant strain for the PNR mechanisms, the assumption is made that the shear modulus of the two networks are changing with the volume ratio of the second network. So the form of the stress and elasticity tensor should be expressed in the following forms:

$$\boldsymbol{\sigma} = \boldsymbol{\sigma}_1 + \boldsymbol{\sigma}_2 \tag{3.47}$$

$$\mathbb{C}^{MZ-J} = \mathbb{C}_1^{MZ-J} + \mathbb{C}_2^{MZ-J} \tag{3.48}$$

Each of the networks is described by the quasi-linear viscoelastic model, and the volume ratio of the second network does not appear in the above the expression explicitly because it will play its role by influencing the shear modulus of the networks, that is $\tilde{u}_i = \tilde{u}_i(\alpha)$, and the volume ratio can be obtain by the evolution equations in Chapter II.

3.3.3.1 neo-Hookean based QLV model

The expression of the quasi-linear viscoelastic model of an incompressible body is:

$$\mathbf{T}(t) = -p\mathbf{I} + \mathbf{F}(t)(\mathbf{S}_D^e(t) + \int_0^t \frac{d\mathbf{D}(t-s)}{d(t-s)}\mathbf{S}_D^e(s)ds)\mathbf{F}^T(t) \tag{3.49}$$

To enforce the constraint of incompressibility, the penalty approach discussed above is used. The second Piola-Kirchhoff stress can be obtained as:

$$\mathbf{S} = KJ(J-1)\mathbf{C}^{-1} + \mathbf{S}_D^e(t) + \int_0^t \frac{d\mathbf{D}(t-s)}{d(t-s)}\mathbf{S}_D^e(s)ds \tag{3.50}$$

By comparing the expression with the one obtained from neo-Hookean model, the volumetric part is the same, so we just need to deal with the deviatoric part $\mathbf{S}_D$.

$$\mathbf{S}_D(t) = \mathbf{S}_D^e(t) + \int_0^t \frac{d\mathbf{D}(t-s)}{d(t-s)}\mathbf{S}_D^e(s)ds \tag{3.51}$$

We need to update the Cauchy stress and determine the updated Jacobian matrix for $\mathbf{S}_D(t)$, which is $\mathbb{C}_D = 2\frac{\partial \mathbf{S}_D(t)}{\partial \mathbf{C}(t)}$

$$\begin{aligned}\mathbf{S}_D(t) &= \mathbf{S}_D^e(t) + \int_0^t \frac{d\mathbf{D}(t-s)}{d(t-s)}\mathbf{S}_D^e(s)ds \\ &= \mathbf{S}_D^e(t_n) + \frac{t_n - t_{n-1}}{2}[(\frac{d\mathbf{D}(t-s)}{d(t-s)}\mathbf{S}_D^e(s))|_{s=t_n} + (\frac{d\mathbf{D}(t-s)}{d(t-s)}\mathbf{S}_D^e(s))|_{s=t_{n-1}}] \\ &\quad + \int_0^{t_{n-1}} \frac{d\mathbf{D}(t-s)}{d(t-s)}\mathbf{S}_D^e(s)ds\end{aligned} \tag{3.52}$$

The total Cauchy stress is:

$$\boldsymbol{\sigma}(t) = K(J-1)\mathbf{I} + J^{-1}\mathbf{F}(t)\mathbf{S}_D(t)\mathbf{F}^T(t) \tag{3.53}$$

The Jacobian Matrix:

$$\begin{aligned}\mathbb{C}_D(t) &= 2\frac{\partial \mathbf{S}_D(t)}{\partial \mathbf{C}(t)} = 2[\frac{\partial \mathbf{S}_D^e(t_n)}{\partial \mathbf{C}(t_n)} + \frac{t_n - t_{n-1}}{2}(\frac{d\mathbf{D}_a(t-s)}{d(t-s)}|_{s=t_n}\ \frac{\partial \mathbf{S}_D^e(t_n)}{\partial \mathbf{C}(t_n)})] \\ &= [1 + \frac{t_n - t_{n-1}}{2}(\frac{d\mathbf{D}_a(t-s)}{d(t-s)}|_{s=t_n})]2\frac{\partial \mathbf{S}_D^e(t_n)}{\partial \mathbf{C}(t_n)} \\ &= [1 + \frac{t_n - t_{n-1}}{2}(\frac{d\mathbf{D}_a(t-s)}{d(t-s)}|_{s=t_n})]\mathbb{C}_D^e(t)\end{aligned} \tag{3.54}$$

By the same manipulations as above, using the push-forward operations, we can obtain the final Jacobian matrix used in ABAQUS UMAT subroutine, where the elastic response function is the neo-Hookean model:

$$\begin{aligned}\mathbb{C}^{\tau c} &= \frac{2}{D_1}J(J-1)(\mathbf{1}\otimes\mathbf{1} - 2\mathbf{I}) + \frac{2}{D_1}J^2\mathbf{1}\otimes\mathbf{1} \\ &\quad + [1 + \frac{t_n - t_{n-1}}{2}(\frac{d\mathbf{D}_a(t-s)}{d(t-s)}|_{s=t_n})](-\frac{2}{3}\mu J^{-2/3}[\mathbf{B}\otimes\mathbf{1} + \mathbf{1}\otimes\mathbf{B}] + \frac{2}{3}\mu\bar{I}_1(\mathbf{I} + \frac{1}{3}\mathbf{1}\otimes\mathbf{1}))\end{aligned} \tag{3.55}$$

and

$$\mathbb{C}^{MZ-J} = \frac{1}{J}\mathbb{C}^{\tau c} + \frac{1}{2}(\delta_{ik}\sigma_{jl} + \sigma_{ik}\delta_{jl} + \delta_{il}\sigma_{jk} + \sigma_{il}\delta_{jk})\ \mathbf{e}_i\otimes\mathbf{e}_j\otimes\mathbf{e}_k\otimes\mathbf{e}_l \tag{3.56}$$

If $\mathbf{D}(t)$ is expressed with one term prony series

$$D(t) = \frac{\mu_\infty}{\mu_o} + (1 - \frac{\mu_\infty}{\mu_o}) e^{-t/\tau} \tag{3.57}$$

Then, $\frac{d\mathbf{D}(t-s)}{d(t-s)} = (1 - \frac{\mu_\infty}{\mu_o})(-\frac{1}{\tau}) e^{-(t-s)/\tau}$

If written in index notation,

$$\begin{aligned}
\mathbb{C}_{ijkl}^{MZ-J} &= \frac{2}{D_1}(J-1)(\delta_{ij}\delta_{kl} - \delta_{ik}\delta_{jl} - \delta_{il}\delta_{jk}) + \frac{2}{D_1} J \delta_{ij}\delta_{kl} \\
&+ (1 - \frac{\triangle \mathrm{t}}{2\tau}(1 - \frac{\mu_\infty}{\mu_o})) \frac{2\mu_0}{3J} [\bar{I}_1 (\frac{1}{2}(\delta_{ik}\delta_{jl} + \delta_{il}\delta_{jk}) + \frac{1}{3}\delta_{ij}\delta_{kl}) - \bar{B}_{ij}\delta_{kl} - \delta_{ij}\bar{B}_{kl}] \\
&+ \frac{1}{2}(\delta_{\mathrm{ik}}\sigma_{jl} + \sigma_{ik}\delta_{\mathrm{jl}} + \delta_{\mathrm{il}}\sigma_{jk} + \sigma_{il}\delta_{\mathrm{jk}})\ \mathbf{e}_i \otimes \mathbf{e}_j \otimes \mathbf{e}_k \otimes \mathbf{e}_l
\end{aligned} \tag{3.58}$$

$$\begin{aligned}
\boldsymbol{\sigma}(t) &= K(J-1)\mathbf{I} + J^{-1}\mathbf{F}(t)\mathbf{S}_D(t)\mathbf{F}^T(t) \\
&= K(J-1)\mathbf{I} + J^{-1}\mathbf{F}(t)(\mathbf{S}_D^e(t) + \int_0^t \frac{d\mathbf{D}(t-s)}{d(t-s)}\mathbf{S}_D^e(s)ds)\mathbf{F}^T(t) \\
&= K(J-1)\mathbf{I} + \boldsymbol{\sigma}_D^e(t) + J^{-1}\mathbf{F}(t)\int_0^t \frac{d\mathbf{D}(t-s)}{d(t-s)}\mathbf{S}_D^e(s)ds\mathbf{F}^T(t) \\
&= K(J-1)\mathbf{I} + \boldsymbol{\sigma}_D^e(t_n) + J^{-1}\mathbf{F}(t)\mathbf{P}(t_n)\mathbf{F}^T(t)
\end{aligned} \tag{3.59}$$

$$\begin{aligned}
\mathbf{P}(t_n) &= \int_0^t \frac{d\mathbf{D}(t-s)}{d(t-s)}\mathbf{S}_D^e(s)ds = \int_{t_{n-1}}^{t_n} \frac{d\mathbf{D}(t-s)}{d(t-s)}\mathbf{S}_D^e(s)ds + \int_0^{t_{n-1}} \frac{d\mathbf{D}(t-s)}{d(t-s)}\mathbf{S}_D^e(s)ds \\
&= -\frac{\triangle \mathrm{t}}{2\tau}(1 - \frac{\mu_\infty}{\mu_o})[\mathbf{S}_D^e(t_n) + e^{-\frac{\triangle \mathrm{t}}{\tau}}\mathbf{S}_D^e(t_{n-1})] + \int_0^{t_{n-1}} (1 - \frac{\mu_\infty}{\mu_o})(-\frac{1}{\tau}) e^{-\frac{t_n - s}{\tau}}\mathbf{S}_D^e(s)ds \\
&= -\frac{\triangle \mathrm{t}}{2\tau}(1 - \frac{\mu_\infty}{\mu_o})[\mathbf{S}_D^e(t_n) + e^{-\frac{\triangle \mathrm{t}}{\tau}}\mathbf{S}_D^e(t_{n-1})] + e^{-\frac{\triangle \mathrm{t}}{\tau}} \int_0^{t_{n-1}} (1 - \frac{\mu_\infty}{\mu_o})(-\frac{1}{\tau}) e^{-\frac{t_{n-1} - s}{\tau}}\mathbf{S}_D^e(s)ds \\
&= -\frac{\triangle \mathrm{t}}{2\tau}(1 - \frac{\mu_\infty}{\mu_o})[\mathbf{S}_D^e(t_n) + e^{-\frac{\triangle \mathrm{t}}{\tau}}\mathbf{S}_D^e(t_{n-1})] + e^{-\frac{\triangle \mathrm{t}}{\tau}}\mathbf{P}(t_{n-1})
\end{aligned} \tag{3.60}$$

where $\boldsymbol{\sigma}_D^e = \frac{\mu}{J}(\bar{\mathbf{B}} - \frac{1}{3}\bar{I}_1\mathbf{1})$, $\mathbf{S}_D^e = \mu(J^{-2/3}\mathbf{1} - \frac{1}{3}\bar{I}_1\mathbf{C}^{-1})$

Since the quasi-linear viscoelastic model is a special case of nonlinear viscoelasticity and also an extension of elastic model, first a uniaxial tension is used to compare the result from degenerated QLV model by eliminating the effects of the time dependent property with the one from built-in neo-Hookean model, and then consider the time dependent behavior of QLV model by comparing with the Matlab result.

1. Reduction to elastic behavior: Uniaxial tension

A stretch loading is imposed on the right side of the body by the displacement control method till the stretch ratio of 3. When the time-dependent property is absent, the model reduces to an elastic response. Then after running the simulation, we can see the displacement contour in Fig. 51 and the stress-stretch relation curve in Fig. 52 are matched very well with the results obtained from built-in neo-Hookean model.

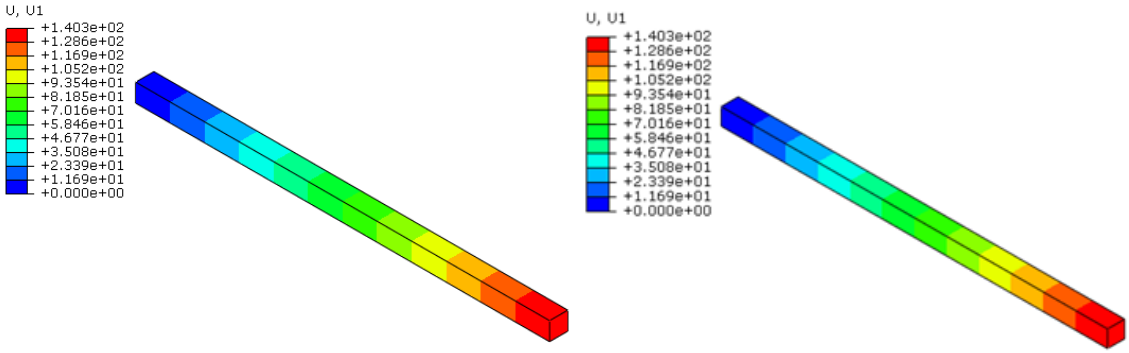

Fig. 51 x- direction displacement: Elastic response from the QLV model (Left) and Abaqus built-in neo-Hookean model (Right)

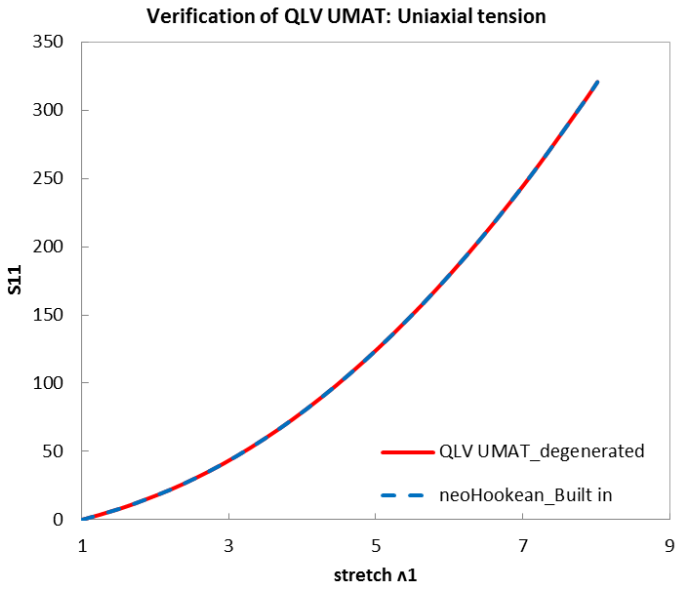

Fig. 52 Comparison of stress vs stretch between degenerated QLV model and Abaqus built-in neo-Hookean model under uniaxial tension

2. Time dependent behavior:

To consider the time dependent response of QLV model, we set up a loading history as shown in Fig. 53. The body is stretch along x direction for 20 seconds till the stretch ratio of 3 and then hold stretch unchanged for another 20 seconds. Fig. 54 showed that the results obtained from UMAT and Matlab match very well.

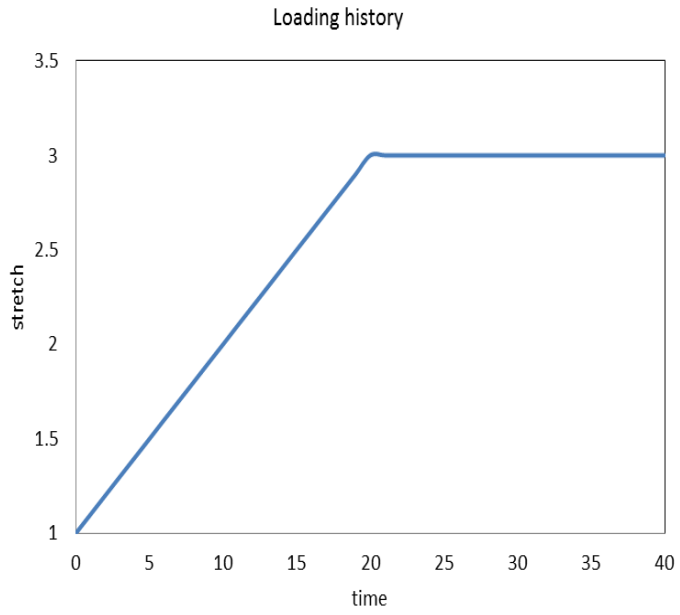

Fig. 53 Loading history for QLV model

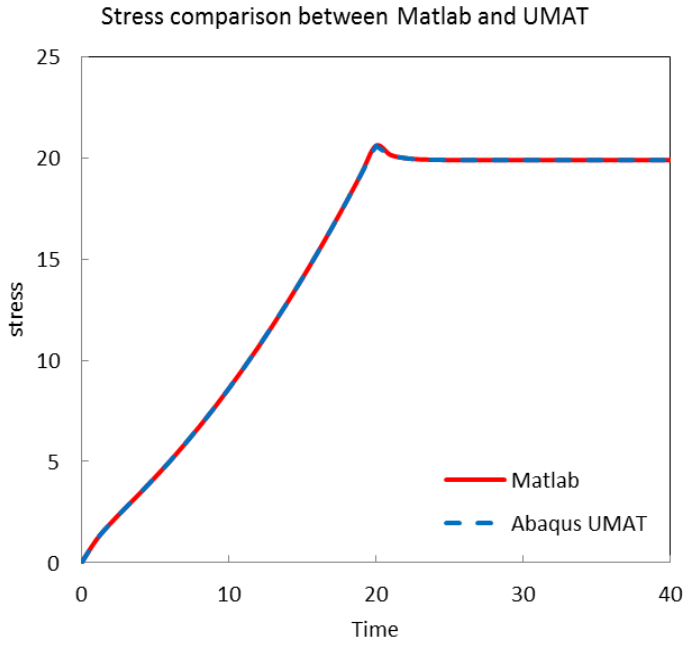

Fig. 54 Comparison of stress vs stretch between UMAT and Matlab under uniaxial tension for QLV model

3.3.3.2 Quasi-linear viscoelastic model of LASMPs

For the QLV model, two cases of uniaxial and biaxial tension problems for analysis to taken here to verify the UMAT code.

1. Uniaxial tension

Four loading steps, as discussed previously, were defined and for each step the time period is set to be 20s. Due to lack of the experimental data, we cannot determine how the formation and cleavage of the new network evolve under the light irradiation, so after 60s we kept the volume ratio of the second network and stress state to see how the body responses.

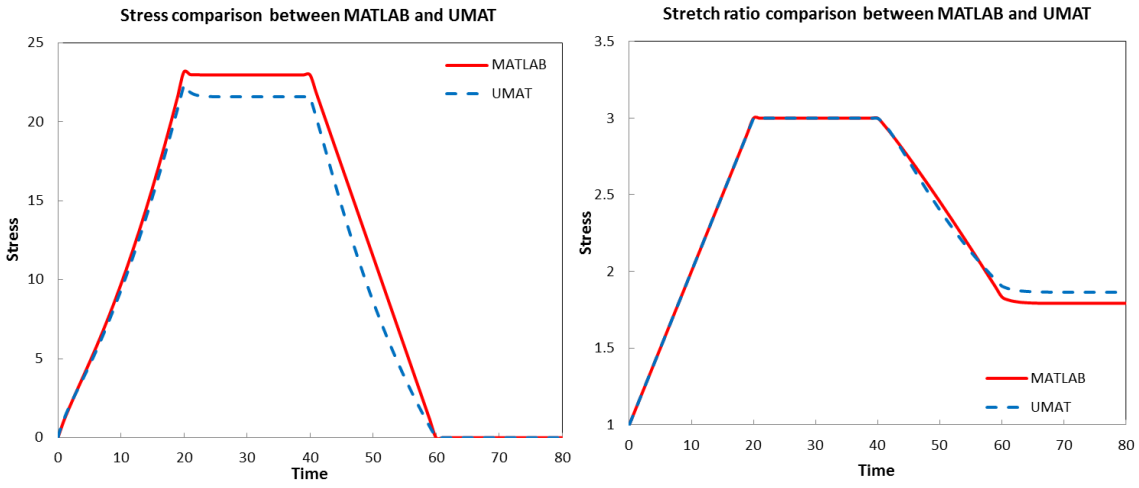

Fig. 55 Comparison between UMAT and Matlab for LASMP QLV model under uniaxial tension: Stress vs time (Left) and Stretch vs time (Right)

From the results, the UMAT code can give a good agreement with Matlab on the stress-stretch-time relationship. The small differences are caused by the numerical treatments, which actually can be reduced by small time increment.

2. Biaxial tension

To verify the capability of QLV UMAT code, we simulate the unequal biaxial tension case which was also calculated in Chapter II. In the first step, the body is stretched 60mm along x direction with stretch ratio of 4 and 40mm along y direction with stretch ratio of 3 in 20 seconds, and then followed by keeping stretch for 20 seconds for light irradiation. The corresponding force is then unloaded to zero in 20 seconds to see the response, and the response is monitored for 20 more seconds.

For the stress contour plots, we can clearly see that the stress relaxed during the light irradiation period although the stretch does not have change which is different from the elastic model. By the relationship curves between stress versus time and stretch versus time we also can find that the UMAT code has a good agreement in the results with Matlab. The small differences can also be reduced further by decreasing the time increment of the analysis.

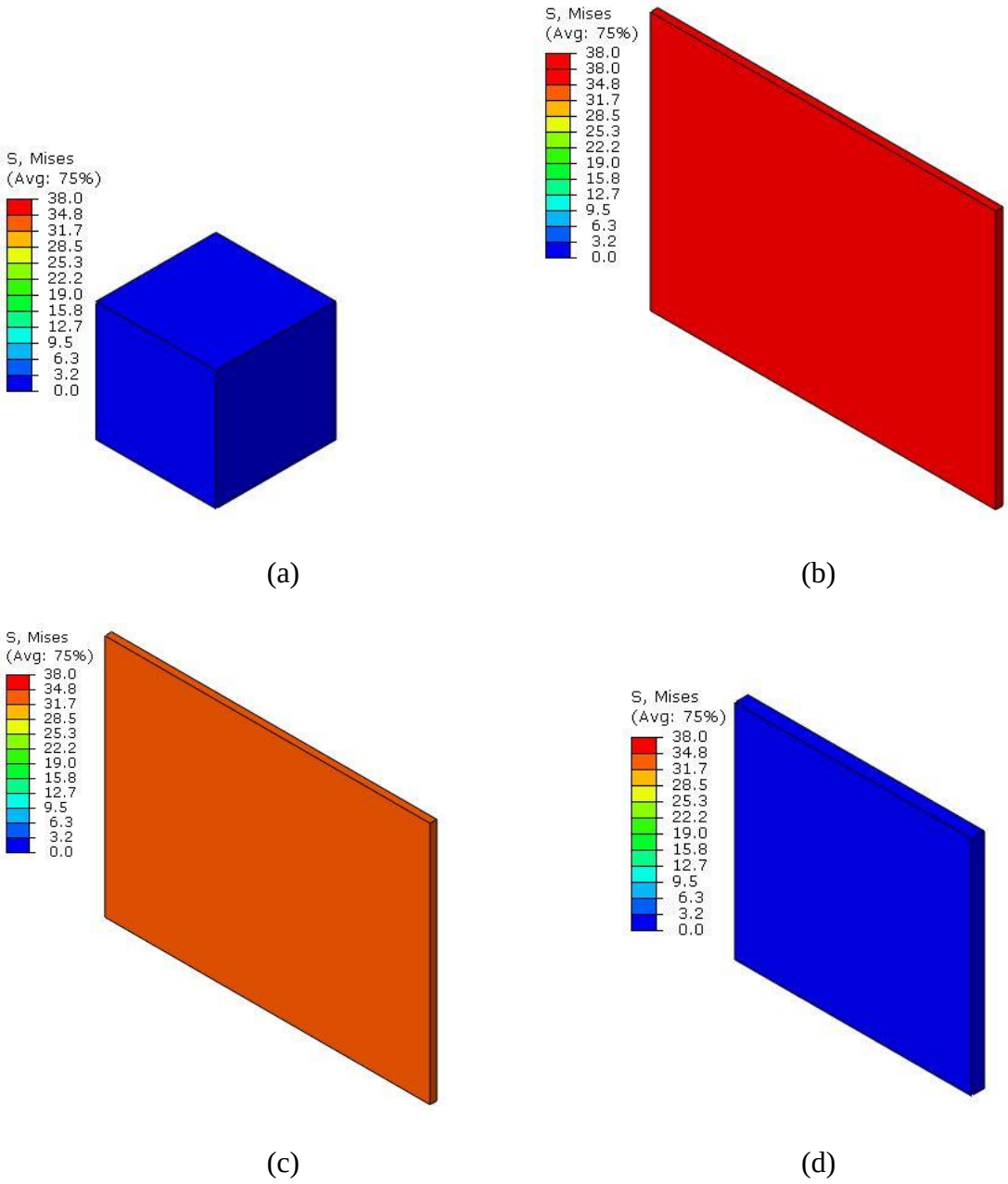

Fig. 56 Von mises stress of LASMP QLV model under biaxial tension: (a) t=0; (b) t=20; (c) t=40; (d) t=60

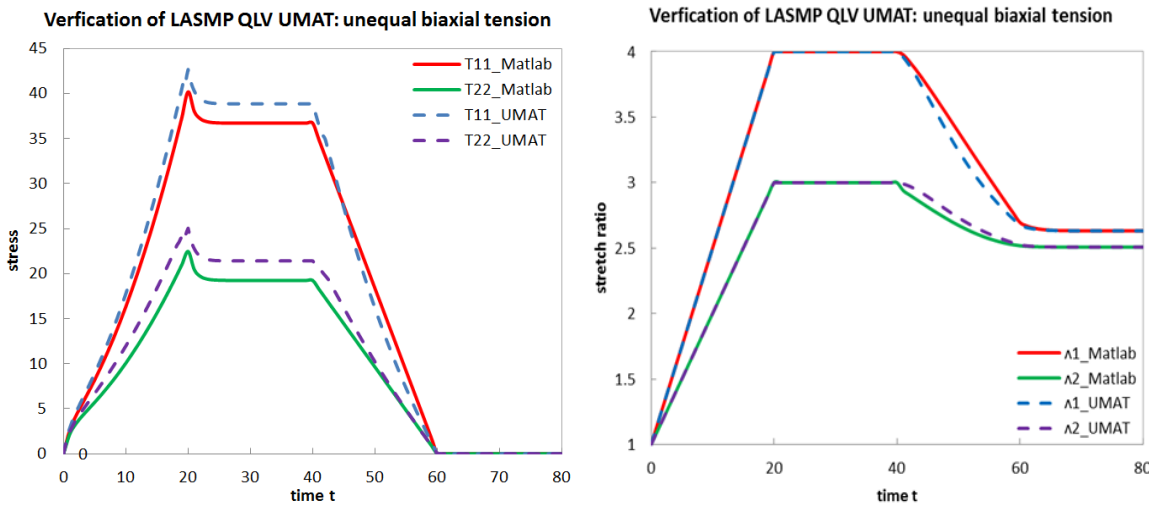

Fig. 57 Comparison between UMAT and Matlab for LASMP QLV model under biaxial tension: Stress vs time (Left) and Stretch vs time (Right)

3.3.3.3 Anisotropic quasi-linear viscoelastic model of LASMPs

If anisotropy of the second network is considered, only the elastic stress $\mathbf{S}_D^e$ of equation (3.49) or (3.50) need to be replaced by the anisotropic form which we have derived in section 3.4.2.

$$\mathbf{S}_D^e = \mu(J^{-2/3}\mathbf{1} - \frac{1}{3}\bar{\mathrm{I}}_1\mathbf{C}^{-1}) + 4C_{201}(J_1 - 1)\mathbf{n}_0 \otimes \mathbf{n}_0 + 4C_{202}(K_1 - 1)\mathbf{m}_0 \otimes \mathbf{m}_0 \tag{3.61}$$

By substituting equations (3.61) and (3.45) into equations (3.58)-(3.60), we can obtain:

$$\mathbb{C}_{ijkl}^{MZ-J} = (\mathbb{C}_{ijkl}^{MZ-J})_{iso} + (\mathbb{C}_{ijkl}^{MZ-J})_{aniso} \tag{3.62}$$

where $(\mathbb{C}_{ijkl}^{MZ-J})_{iso}$ is isotropic elastic material Jocobian same as (3.58) and $(\mathbb{C}_{ijkl}^{MZ-J})_{aniso}$ is anisotropic term which is expressed as:

$$
\begin{aligned}
(\mathbb{C}_{ijkl}^{MZ-J})_{aniso} = (1-\frac{\triangle \mathrm{t}}{2\tau}(1-\frac{\mu_\infty}{\mu_o}))[&\frac{8C_{201}}{J}(Fn_0)_i(Fn_0)_j(Fn_0)_k(Fn_0)_l \\
&+\frac{8C_{202}}{J}(Fm_0)_i(Fm_0)_j(Fm_0)_k(Fm_0)_l] \\
&+\frac{1}{2}\delta_{ik}[\frac{4C_{201}}{J}(J_1-1)(Fn_0)_j(Fn_0)_l+\frac{4C_{202}}{J}(K_1-1)(Fm_0)_j(Fm_0)_l] \\
&+\frac{1}{2}\delta_{jl}[\frac{4C_{201}}{J}(J_1-1)(Fn_0)_i(Fn_0)_k+\frac{4C_{202}}{J}(K_1-1)(Fm_0)_i(Fm_0)_k] \\
&+\frac{1}{2}\delta_{il}[\frac{4C_{201}}{J}(J_1-1)(Fn_0)_j(Fn_0)_k+\frac{4C_{202}}{J}(K_1-1)(Fm_0)_j(Fm_0)_k] \\
&+\frac{1}{2}\delta_{jk}[\frac{4C_{201}}{J}(J_1-1)(Fn_0)_i(Fn_0)_l+\frac{4C_{202}}{J}(K_1-1)(Fm_0)_i(Fm_0)_l]
\end{aligned}
\tag{3.63}
$$

For the Cauchy stress we need to update two terms: $\boldsymbol{\sigma}_D^e(t_n)$ and $\mathbf{P}(t_n)$.

$$
\boldsymbol{\sigma}_D^e = \frac{\mu}{J}(\bar{\mathbf{B}}-\frac{1}{3}\bar{\mathrm{I}}_1\mathbf{1})+\frac{4C_{201}}{J}(J_1-1)\mathbf{Fn}_0\otimes\mathbf{Fn}_0+\frac{4C_{202}}{J}(K_1-1)\mathbf{Fm}_0\otimes\mathbf{Fm}_0
$$

$\mathbf{P}(t_n)$ should be calculated by using anisotropic elastic stress of (3.61). Then by preserving the first network of LASMPs with isotropic QLV model and considering the second network with anisotropic QLV model, we use the simple uniaxial tension problem to investigate the responses. From the left picture of Fig. 58, we can see that the stress vs. time curves are same between anisotropic and isotropic QLV model, and the reason lies on that only first network is involved to carry the total stress before unloading and the unloading period is controlled by stress itself. From the right picture of Fig. 58 in the unloading period, the stretch decreases in a different way. The anisotropic model relaxes much slower since the anisotropic part of the second network stiffens the material.

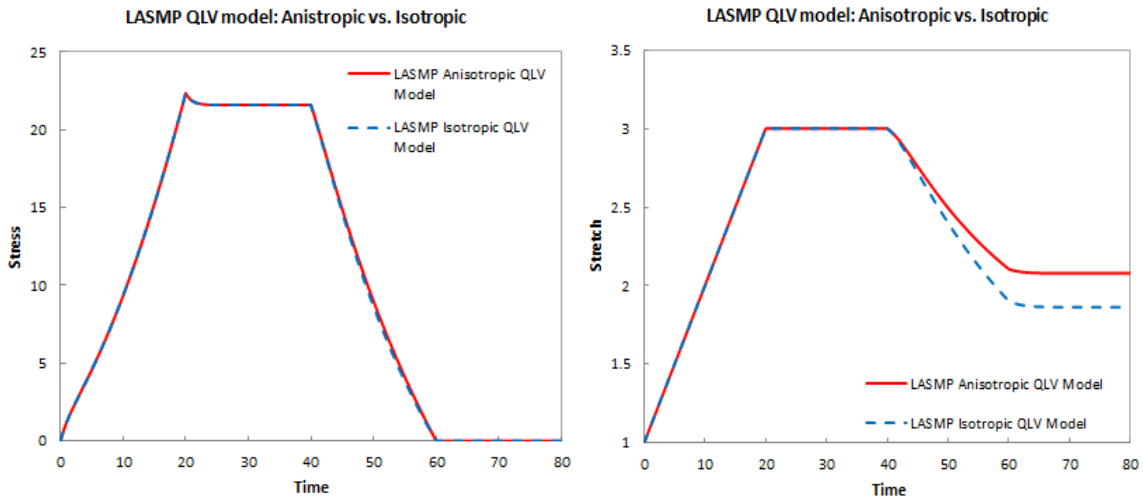

Fig. 58 Comparison between LASMP anisotropic QLV model and isotropic QLV model: Stress vs. time (Left) and Stretch vs. time (Right)

In this chapter, implementation of LASMPs models (elastic isotropic, elastic anisotropic, viscoelastic isotropic and anisotropic) in UMAT ABAQUS subroutine is presented. The responses from UMAT subroutine were compared with responses available in ABAQUS library and also analytical solutions, in order to validate the accuracy of the UMAT code. In the next chapter, several structural analyses on adaptive and shape reconfiguration structures are presented.

CHAPTER IV

ANALYSES OF FLEXIBLE AND FOLDABLE STRUCTURES

This chapter presents several structural analyses of flexible and foldable structures that can be deformed by mechanical or thermal stimulus and whose shapes are retained by light irradiation in the LASMP components. The influence of material isotropy and anisotropy, and stress relaxation behavior on the shape reconfiguration is also examined.

4.1 Bending and torsion

Let us first consider a LASMP plate of dimension 60mm x 20mm x 4 mm, as illustrated in Fig. 59. The plate is fixed on the left end. The initial deformation is produced by imposing a bending moment of 80N·M on the right end. Once bending is achieved, light irradiation is prescribed followed by releasing the bending moment. Upon removing the moment, the plate only partially just relaxes back and retaining a bending shape. In the simulation, the shear modulus of 5MPa for the first network and 20MPa for the second network and a volume ratio of 1.0 are used. A similar plate is now subjected to a twisting moment of 40 N·M, and the response of the plate is shown in Fig 60. After light activation and releasing the moment, the body still preserves a large twist deformation.

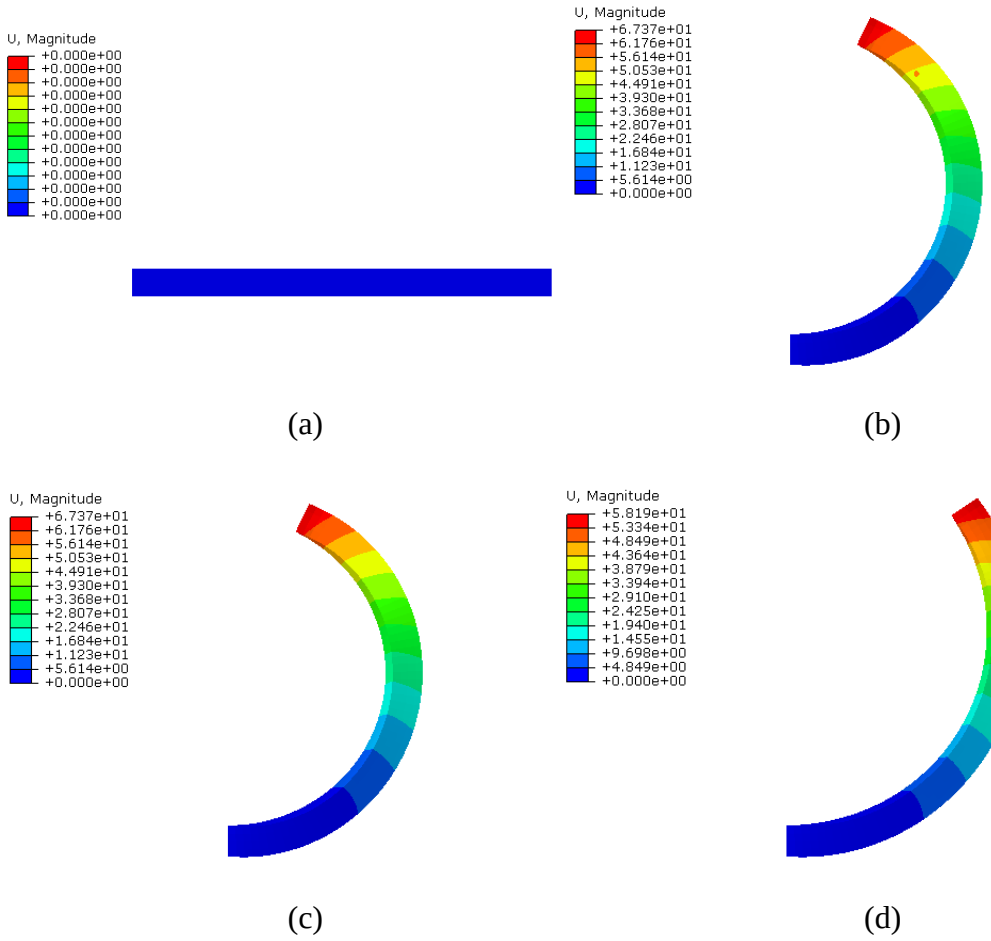

Fig. 59 Displacement magnitude of LASMP plate under bending: (a) original shape (b) intermediate shape after loading but before light activation; (c) intermediate shape after light activation; (d) shape after unloading

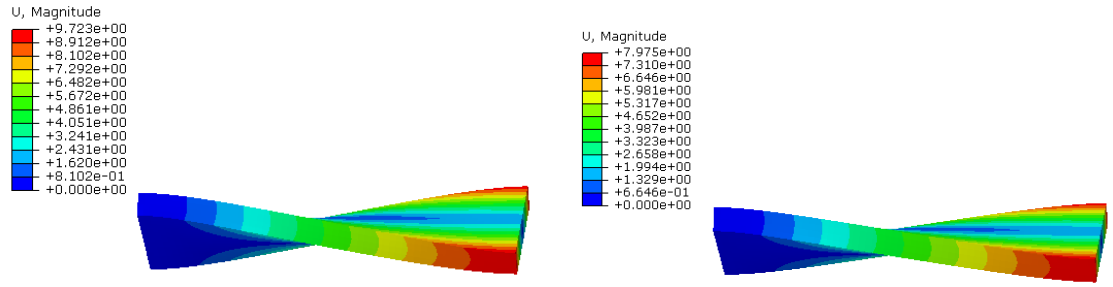

Fig. 60 Displacement magnitude under torsion: Before unloading (Left) and After unloading (Right)

4.2 Two-layer composite under tension

Next we will consider a composite structure made of LASMPs and inactive material. As shown in Fig.61, the structure is made of two layers with hyperelastic material on the top and LASMP at the bottom, and each layer is a plate geometry of 60mm x 20mm x 2 mm. The bilayer is first stretched uniaxially along its longitudinal axis to a stretch ratio of 2. At this stretch ratio, the LASMP is radiated to induce phase transformation and retain the current shape. The material parameters for LASMPs are $\mu_a = 5MPa,\ \mu_b = 20MPa,\ \alpha$=1.0 , and the top layer is an incompressible neo-Hookean solid with shear modulus of 5MPa. When the left side of the body is totally fixed, upon removing the axial loading that causes the stretching, bending deformation is achieved as shown in Fig. 62.

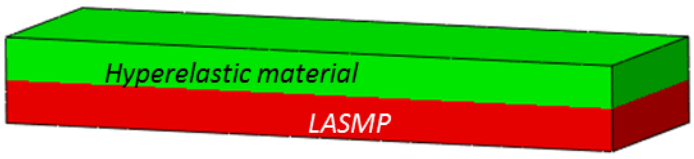

Fig. 61 Geometry of two-layer composite

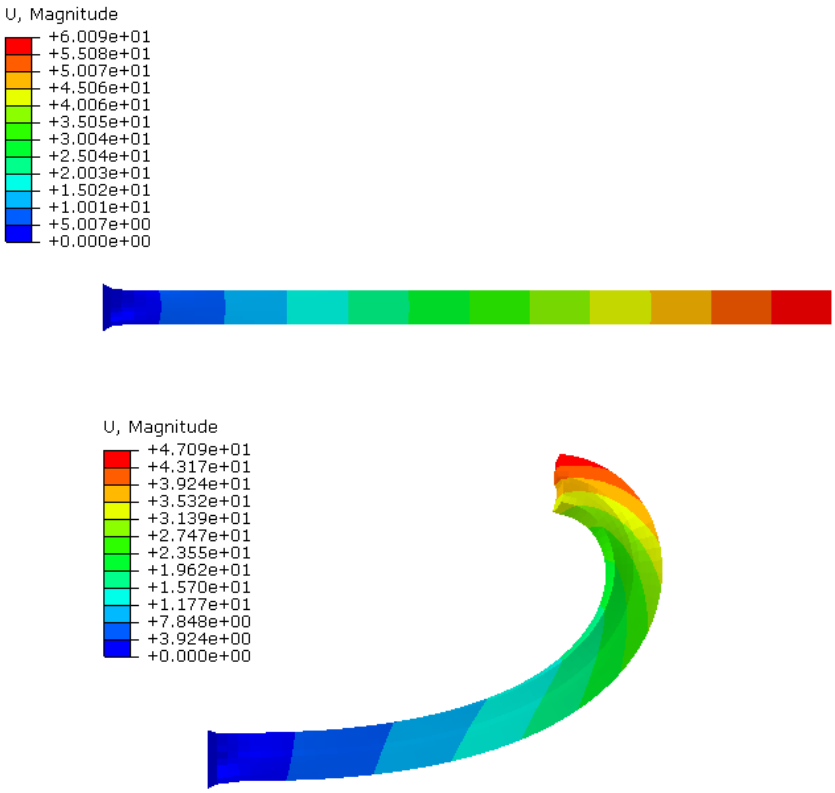

Fig. 62 Displacement magnitude of two-layer composite under stretch with fixed end constraint: Before unloading (Above) and After unloading (Below)

4.3 Multiple patches tension

Another example is on placing LASMP patches on elastic substrates and depending on the locations and arrangements of patches and external prescribed stimuli, various shape configurations can be obtained. The structure is mechanically stretched along the x direction and followed by releasing the load. The following cases are considered:

(1) Two LASMP patches are integrated to an elastic body as shown in Fig. 63. The body is an incompressible neo-Hookean plate with dimension of 60 mm x 20mm x 8mm, and the patch dimension is 8mm x 8mm x 4mm. We stretch the body along x

direction by displacement of 60mm and then keep the stretch constant for light activation, and then unload the force completely. The shear modulus of the main body is $\mu = 20MPa$ and the parameters for LASMPs are $\mu_a = 5MPa$, $\mu_b = 20MPa$, α=1.0.

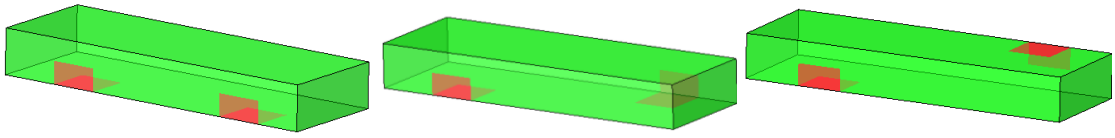

(a) (b) (c)

Fig. 63 Geometry of plates with two LASMP patches

Fig. 64 shows the von Mises stress contour after loading and unloading and also the displacement magnitude after unloading. Similar to the result of two-layer composite plate tension problem, the body will curve up after releasing the force. But due to the location of the patches, the body is also twisted at the free end. Since the LASMP patches are much softer than the elastic body, the LASMP parts experience much large strain during loading that causes larger stress of the elastic body that is bonded with LASMP patches. After unloading, the elastic body tends to return back to the original shape while LASMPs become much stiffer and tends to retain the deformation. The results in Fig. 65 and Fig. 66 show different responses when different patches are arranged.

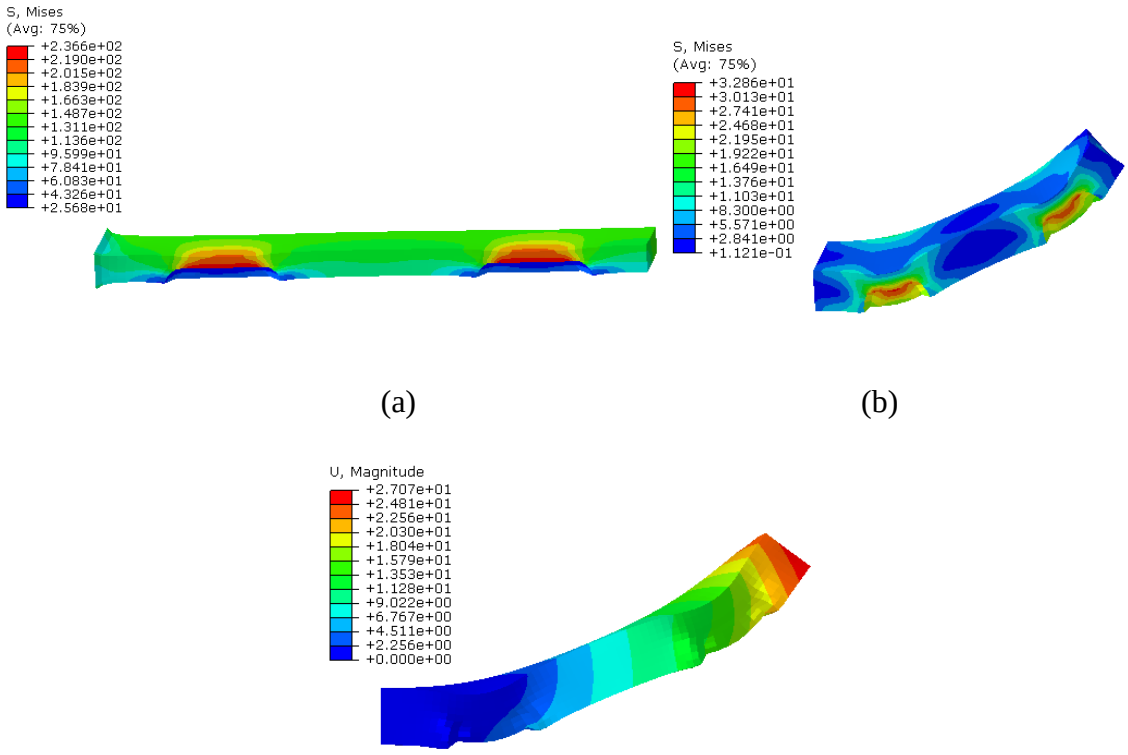

Fig. 64 Output of plate with geometry Fig 63(a) under stretch: (a) Von mises stress before unloading; (b) von-Mises stress after unloading; (c) displacement magnitude after unloading

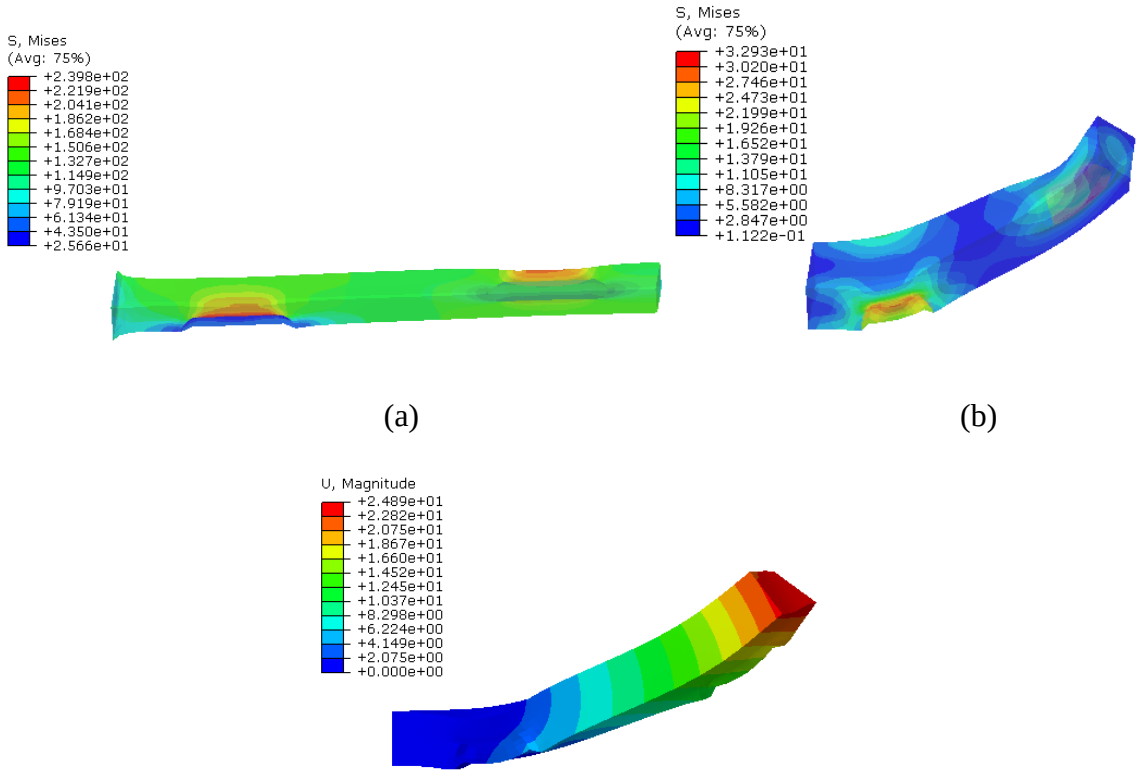

Fig. 65 Output of plate with geometry Fig 63(b) under stretch: (a) Von mises stress before unloading; (b) Von-mises stress after unloading; (c) displacement magnitude after unloading

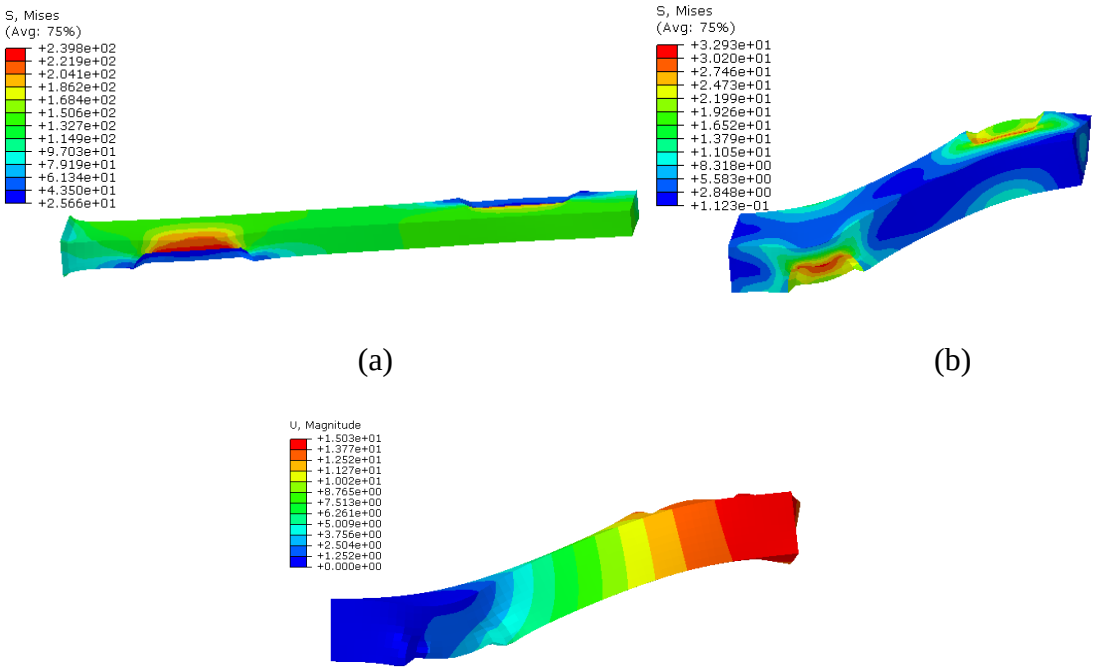

Fig. 66 Output of plate with geometry Fig 63(c) under stretch: (a) Von mises stress before unloading; (b) Von-mises stress after unloading; (c) displacement magnitude after unloading

(2) Three patches incorporated in the elastic body as shown in Fig. 67. Different deformed shapes are expected in these arrangements. Upon unloading, the existence of the new patch tries to pull back the body to the opposite direction. From the displacement magnitude, it is seen that when the three patches are on the same side (up or down), the body will significantly curve upward, while Fig. 70(c) showed less twisting but a wavy shape.

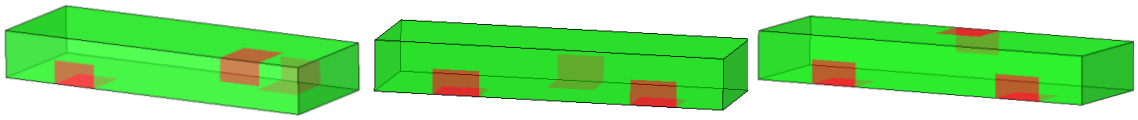

(a) (b) (c)

Fig. 67 Geometry of plates with three LASMP patches

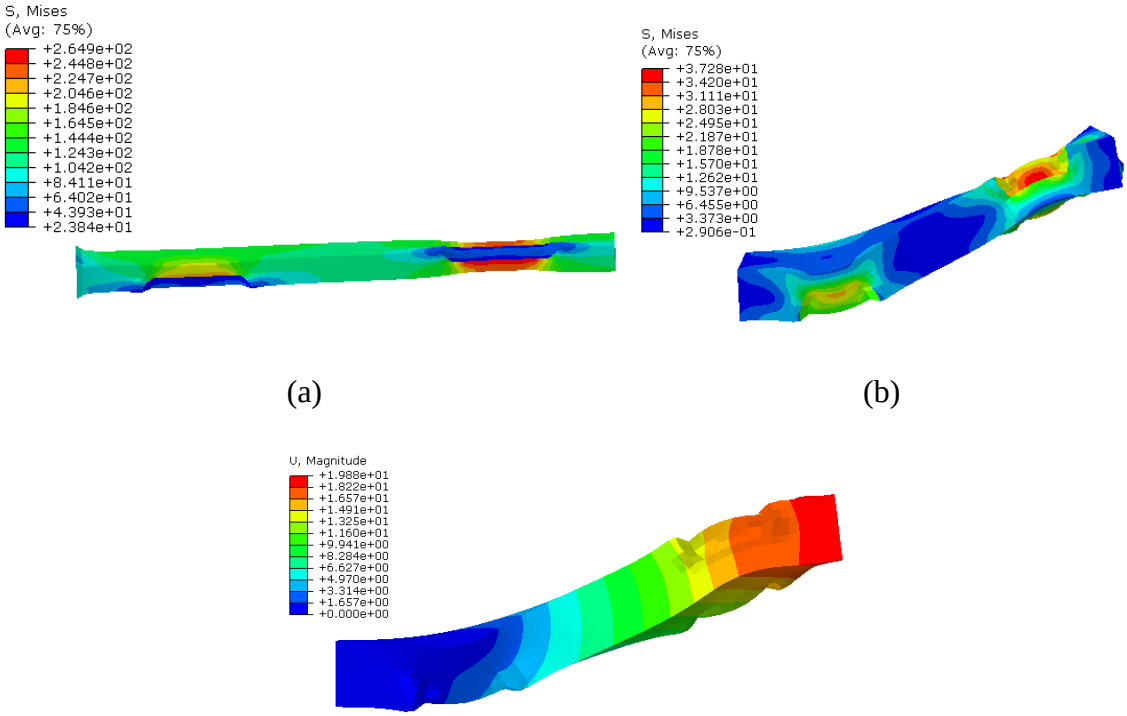

(a) (b)

(c)

Fig. 68 Output of plate with geometry Fig. 67(a) under stretch: (a) Von mises stress before unloading; (b) Von-mises stress after unloading; (c) displacement magnitude after unloading

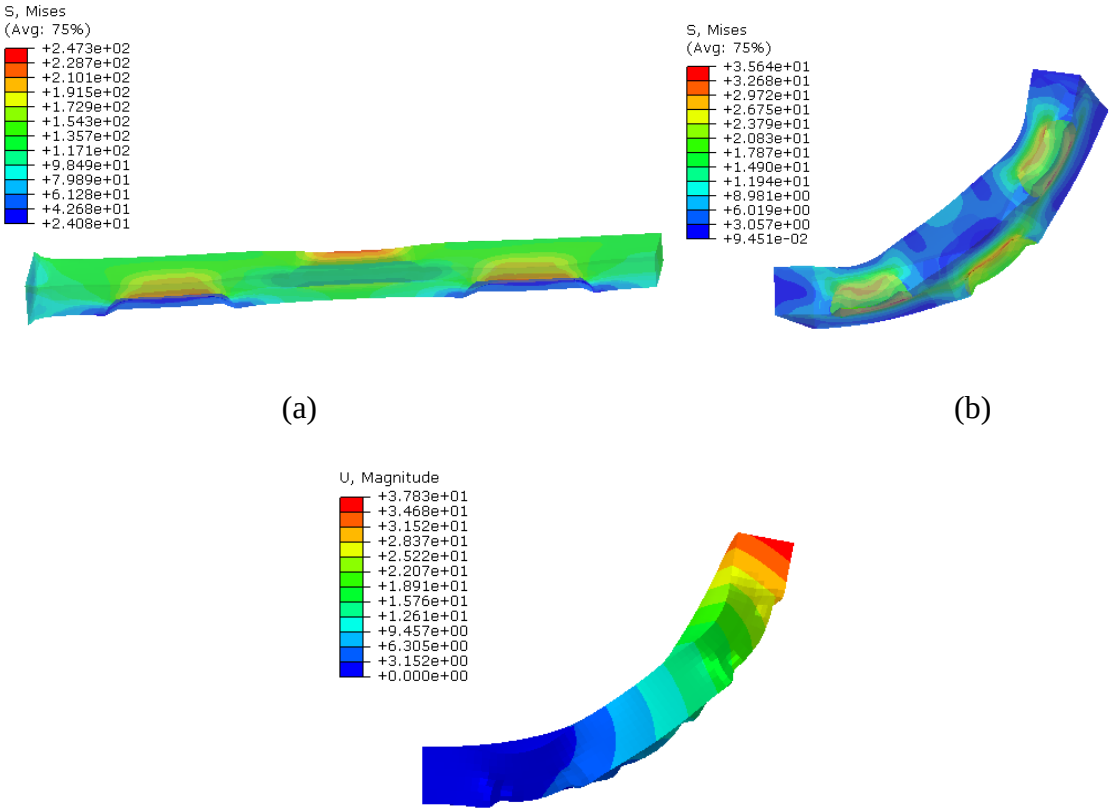

Fig. 69 Output of plate with geometry Fig 67(b) under stretch: (a) Von mises stress before unloading; (b) Von-mises stress after unloading; (c) displacement magnitude after unloading

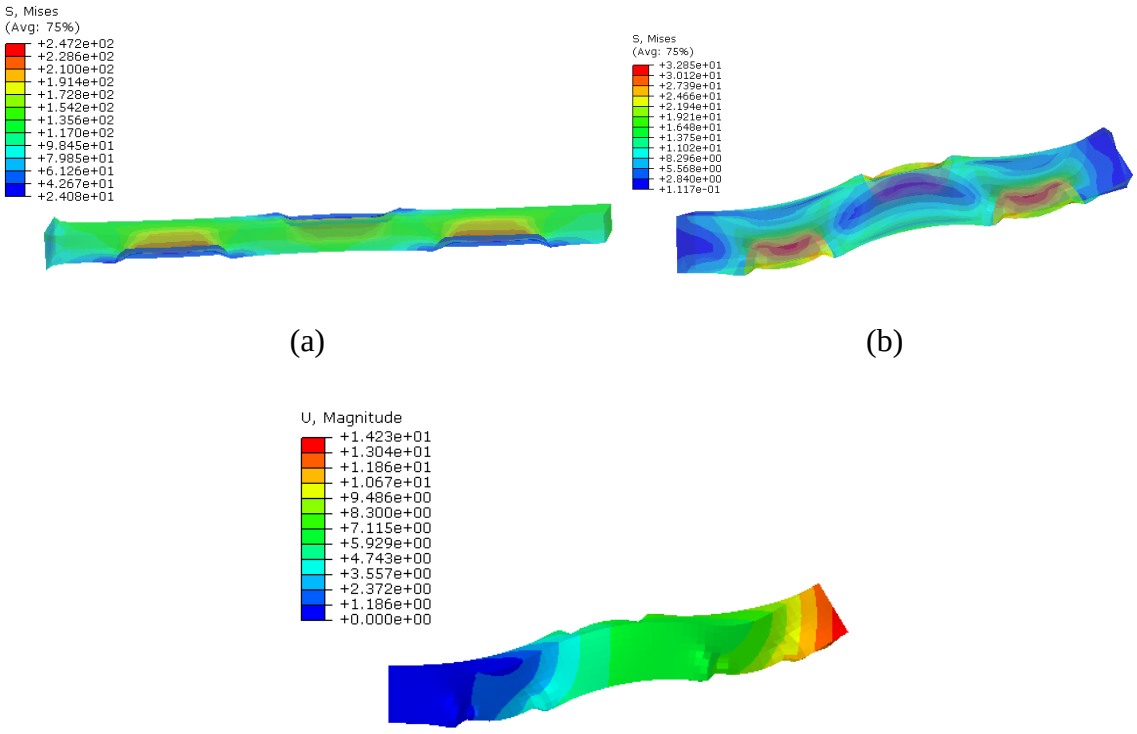

Fig. 70 Output of plate with geometry Fig 67(c) under stretch: (a) Von mises stress before unloading; (b) Von-mises stress after unloading; (c) displacement magnitude after unloading

(3) Finally we consider a case of four LASMP patches distributed as below. Because the patches are distributed in an even and regular way, after releasing the load it shows a obvious twisted shape other than a bending bebavior

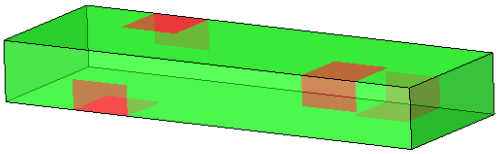

Fig. 71 Geometry of plates with four LASMP patches

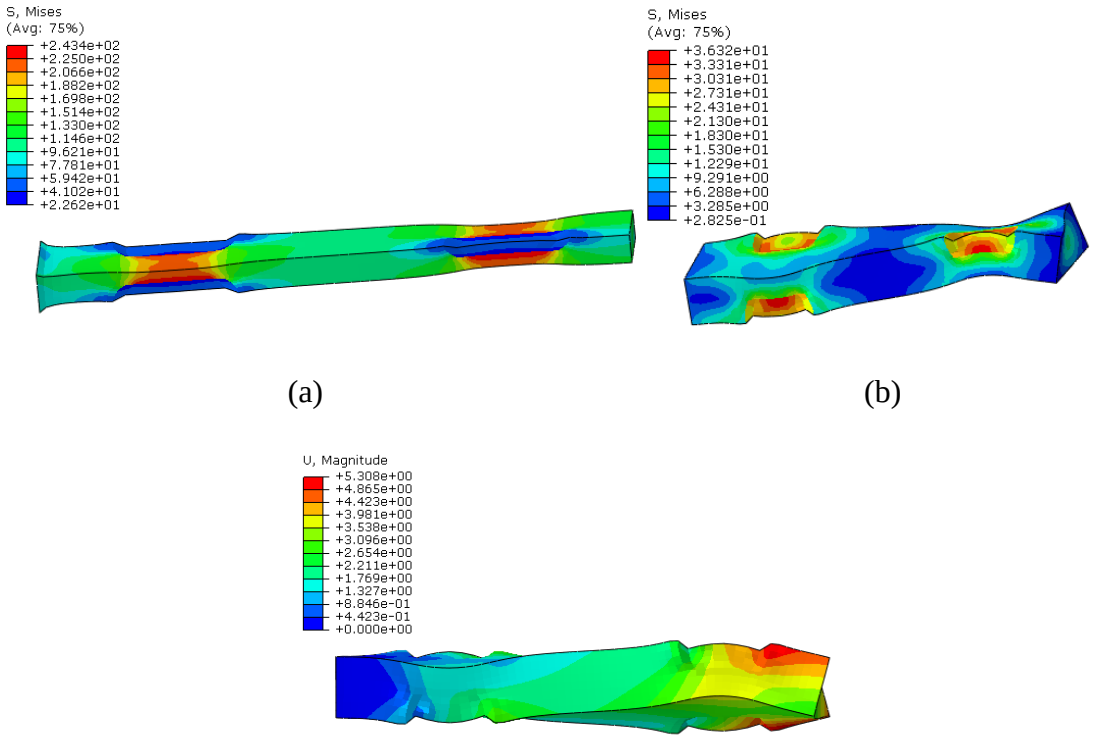

Fig. 72 Output of plate with geometry Fig. 71 under stretch: (a) Von mises stress before unloading; (b) Von-mises stress after unloading; (c) displacement magnitude after unloading

From the above analysis, we can design different geometries by adjusting the quantities and location of the LASMP patches to induce various shape changes. One can also consider a whole plate made of LASMP materials, but radiating it at different locations can induce different shape reconfigurations.

4.4 Flapping wing

LASMPs can also potentially be used to control shape changes in wing systems. Here we show an example of a flapping wing structure as shown in Fig. 73 which uses

the LASMPs to connect the other two elastic wings. Since the LASMPs have the shape memory functionality, the structure will have the flexibility to change its configurations at different state.

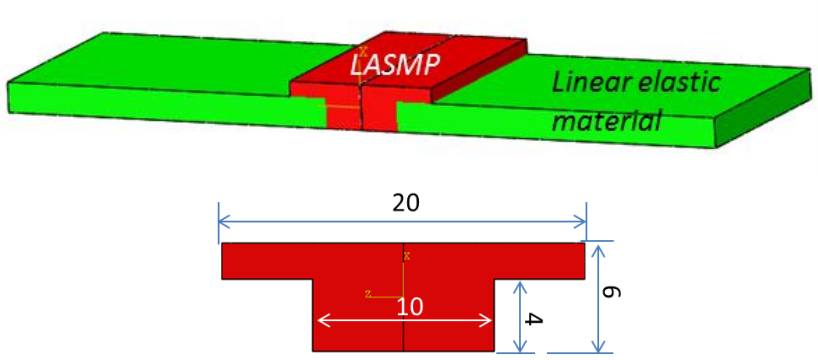

Fig. 73 Geometry of soldered plate

The structure is made of two linear elastic materials with modulus $\mu = 10^5 MPa$ and Poisson ratio $\nu = 0.3$, connected by LASMPs with the properties $\mu_a = 5MPa$, $\mu_b = 20MPa$, α=1.0. The linear elastic material has much larger modulus compared to that of LASMPs. Two calculations are carried out by imposing the bending moment of negative and positive 800 N·M on the outer edge of the structure along the width direction。

From the results we can see that the flat wing structures bend with an angle of 155^o due to the bending moment. After the light irradiation and unloading the force, the wing structure slightly springs back to a bending angle of 160^o. Further exposing the LASMPs to light of a specific frequency, shape recovery can be achieved. This flapping

wing analysis provides an example of the possibility using LASMPs to induce large deformation needed or different desired shapes during service.

1. Moment: -800 N·M

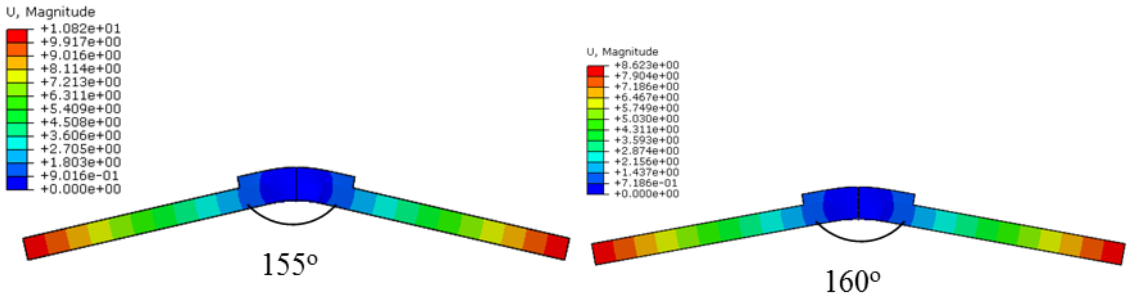

Fig. 74 Displacement magnitude of soldered plate under bending of -800 N·M: Before unloading (Left) and After unloading (Right)

2. Moment: 800 N·M

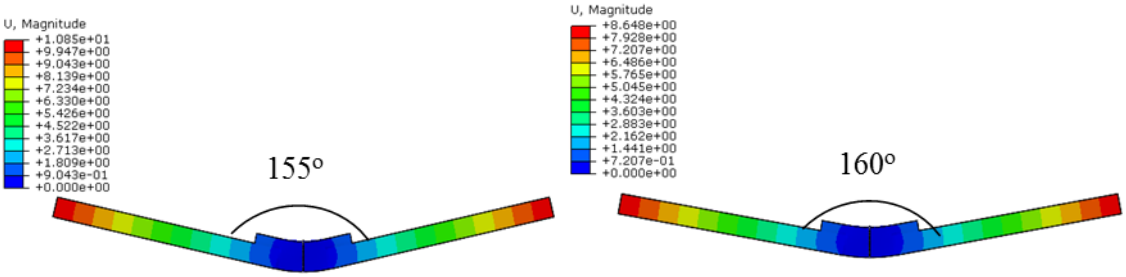

Fig. 75 Displacement magnitude of soldered plate under bending of 800 N·M: Before unloading (Left) and After unloading (Right)

4.5 Foldable structures

(1) Single winglet

Shape memory materials have promising applications in airplane or spacecraft engineering. By employing the shape memory materials, the structures can morph into

different shapes. Fig.76 shows a single winglet structure made of two linear elastic plates and LASMP curved plated connected in between the two plates.

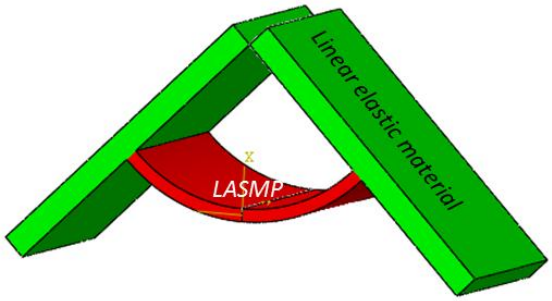

Fig. 76 Geometry of single winglet

Two simulations were carried out: one is to impose a bending moment of 200MPa to open up the wings and the other is to impose a bending moment of -400MPa to close off the wings. Fig.77 is the initial state of the wings with angle of 90^{o}.

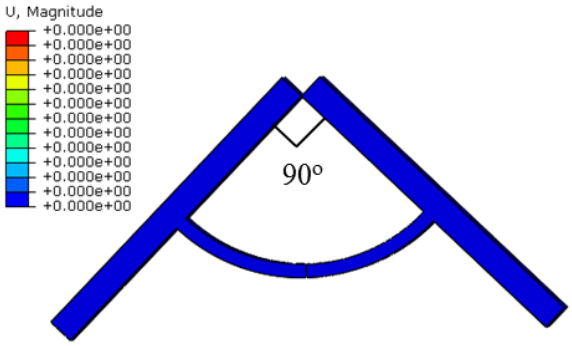

Fig. 77 Initial state of single winglet

When the bending moment is 200 N·M, the angle of wings opens up to 94.8^{o}, and after light irradition and removal of the moment the angle decerases slightly to 94^{o}. Figure 78 illustrates the shape changes before and after removal of the moment.

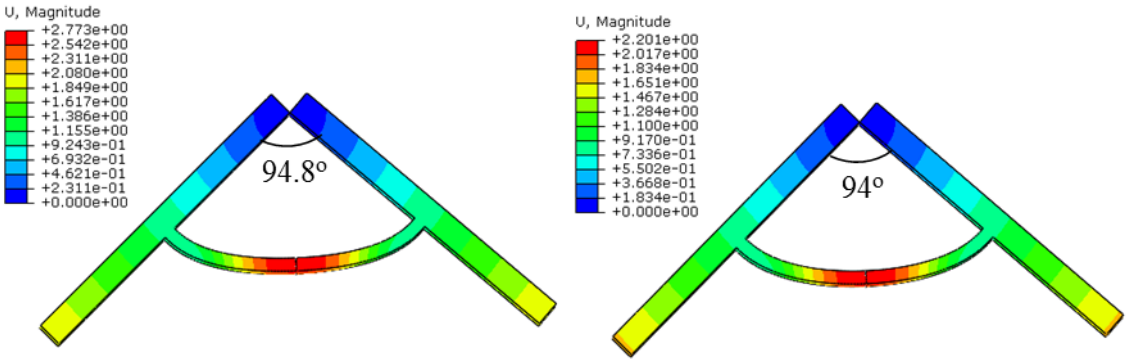

Fig. 78 Deformed state of single winglet under bending moment of 200N·M: Before unloading (Left) and After unloading (Right)

When a moment of -400MPa is considered, the wings bends to be an angle of 67.6°, and go back and keep at the angle of 72.6° after the light activation and release of the moment (Fig. 79).

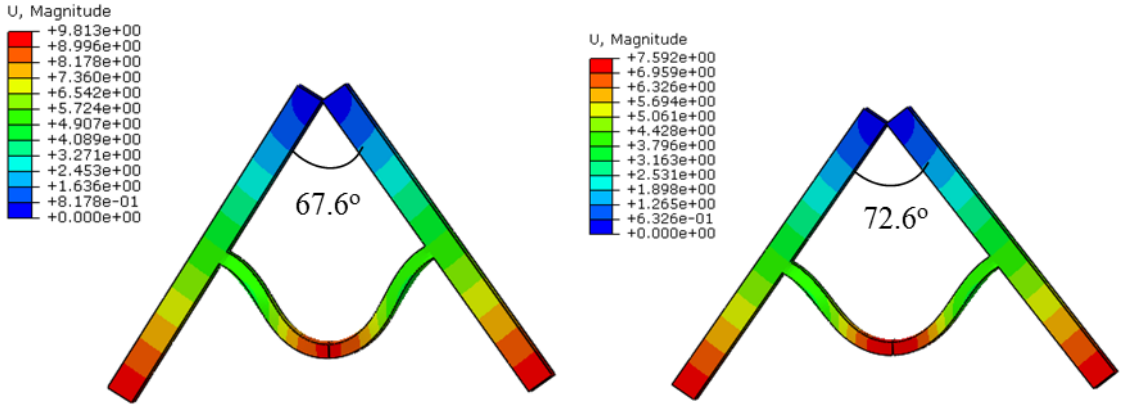

Fig. 79 Deformed state of single winglet under bending moment of -400N·M: Before unloading (Left) and After unloading (Right)

(2) Multi- winglets

After simulating the deformation of a single wing structure, we can create folding systems by combining multiple wings with LASMPs as connectors for controlling shape configurations (Fig. 80). Plates A, B and C are elastic panels and the red curved plates in

between are LASMP materials. The three wings are jointed at the top and can rotate with the same pivot center.

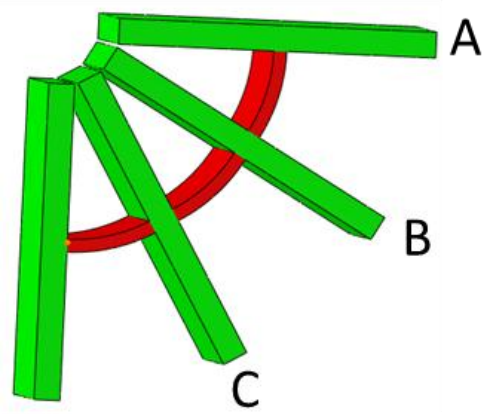

Fig. 80 Geometry of multi-winglets

Several cases are studied which will be demonstrated below.

1. Imposing different magnitude of bending moments to plates A, B, C at the same time. The bending moments exerted on plates A, B, and C are -1500 N·mm, -600 N·mm and -300 N·mm, respectively. Fig.81 showed four deformation states of displacement magnitude.

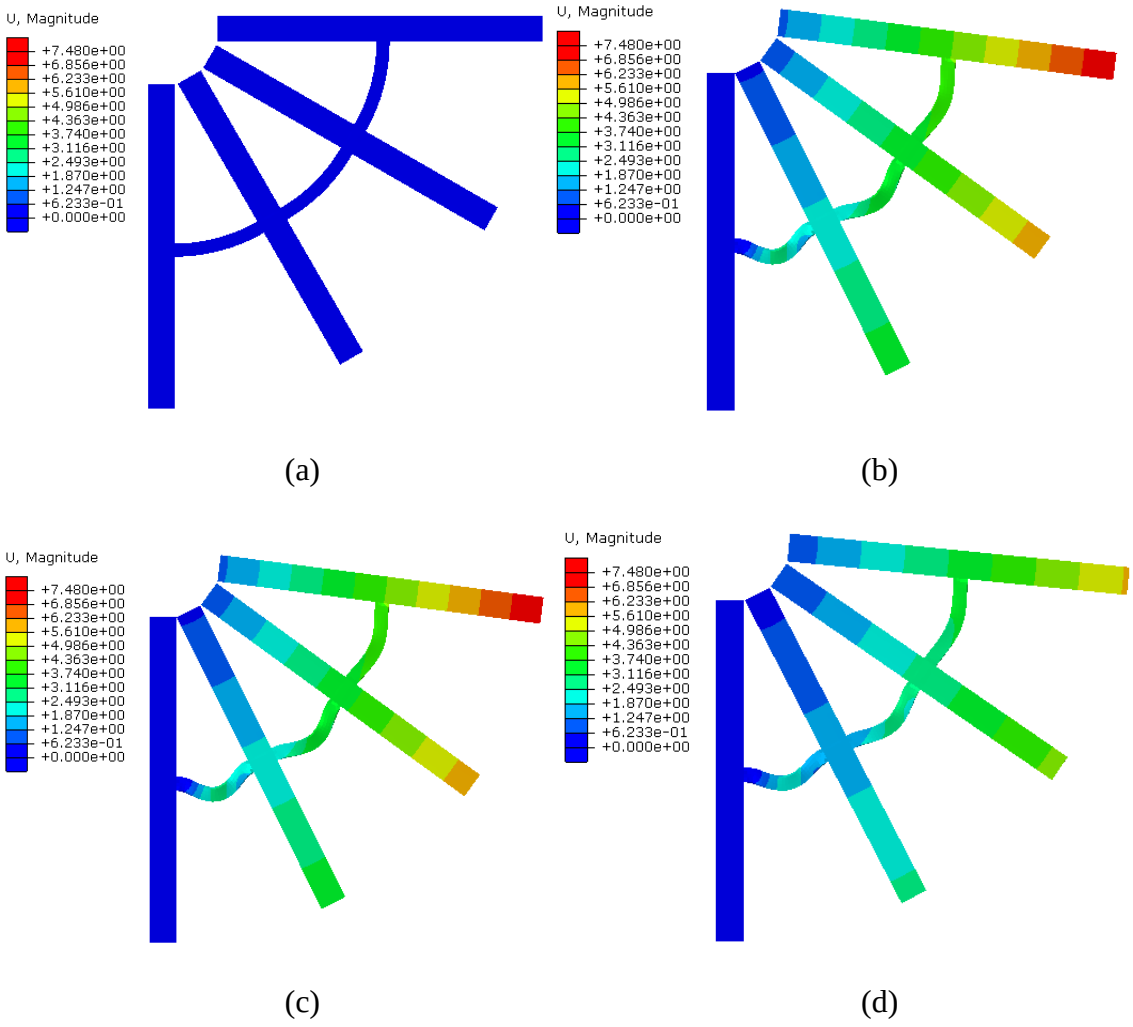

Fig. 81 Multi-winglets by imposing different bending moments simultaneously: (a) initial state; (b) intermediate state after loading but before activation; (c) intermediate state after activation; (d) after unloading state

2. Imposing the same magnitude of bending moment to plates A, B, and C sequentially. The bending moment is -2000 N·mm which is exerted on plate C first and then on plate B, followed by plate A. At each loading period, we keep the folded plates fixed and further deform the unfolded plates. For example, when we analyze the step of bending moment placing on the plate B, we fixed the plate C since it has already folded

completely, and similarly we fixed plate C and B for analyzing the step of bending moment placing on plate A. The simulation results are shown in Fig. 82, and the angle is changed from 90^{o} to 83.3^{o} to 84.7^{o}.

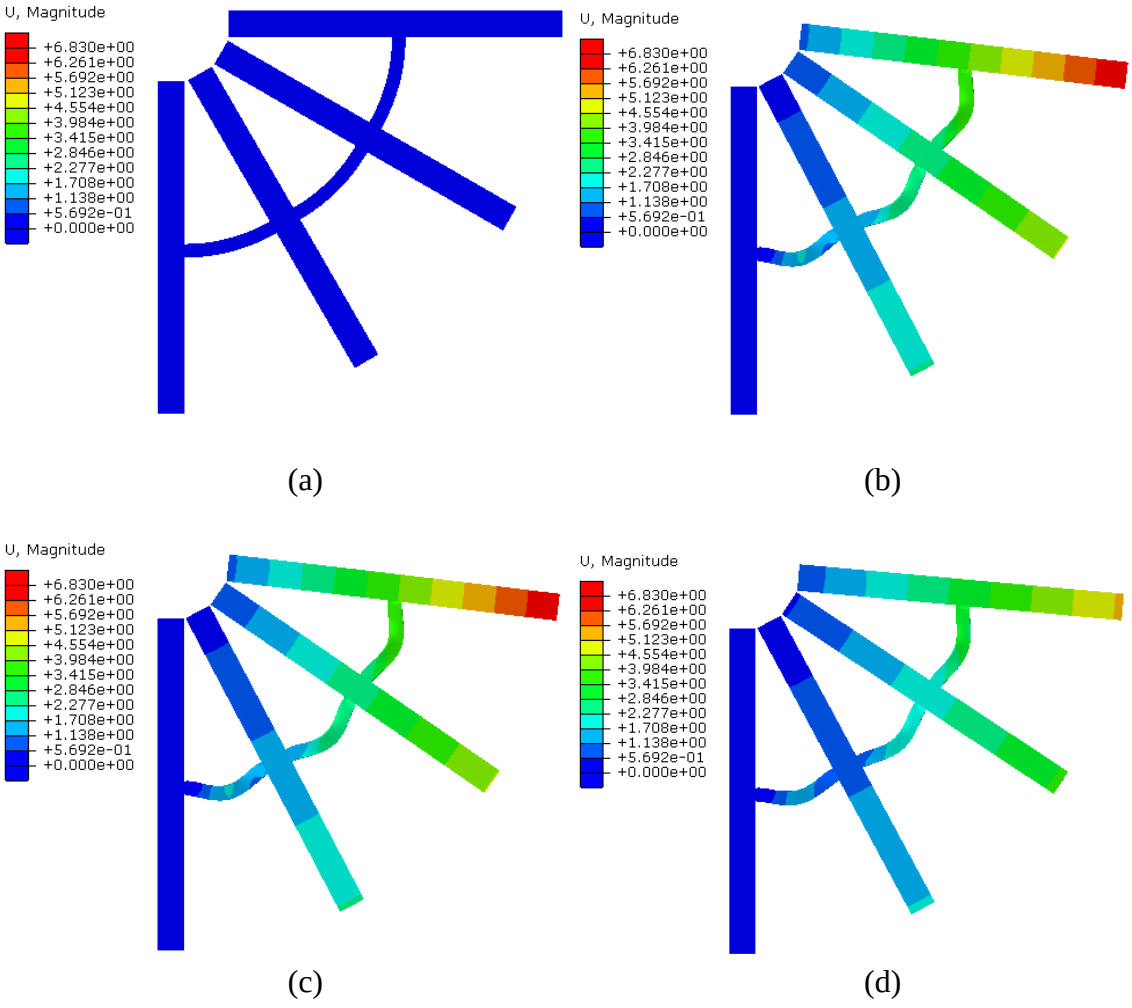

Fig. 82 Multi-winglets by imposing same bending moments sequentially: (a) initial state; (b) intermediate state after loading but before activation; (c) intermediate state after activation; (d) after unloading state

3. Based on the above case, we increase the bending moment to 2500 N·mm and load sequentially. To simulate the folding procedure much accurately, we cut the top of the

plate a little bit in order to all the plate rotate around the same pivot center. The results are shown below, and the angle changes from 90^o to 78^o to 81^o.

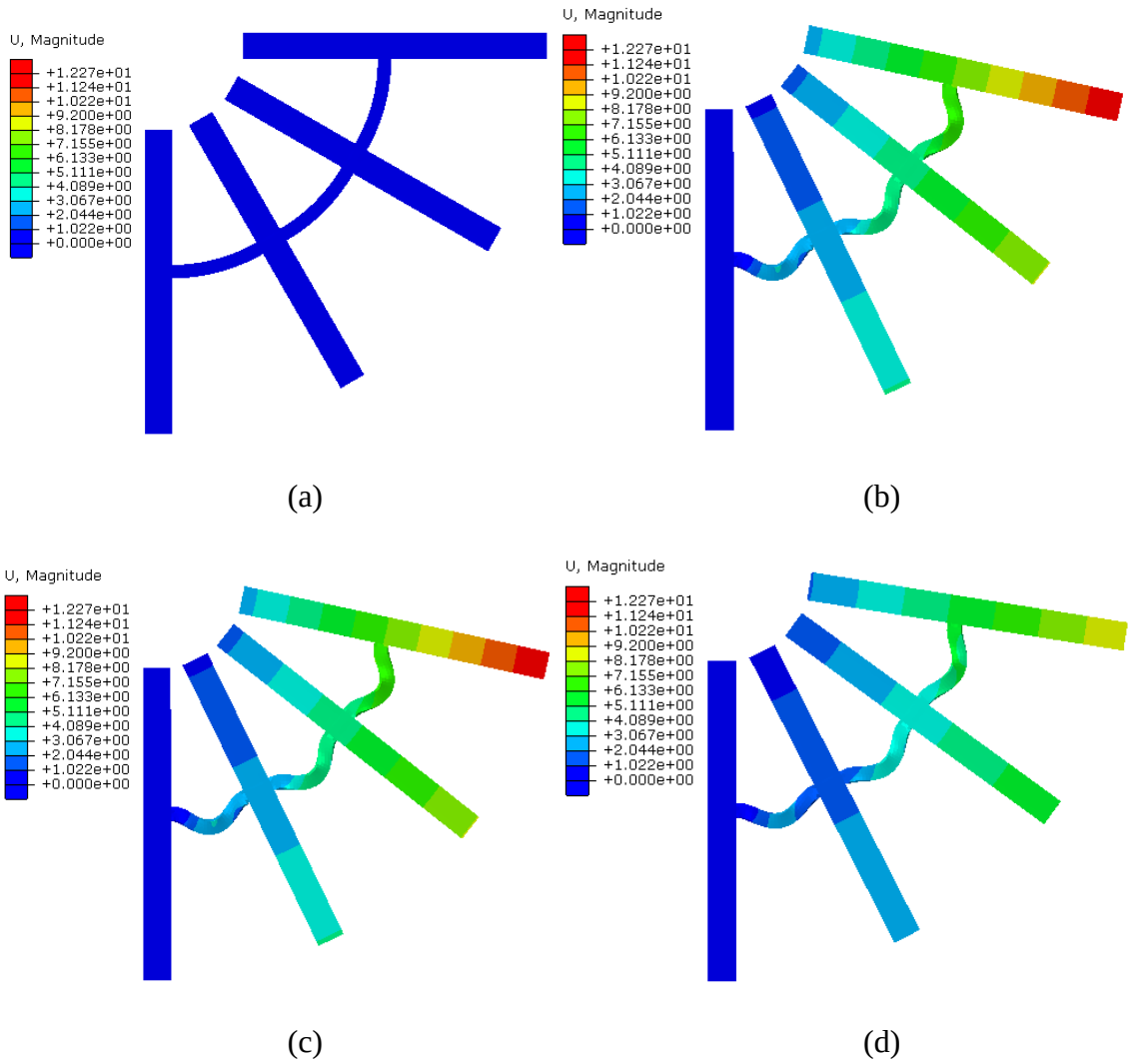

Fig. 83 Multi-winglets by imposing same bending moments sequentially: (a) initial state; (b) intermediate state after loading but before activation; (c) intermediate state after activation; (d) after unloading state

However, in all the above calculations the angle does not change large enough. So to address this problem, we change the geometry a little bit and place the LASMP plate connected at the distance of 5mm away from the edge of the wings as shown in Fig.

84. The same magnitude of -2000MPa of the bending moment are exerted on plate A, B, C sequentially again, and from the results we can see that the structure experienced a very large deformation now.

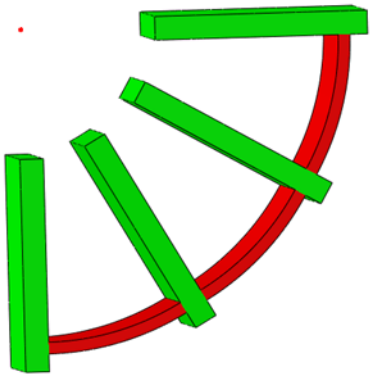

Fig. 84 New geometry of multi-winglets

Fig. 85 presents the deformation at different states. Upon loading, the angle can achieve to 37.6^{o}, and after light irradiation the angle can keep at 53^{o} when stress free. And furthermore, the angle can be decreased more by optimizing the geometry.

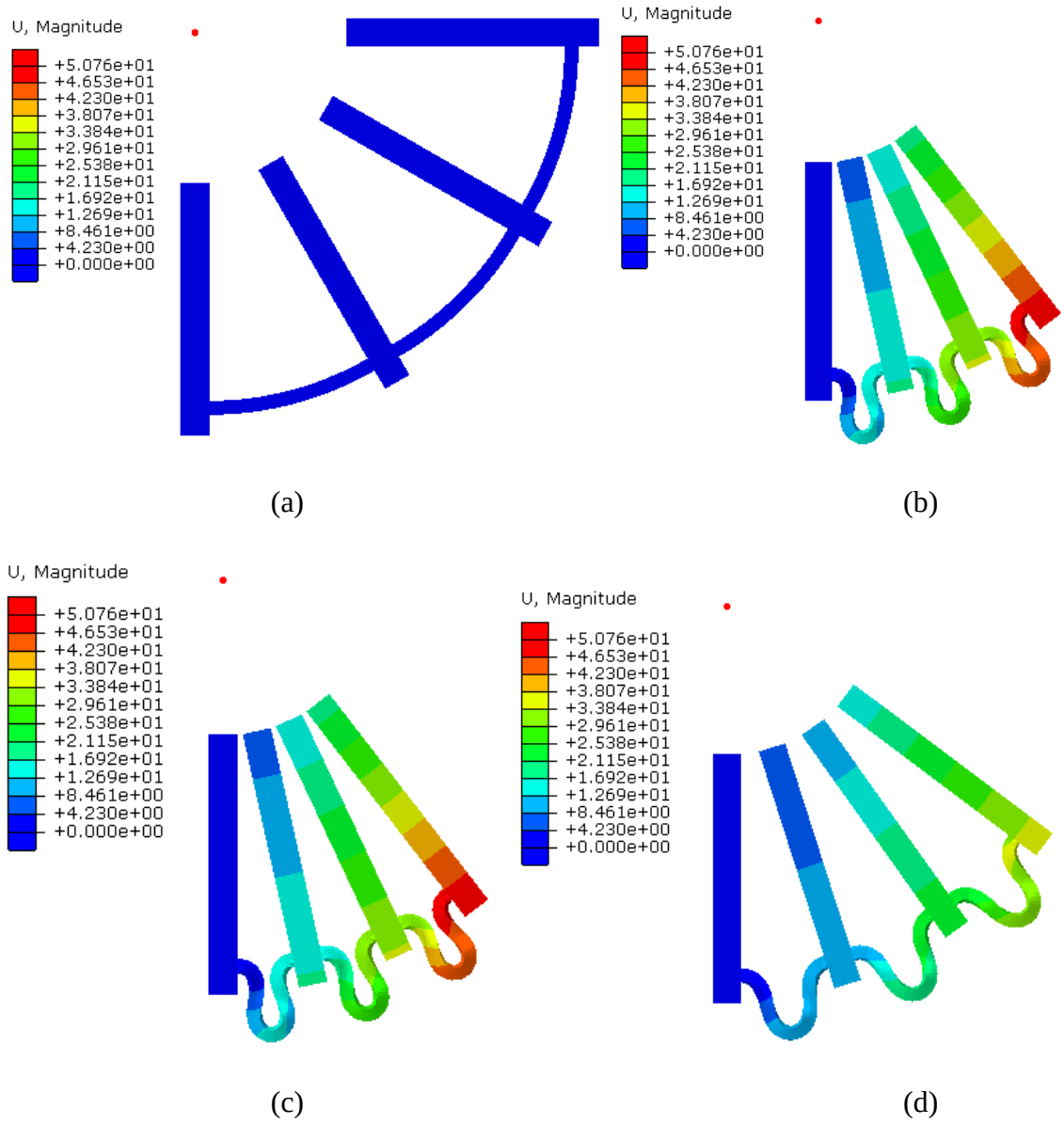

Fig. 85 New multi-winglets by imposing same bending moments sequentially: (a) initial state; (b) intermediate state after loading but before activation; (c) intermediate state after activation; (d) after unloading state

4.6 Thermal expansion induced shape deformation

All the above discussions are based on that the initial deformation of the LASMPs that are caused by the mechanical loading, but actually the deformation can be

achieved by many ways, here we just show one example which is a thermal expansion induced shape deformation.

For example, we can consider a lattice structure below, which was discussed in Janbaz et al. 2016 [81], for demonstration. The green parts are an elastic solid with neo-Hookean material model and the red parts are made of a LASMP. These two kinds of materials have different thermal expansion coefficients, so when undergoing the same temperature changes the structures will bend and be curved. Similarly four analysis steps are created to simulate the full cycle of the mechanism:

(1) Predefine the temperature of whole structure at T_0, and then decrease the temperature to T_1.

(2) Keep the temperature at T_1 and hold the deformation fixed for the light irradiation.

(3) Return back the temperature to T_0.

(4) Expose the structure to the light that cause the volume ratio of the second network decreased.

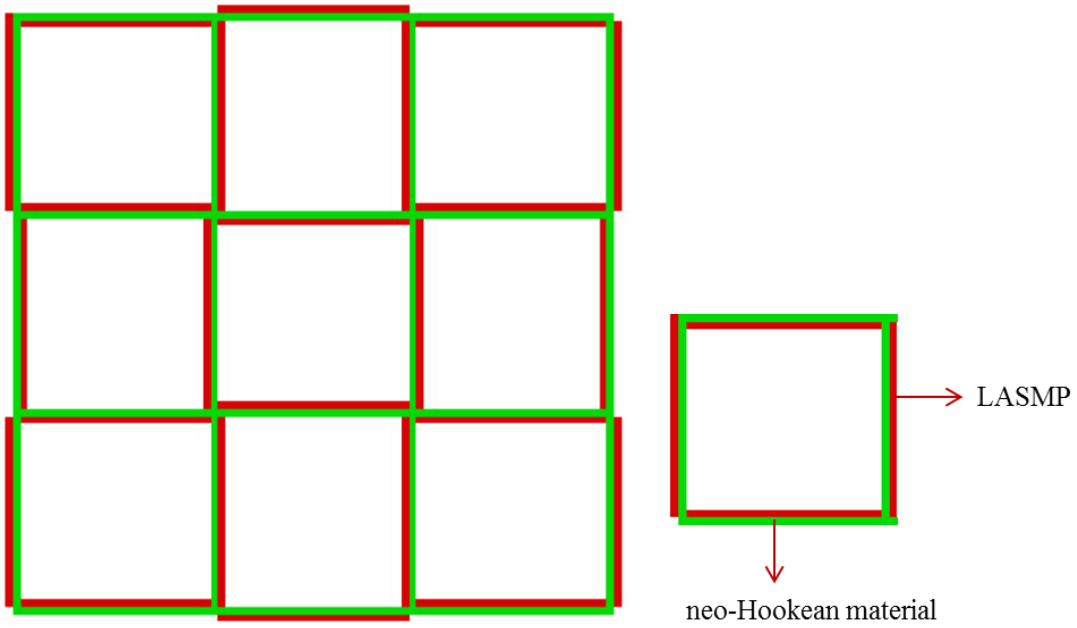

Fig. 86 Geometry of the lattice composite structure

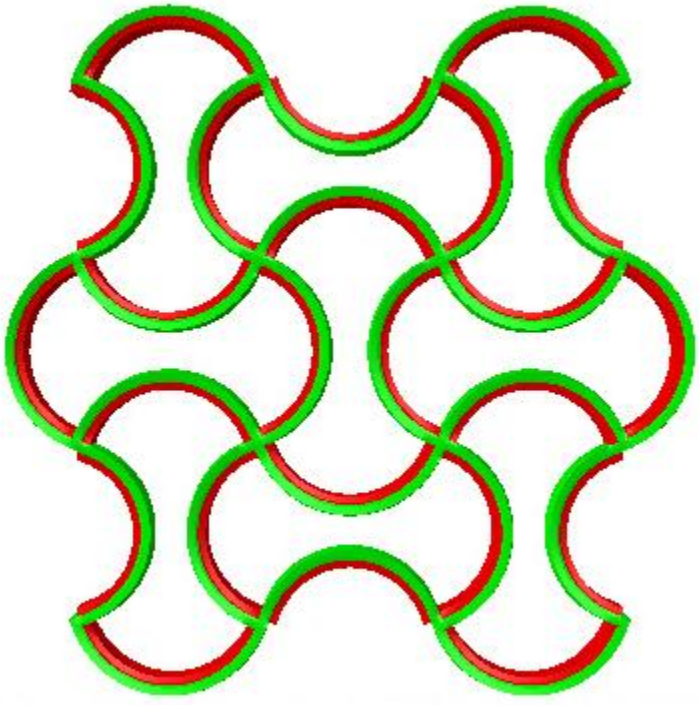

Fig. 87 Deformed state after cooling down

Fig. 87 showed the result of the first analysis step, the structures is deformed severely due to different thermal property. Fig. 88 shows the shape after the temperature returns back to the initial value and we can find that the structure does not completely recover. The values of the parameters are given in the calculation as follows:

(1) Temperature $T_0 = 325^o C$, $T_1 = 200^o C$

(2) Thermal coefficient for neo-Hookean solid is $c_1 = 0.001$ and for LASMPs for 0,

(3) The material parameters for neo-Hookean solid are μ=5 MPa with incompressibility, and for LASMPs are μ_a=5 MPa, μ_b=20 MPa

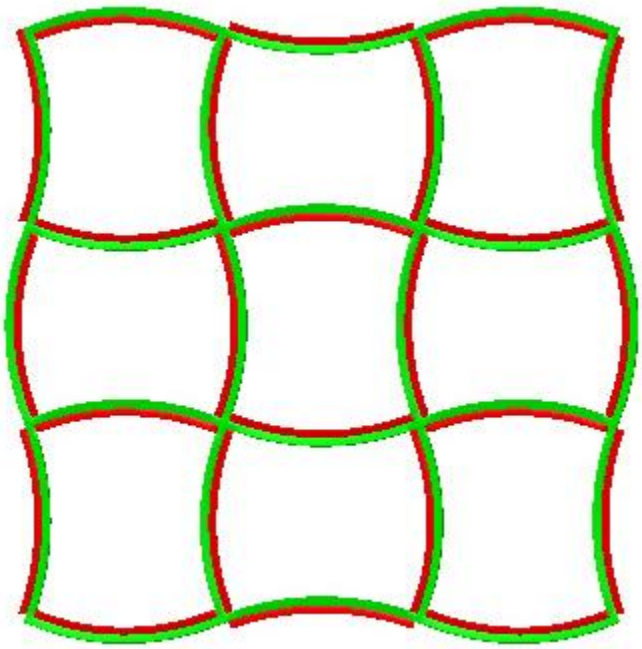

Fig. 88 Deformed state after heating up

Therefore from the viewpoint of shape memory function, thermal expansion can also work as a stimulus to induce the initial deformation of the structures.

4.7 Comparison between different models

In this section, all the four constitutive models (elastic isotropy, elastic anisotropy, viscoelastic isotropy, and viscoelastic anisotropy) developed in Chapter II and III are examined and the responses due to different material models are compared.

1. Bending

Fig. 89 showed the results of four constitutive models used in the bending case of 4.1. By comparing Fig. 89(a) and (b), (c) and (d) we can find that the anisotropy caused by the second network behaves much stiffer by fixing at a larger deformation after unloading, but the differences are not too much. While by comparing Fig.(a) and (c), (b) and (d), a very big difference caused by time dependent property can be observed. During loading, even only original network plays the role, the time dependent viscoelasticity produces a much larger bending shape. And also when unloading it still can be fixed at a large bending position.

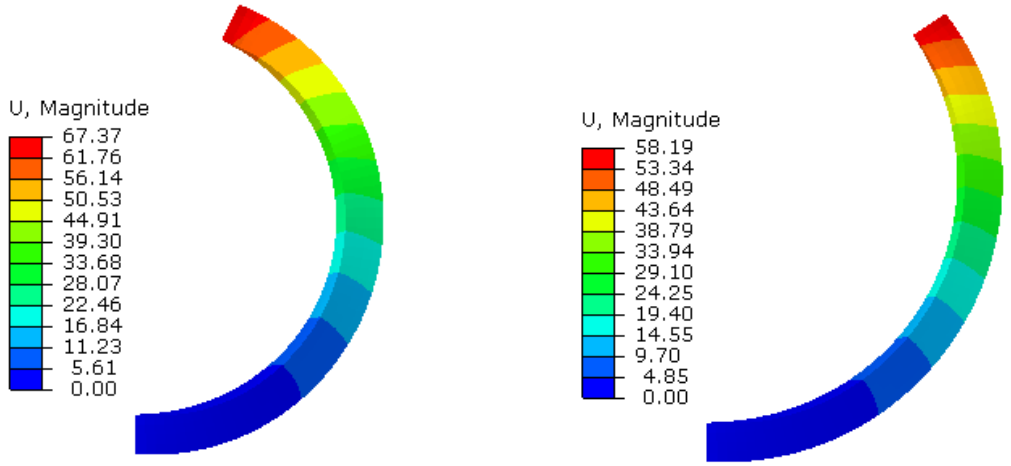

(a)

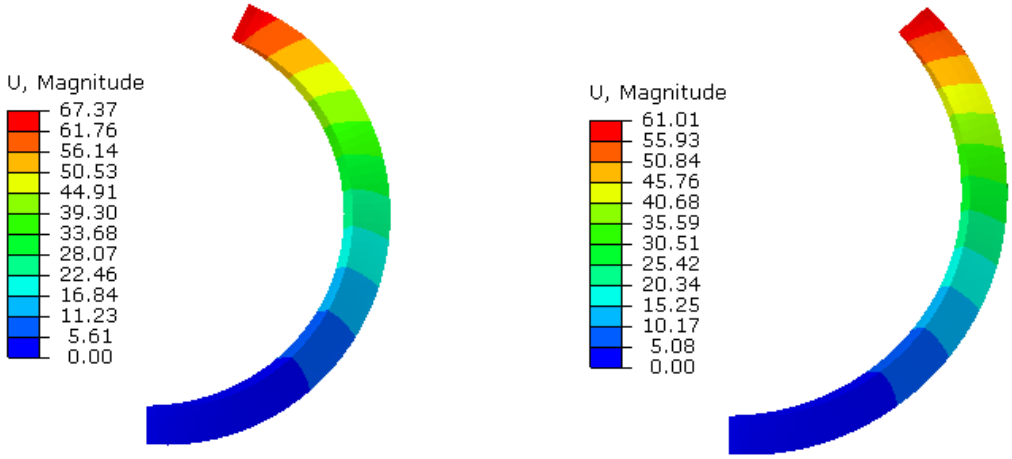

(b)

Fig. 89 The responses of LASMP plate with different constitutive models under bending moment of 80N·M. (a) Isotropic elastic model: loading (Left) and unloading (Right); (b) Anisotropic elastic model: loading (Left) and unloading (Right); (c) Isotropic viscoelastic model: loading (Left) and unloading (Right); (d) Anisotropic viscoelastic model: loading (Left) and unloading (Right)

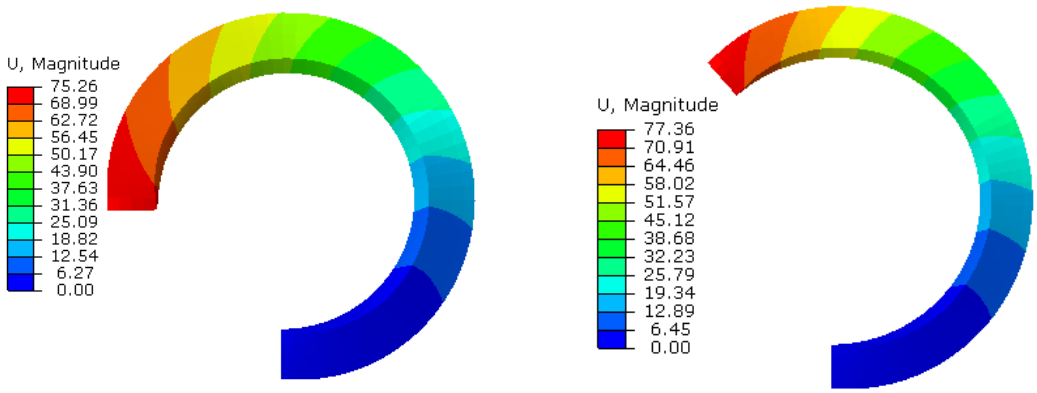

(c)

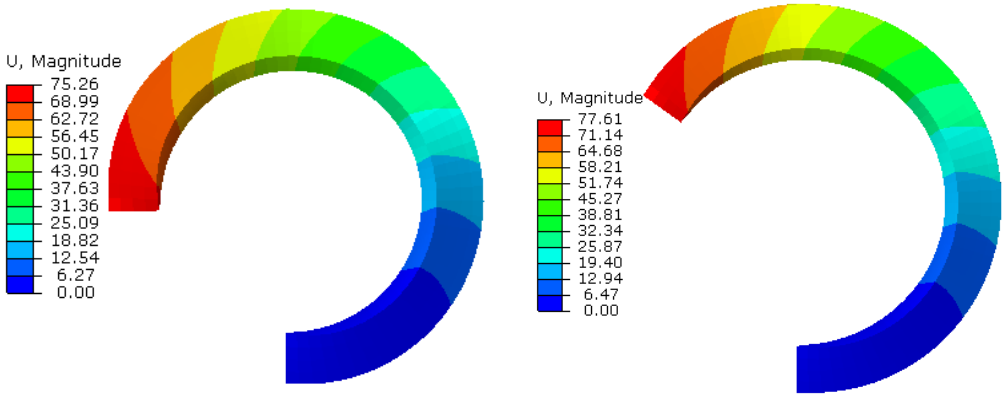

(d)

Fig. 89 Continued.

2. Flapping wing

Fig. 90 showed the results of flapping wing structure for different models. By comparison, we can get the similar conclusion as above. The viscoelasticity can produce a much larger deformation, and the anisotropy leads to smaller recovery.

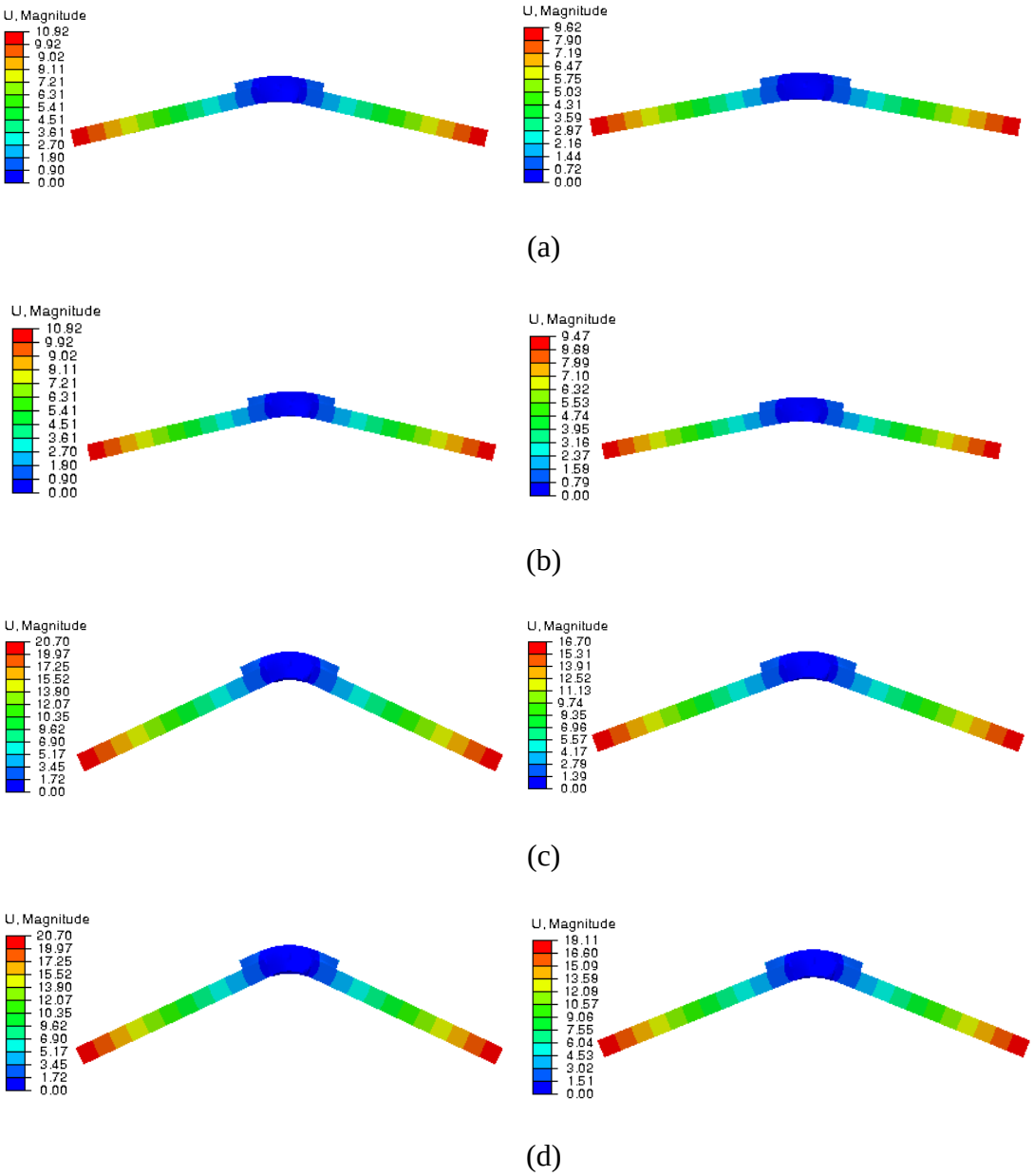

Fig. 90 The responses of flapping wing with different constitutive models under bending moment of -800N·M. (a) Isotropic elastic model: loading (Left) and unloading (Right); (b) Anisotropic elastic model: loading (Left) and unloading (Right); (c) Isotropic viscoelastic model: loading (Left) and unloading (Right); (d) Anisotropic viscoelastic model: loading (Left) and unloading (Right)

3. Unit cell

We further study the non-mechanical stimuli case. A unit cell from the lattice structure in 4.7 is used in the analysis. The initial deformation is caused by thermal expansion by heating up and releasing by cooling down. From the results, we can see that there are no big differences of the deformation after cooling down and heating up that indicates the deformation is mainly dominated by the thermal expansion rather than mechanical property. And the viscoelasticity weaken its role further on shape change, so viscoelasticity leads to much closer to the original configuration after cooling down, while the anisotropy can help fix a larger deformation.

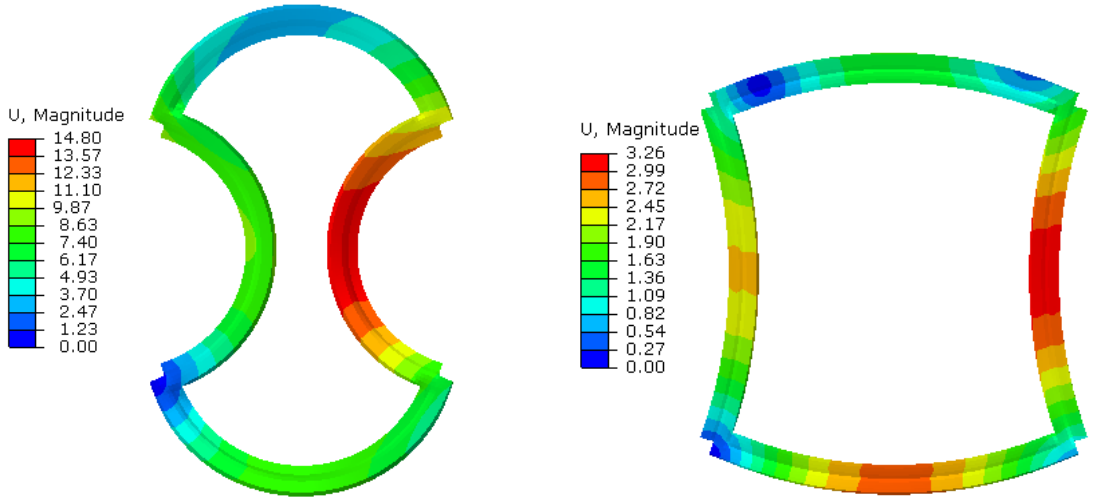

(a)

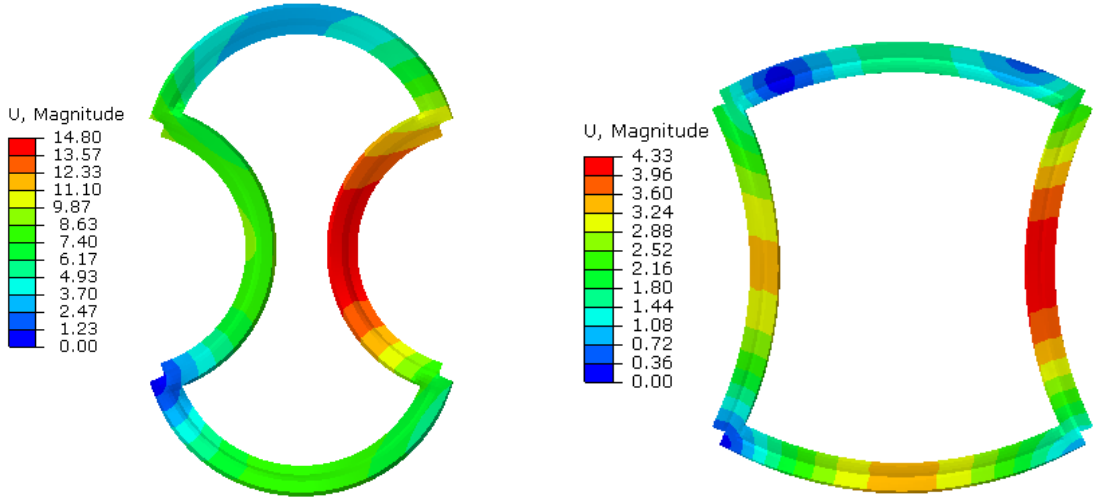

(b)

Fig. 91 The responses of unit cell with different constitutive models due to thermal expansion. (a) Isotropic elastic model: loading (Left) and unloading (Right); (b) Anisotropic elastic model: loading (Left) and unloading (Right); (c) Isotropic viscoelastic model: loading (Left) and unloading (Right); (d) Anisotropic viscoelastic model: loading (Left) and unloading (Right)

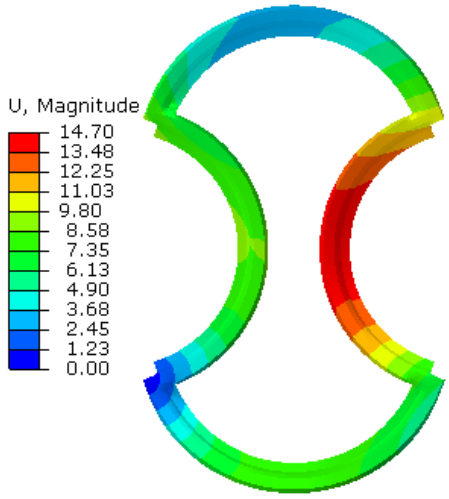

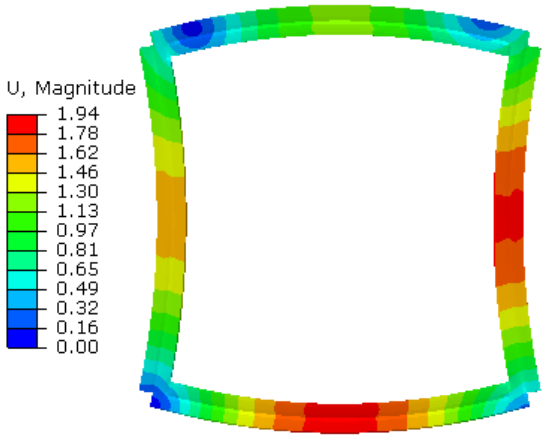

(c)

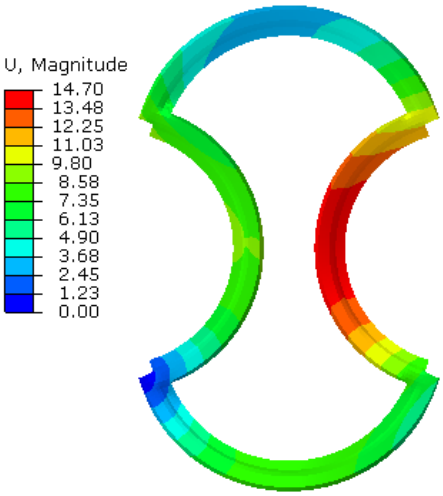

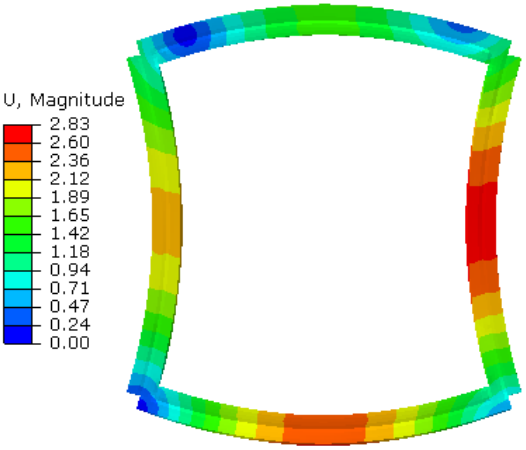

(d)

Fig. 91 Continued.

CHAPTER V

SUMMARY AND FUTURE WORK

5.1 Summary

The present work is focused on developing a constitutive model to describe the mechanical behavior of light-activated shape memory polymers. The constitutive framework is based on the theory of multiple natural configurations which has been widely used to describe a wide variety of material behaviors undergoing microstructural changes. Elastic and viscoelastic models are developed to describe the material behaviors. The original material configuration is assumed isotropic and as the material is being deformed the newly formed microstructure is modeled as either isotropic or anisotropic. Responses from different material behaviors and material symmetric are compared. The main accomplishments of this study are summarized as follows:

1. An elastic model is developed for the PMC LASMPs and the new network is formed by activating the photoactive molecules without breaking of the original network. Both networks are assumed to behave like entropic elastic materials but with and without consideration of the material symmetry change.

    a. It is first assumed that both networks are isotropic and nonlinear elastic. If two networks involved in the body, they are assumed to have the same displacements when deformed, so the total stress is the summation of the stress from the two networks.

b. The second network is experienced anisotropic induced deformation within nonlinear elastic behavior. Since the second network is formed based on a deformed configuration which may cause some preferred orientation, and will show anisotropy mechanically. Two invariant terms relating anisotropic directions are incorporated in order to describe the anisotropic behaviors.

2. A viscoelastic model is formulated in order to capture the stress relaxation behavior appeared in LASMPs. Within this framework, PMC and PNR mechanisms are considered. The latter one has obvious stress relaxation behavior due to the light irradiation and the new network is formed based on the cleavage of the original network. For simplicity, a quasi-linear viscoelastic model is adopted. The volume ratios of the networks do not appear in the expression of the constitutive models explicitly, but play their role implicitly through changing the mechanical property of the networks such as shear modulus and relaxation time.

3. The above constitutive models are implemented in ABAQUS user material (UMAT) subroutines for solving problems with complex geometries and boundary conditions. The UMAT formulations start from the strain energy in terms of invariants. For the anisotropic model, instead of using the deviatoric form of the invariants of Cauchy-Green tensor in the anisotropic terms, the full form of the invariants is involved. The verification of UMAT codes are done by comparing the results with the one from Abaqus built-in models and/or analytical calculations.

4. Finally, several shape changes in more complex geometries and boundary conditions are simulated to evaluate the ability of LASMPs in inducing and retaining shape changes. In addition to prescribing mechanical loading to induce the deformation before light activation, a thermal stimulus is also taken into account for inducing shape changes and LASMPs are used for shape retention.

5.2 Future work

Several constitutive models have been developed and implemented into three dimensional finite element models in this work. Suggestions for further studies are as follow:

1. More experimental data need to be explored to validate the models. In this work, due to lack of experiment data, we conducted parametric studies on understanding the response of PMC mechanism, and for PNR mechanism we calibrate the mechanical parameters with limited experimental data.

2. A more general method of solutions is required. In the above analytical and numerical implementations, we just consider that case of keeping stretch or strain constant when light irradiation. However, the general scenario should be that light irradiation can be occurred at any time even when stretching. There are two ways to characterize the evolution process of the new networks, one is a phenomenological

method to capture the change of the volume ratio [69], and the other is to describe the process microscopically from the photochemistry point view [42].

For a more general model, there are several aspects can be considered:

a. Light propagation in the media: The formation and cleavage of the networks in LASMPs take place under the activation of light of specific frequencies or wavelength, so when light propagates in the media the intensity will change. In our model, we mainly focus on the thin structures and neglect the variations of the light throughout the thickness. Besides, when the structure experiencing a large deformation, the incident light direction will be different as the body deforms. Therefore for accurate modeling, we need to consider the light change and its propagation in the body.

b. Inhomogeneous property: For a thicker body, due to the light intensity weakening along the thickness the evolution of the microstructures will be different. For instance, some parts of the body may receive larger light intensity and the evolution of the new networks in that region is faster, while in contrast the evolution may not be initiated in some other parts. Different volume ratios of the networks in the body will produce different inhomogeneous property.

c. Incorporating other stimuli to the structures: In this work we present the constitutive models mainly upon the mechanical loading induced the initial deformation and we also mentioned the case of shape deformation programmed

by the thermal stimulus. There are other stimuli possible to induce the deformation such as electricity, diffusion and so on.

REFERENCES

[1] Ashby, Michael F., and Kara Johnson. Materials and design: the art and science of material selection in product design. Butterworth-Heinemann, 2013.

[2] van Kesteren, I. E. H., P. J. Stappers, and J. C. M. de Bruijn. "Defining user-interaction aspects for materials selection: Three tools." the Web Proceedings of Nordic Design Research. Retrieved April 1 (2007): 2007.

[3] Van Kesteren, I. E. H., Pieter Jan Stappers, and J. C. M. De Bruijn. "Materials in products selection: tools for including user-interaction in materials selection." International journ al of sedign, 1 (3) 2007 (2007).

[4] Crilly, Nathan, James Moultrie, and P. John Clarkson. "Seeing things: consumer response to the visual domain in product design." Design studies 25, no. 6 (2004): 547-577.

[5] Jahan, A., M. Y. Ismail, S. M. Sapuan, and F. Mustapha. "Material screening and choosing methods–a review." Materials & Design 31, no. 2 (2010): 696-705.

[6] Immarigeon, J. P., R. T. Holt, A. K. Koul, L. Zhao, W. Wallace, and J. C. Beddoes. "Lightweight materials for aircraft applications." Materials characterization 35, no. 1 (1995): 41-67.

[7] Reece, Peter L. Smart materials and structures: new research. Nova Publishers, 2007.

[8] Meng, Harper, and Jinlian Hu. "A brief review of stimulus-active polymers responsive to thermal, light, magnetic, electric, and water/solvent stimuli." Journal of Intelligent Material Systems and Structures 21, no. 9 (2010): 859-885.

[9] Duerig, Thomas W., K. N. Melton, and D. Stöckel. “Engineering aspects of shape memory alloys.” Butterworth-Heinemann, 2013.

[10] Behl, Marc, and Andreas Lendlein. "Shape-memory polymers." Materials today 10, no. 4 (2007): 20-28.

[11] Wache, H. M., D. J. Tartakowska, A. Hentrich, and M. H. Wagner. "Development of a polymer stent with shape memory effect as a drug delivery system." Journal of Materials Science: Materials in Medicine 14, no. 2 (2003): 109-112.

[12] Lendlein, Andreas, Marc Behl, Bernhard Hiebl, and Christian Wischke. "Shape-memory polymers as a technology platform for biomedical applications." Expert Review of Medical Devices 7, no. 3 (2010): 357-379.

[13] Bar-Cohen, Yoseph, T. Xue, Mohsen Shahinpoor, Joycelyn S. Harrison, and Joseph G. Smith. "Flexible low-mass robotic arm actuated by electroactive polymers." In 5th Annual International Symposium on Smart Structures and Materials, pp. 52-57. International Society for Optics and Photonics, 1998.

[14] Nemat-Nasser, Sia, and Chris Thomas. "Electroactive polymer (EAP) actuators as artificial muscles. Reality, potential and challenges." Bellingham, WA: SPIE (2001): 139-191.

[15] Hu, J. 2007. Shape Memory Polymers and Textiles, Vol. 1, 1st edn, pp. 15 25, Woodhead Publishing Limited, Cambridge, England, ISBN-13: 978-1-84569-047-2; ISBN-10: 1-84569-047-8.

[16] Leng, Jinsong, Haibao Lu, Yanju Liu, and Shanyi Du. "Conductive nanoparticles in electro activated shape memory polymer sensor and actuator." In The 15th International Symposium on: Smart Structures and Materials & Nondestructive Evaluation and Health Monitoring, pp. 693109-693109. International Society for Optics and Photonics, 2008.

[17] Havens, Ernie, Emily A. Snyder, and Tat H. Tong. "Light-activated shape memory polymers and associated applications." In Smart structures and materials, pp. 48-55. International Society for Optics and Photonics, 2005.

[18] Pastor, Christine, Brian Sanders, James J. Joo, and Robin McCarty. "Kinematically designed flexible skins for morphing aircraft." ASME Paper No. IMECE2006-69674 (2006).

[19] Liu, C., H. Qin, and P. T. Mather. "Review of progress in shape-memory polymers." Journal of Materials Chemistry 17, no. 16 (2007): 1543-1558.

[20] Lee, Bo Sun, Byoung Chul Chun, Yong-Chan Chung, Kyung Il Sul, and Jae Whan Cho. "Structure and thermomechanical properties of polyurethane block copolymers with shape memory effect." Macromolecules 34, no. 18 (2001): 6431-6437.

[21] Beblo, Richard V., and Lisa Mauck Weiland. "Light activated shape memory polymer characterization." Journal of Applied Mechanics 76, no. 1 (2009): 011008.

[22] El Feninat, Fatiha, Gaetan Laroche, Michel Fiset, and Diego Mantovani. "Shape memory materials for biomedical applications." Advanced Engineering Materials 4, no. 3 (2002): 91-104.

[23] Langer, Robert, and David A. Tirrell. "Designing materials for biology and medicine." Nature 428, no. 6982 (2004): 487-492.

[24] Maitland, Duncan J., Melodie F. Metzger, Daniel Schumann, Abraham Lee, and Thomas S. Wilson. "Photothermal properties of shape memory polymer micro-actuators for treating stroke." Lasers in Surgery and Medicine 30, no. 1 (2002): 1-11.

[25] Beblo, Richard Vincent. "Characterization and modeling of light activated shape memory polymer." PhD diss., University of Pittsburgh, 2010.

[26] Eisenbach, Claus D. "Isomerization of aromatic azo chromophores in poly (ethyl acrylate) networks and photomechanical effect." Polymer 21, no. 10 (1980): 1175-1179.

[27] Yu, Yanlei, Makoto Nakano, and Tomiki Ikeda. "Photomechanics: directed bending of a polymer film by light." Nature 425, no. 6954 (2003): 145-145.

[28] Irie, Masahiro, and Dawan Kunwatchakun. "Photoresponsive polymers. 8. Reversible photostimulated dilation of polyacrylamide gels having triphenylmethane leuco derivatives." Macromolecules 19, no. 10 (1986): 2476-2480.

[29] Mamada, Akira, Toyoichi Tanaka, Dawan Kungwatchakun, and Masahiro Irie. "Photoinduced phase transition of gels." Macromolecules 23, no. 5 (1990): 1517-1519.

[30] Lendlein, Andreas, Hongyan Jiang, Oliver Jünger, and Robert Langer. "Light-induced shape-memory polymers." Nature 434, no. 7035 (2005): 879-882.

[31] Scott, Timothy F., Andrew D. Schneider, Wayne D. Cook, and Christopher N. Bowman. "Photoinduced plasticity in cross-linked polymers." Science 308, no. 5728 (2005): 1615-1617.

[32] Gaur, Umesh, Suk‐fai Lau, Brent B. Wunderlich, and Bernhard Wunderlich. "Heat capacity and other thermodynamic properties of linear macromolecules VI. Acrylic polymers." Journal of Physical and Chemical Reference Data 11, no. 4 (1982): 1065-1089.

[33] Long, Kevin Nicholas. Mechanics of light-activated network polymers. University of Colorado at Boulder, 2010.

[34] Beblo, Richard V., and Lisa Mauck Weiland. "Light activated shape memory polymer characterization." Journal of Applied Mechanics 76, no. 1 (2009): 011008.

[35] Beblo, Richard V., and Lisa Mauck Weiland. "Demonstration of a multiscale modeling technique: prediction of the stress–strain response of light activated shape memory polymers." Smart Materials and Structures 19, no. 9 (2010): 094012.

[36] Li, Huiyu, Hua Li, and Hornsen Tzou. "Frequency Control of Beams and Cylindrical Shells With Light-Activated Shape Memory Polymers." Journal of Vibration and Acoustics 137, no. 1 (2015): 011006.

[37] Li, Huiyu, Hua Li, and Hornsen Tzou. "Neural-Network Vibration Control of Rings With Light-Activated Shape Memory Polymer Actuators." In ASME 2015 International Design Engineering Technical Conferences and Computers and Information in Engineering Conference, pp. V008T13A006-V008T13A006. American Society of Mechanical Engineers, 2015.

[38] Sodhi, J. S., and I. J. Rao. "Modeling the mechanics of light activated shape memory polymers." International Journal of Engineering Science 48, no. 11 (2010): 1576-1589.

[39] Rajagopal, Kumbakonam R., and Alan S. Wineman. "A constitutive equation for nonlinear solids which undergo deformation induced microstructural changes." International Journal of Plasticity 8, no. 4 (1992): 385-395.

[40] Wineman, A. S., and K. R. Rajagopal. "On a constitutive theory for materials undergoing microstructural changes." Archives of Mechanics 42, no. 1 (1990): 53-75.

[41] Sodhi, J. S., P. R. Cruz, and I. J. Rao. "Inhomogeneous deformations of light activated shape memory polymers." International Journal of Engineering Science 89 (2015): 1-17.

[42] Long, Kevin N., Timothy F. Scott, H. Jerry Qi, Christopher N. Bowman, and Martin L. Dunn. "Photomechanics of light-activated polymers." Journal of the Mechanics and Physics of Solids 57, no. 7 (2009): 1103-1121.

[43] Long, Kevin N., Timothy F. Scott, Martin L. Dunn, and H. Jerry Qi. "Photo-induced deformation of active polymer films: Single spot irradiation." International Journal of Solids and Structures 48, no. 14 (2011): 2089-2101.

[44] Ryu, Jennie, Matteo D'Amato, Xiaodong Cui, Kevin N. Long, H. Jerry Qi, and Martin L. Dunn. "Photo-origami—Bending and folding polymers with light." Applied Physics Letters 100, no. 16 (2012): 161908.

[45] Rajagopal, K. R., and A. R. Srinivasa. "Mechanics of the inelastic behavior of materials—Part 1, theoretical underpinnings." International Journal of Plasticity 14, no. 10 (1998): 945-967.

[46] Rajagopal, K. R., and A. R. Srinivasa. "On the inelastic behavior of solids—Part 1: Twinning." International Journal of Plasticity 11, no. 6 (1995): 653-678.

[47] Rajagopal, K. R., and A. R. Srinivasa. "A thermodynamic frame work for rate type fluid models." Journal of Non-Newtonian Fluid Mechanics 88, no. 3 (2000): 207-227.

[48] Rajagopal, K. R., and A. R. Srinivasa. "On the thermomechanics of shape memory wires." Zeitschrift für angewandte Mathematik und Physik ZAMP 50, no. 3 (1999): 459-496.

[49] I. J. Rao, I. J., and K. R. Rajagopal. "Phenomenological modelling of polymer crystallization using the notion of multiple natural configurations." Interfaces and free boundaries 2, no. 1 (2000): 73-94. Rao, and K. R. Rajagopal, "Phenomenological modelling of polymer crystallization using the notion of multiple natural configurations." Interfaces and free boundaries 2.1 (2000): 73-94.

[50] Rajagopal, K. R., and A. R. Srinivasa. "Modeling anisotropic fluids within the framework of bodies with multiple natural configurations." Journal of Non-Newtonian Fluid Mechanics 99, no. 2 (2001): 109-124.

[51] Yuan, Zhi, Anastasia Muliana, and Kumbakonam Ramamani Rajagopal. "Modeling the response of light-activated shape memory polymers." Mathematics and Mechanics of Solids 22, no. 5 (2017): 1116-1143.

[52] Akabori, Sadatoshi, Yoichi Habata, Misako Nakazawa, Yoko Yamada, Yoichi Shindo, Tokuko Sugimura, and Sadao Sato. "The novel syntheses of photoreversible cyclobutanocrown ethers by the intramolecular photoaddition of α, ω-dicinnamoyl polyethylene glycol derivatives." Bulletin of the Chemical Society of Japan 60, no. 9 (1987): 3453-3455.

[53] Tanaka, Hideaki, and Koichi Honda. "Photoreversible reactions of polymers containing cinnamylideneacetate derivatives and the model compounds." Journal of Polymer Science Part A: Polymer Chemistry 15, no. 11 (1977): 2685-2689.

[54] Rajagopal, K. R. "Multiple configurations in continuum mechanics." Reports of the institute for computational and applied mechanics 6 (1995).

[55] Zhi, Yuan, Anastasia Muliana, and K. R. Rajagopal. "Quasi-linear viscoelastic modeling of light-activated shape memory polymers." Journal of Intelligent Material Systems and Structures (2017): 1045389X17689936.

[56] Fung, Yuan-Cheng. “Biomechanics: mechanical properties of living tissues.” Springer Science & Business Media, 2013.

[57] De Pascalis, Riccardo, I. David Abrahams, and William J. Parnell. "On nonlinear viscoelastic deformations: a reappraisal of Fung's quasi-linear viscoelastic model." Proceedings of the Royal Society of London A: Mathematical, Physical and Engineering Sciences. Vol. 470. No. 2166. The Royal Society, 2014.

[58] Rajagopal, Kumbakonam Ramamani. "Mechanics of mixtures." World scientific, 1995.

[59] Burden, Richard L., and J. Douglas Faires. "Numerical analysis ", 1989

[60] Hu, Jinlian, Yong Zhu, Huahua Huang, and Jing Lu. "Recent advances in shape–memory polymers: Structure, mechanism, functionality, modeling and applications." Progress in Polymer Science 37, no. 12 (2012): 1720-1763.

[61] Ratna, Debdatta, and J. Karger-Kocsis. "Recent advances in shape memory polymers and composites: a review." Journal of Materials Science 43, no. 1 (2008): 254-269.

[62] Qi, H. Jerry, Thao D. Nguyen, Francisco Castro, Christopher M. Yakacki, and Robin Shandas. "Finite deformation thermo-mechanical behavior of thermally induced shape memory polymers." Journal of the Mechanics and Physics of Solids 56, no. 5 (2008): 1730-1751.

[63] Xu, We, and Guoqiang Li. "Constitutive modeling of shape memory polymer based self-healing syntactic foam." International Journal of Solids and Structures 47, no. 9 (2010): 1306-1316.

[64] Diani, Julie, Pierre Gilormini, Carole Frédy, and Ingrid Rousseau. "Predicting thermal shape memory of crosslinked polymer networks from linear viscoelasticity." International Journal of Solids and Structures 49, no. 5 (2012): 793-799.

[65] Abramowitch, Steven D., Savio LY Woo, Theodore D. Clineff, and Richard E. Debski. "An evaluation of the quasi-linear viscoelastic properties of the healing medial collateral ligament in a goat model." Annals of biomedical engineering 32, no. 3 (2004): 329-335.

[66] Drapaca, C. S., G. Tenti, K. Rohlf, and S. Sivaloganathan. "A quasi-linear viscoelastic constitutive equation for the brain: application to hydrocephalus." Journal of Elasticity 85, no. 1 (2006): 65-83.

[67] Suchocki, Cyprian. "A quasi-linear viscoelastic rheological model for thermoplastics and resins." Journal of Theoretical and Applied Mechanics 51, no. 1 (2013): 117-129.

[68] Muliana, A., K. R. Rajagopal, and D. Tscharnuter. "A nonlinear integral model for describing responses of viscoelastic solids." International Journal of Solids and Structures 58 (2015): 146-156.

[69] Kim, Whan Gun. "Photocure properties of high‐heat‐resistant photoreactive polymers with cinnamate groups." Journal of applied polymer science 107, no. 6 (2008): 3615-3624.

[70] Weiss, Jeffrey A., Bradley N. Maker, and Sanjay Govindjee. "Finite element implementation of incompressible, transversely isotropic hyperelasticity." Computer methods in applied mechanics and engineering 135, no. 1-2 (1996): 107-128.

[71] Vergori, Luigi, Michel Destrade, Patrick McGarry, and Ray W. Ogden. "On anisotropic elasticity and questions concerning its finite element implementation." Computational Mechanics 52, no. 5 (2013): 1185-1197.

[72] Gilchrist, M. D., Jeremiah G. Murphy, W. Parnell, and B. Pierrat. "Modelling the slight compressibility of anisotropic soft tissue." International Journal of Solids and Structures 51, no. 23 (2014): 3857-3865.

[73] Nolan, D. R., A. L. Gower, M. Destrade, R. W. Ogden, and J. P. McGarry. "A robust anisotropic hyperelastic formulation for the modelling of soft tissue." Journal of the mechanical behavior of biomedical materials 39 (2014): 48-60.

[74] Annaidh, A. N ́ Michel Destrade, M. D. Gilchrist, and J. G. Murphy. "Deficiencies in numerical models of anisotropic nonlinearly elastic materials." Biomechanics and modeling in mechanobiology 12, no. 4 (2013): 781-791.

[75] Pierrat, B., J. G. Murphy, D. B. MacManus, and M. D. Gilchrist. "Finite element implementation of a new model of slight compressibility for transversely isotropic materials." Computer methods in biomechanics and biomedical engineering 19, no. 7 (2016): 745-758.

[77] Suchocki, Cyprian. "A finite element implementation of Knowles stored-energy function: theory, coding and applications." Archive of Mechanical Engineering 58, no. 3 (2011): 319-346.

[78] Holzapfel, Gerhard A. Nonlinear solid mechanics. Vol. 24. Chichester: Wiley, 2000.

[79] Abaqus, Ver. "6.14 Documentation." Dassault Systemes Simulia Corporation (2014).

[80] Prasad, Sharat C., K. R. Rajagopal, and I. J. Rao. "A continuum model for the anisotropic creep of single crystal nickel-based superalloys." Acta materialia 54, no. 6 (2006): 1487-1500.

[81] Janbaz, S., R. Hedayati, and A. A. Zadpoor. "Programming the shape-shifting of flat soft matter: from self-rolling/self-twisting materials to self-folding origami." Materials Horizons 3, no. 6 (2016): 536-547.

APPENDIX A

This appendix provides a description of the numerical method used to solve the integral equations. When the equations have two unknown variables existing in a nonlinear and coupled manner, it is not easy to obtain analytical solutions. For example, in the case of unequal biaxial tension problem in this paper, we need to obtain the two unknown stretches when unloading by prescribing the stress. In order to demonstrate the numerical algorithm, equations (4.18)-(4.19) are used. Equations (4.18)-(4.19) can be rewritten as:

$$T_{11}(t) = \{\Lambda_1^2(t)S_{D11}^e(t) - \frac{1}{\Lambda_1^2(t)\Lambda_2^2(t)}S_{D33}^e(t) - \int_0^t \frac{1}{\tau}(1-\frac{\mu_\infty}{\mu_a})e^{-\frac{t-s}{\tau}}[\Lambda_1^2(t)S_{D11}^e(s) - \frac{1}{\Lambda_1^2(t)\Lambda_2^2(t)}S_{D33}^e(s)]ds\} \tag{A.1}$$

and

$$T_{22}(t) = \{\Lambda_2^2(t)S_{D22}^e(t) - \frac{1}{\Lambda_1^2(t)\Lambda_2^2(t)}S_{D33}^e(t) - \int_0^t \frac{1}{\tau}(1-\frac{\mu_\infty}{\mu_a})e^{-\frac{t-s}{\tau}}[\Lambda_2^2(t)S_{D22}^e(s) - \frac{1}{\Lambda_1^2(t)\Lambda_2^2(t)}S_{D33}^e(s)]ds\} \tag{A.2}$$

In the above equations, the integral function is calculated by using the classical trapezoidal and recursive methods. Therefore, (A.1) and (A.2) can be expressed as:

$$T_{11}(t) = \Lambda_1^2(t) S_{D11}^e(t) - \frac{1}{\Lambda_1^2(t)\Lambda_2^2(t)} S_{D33}^e(t) - (\Lambda_1^2(t) P_a(t) - \frac{Q_a(t)}{\Lambda_1^2(t)\Lambda_2^2(t)}) \tag{A.3}$$

$$T_{22}(t) = \Lambda_2^2(t) S_{D22}^e(t) - \frac{1}{\Lambda_1^2(t)\Lambda_2^2(t)} S_{D33}^e(t) - (\Lambda_2^2(t) U_a(t) - \frac{Q_a(t)}{\Lambda_1^2(t)\Lambda_2^2(t)}) \tag{A.4}$$

Where the history variables are

$$P_a(t) = e^{-\frac{\Delta t}{\tau}} P_a(t-\Delta t) + \frac{\Delta t}{2}\frac{1}{\tau}(1-\frac{\mu_\infty}{\mu_a})(S_{D11}^e(t) + e^{-\frac{\Delta t}{\tau}} S_{D11}^e(t-\Delta t)) \tag{A.5}$$

$$Q_a(t) = e^{-\frac{\Delta t}{\tau}} Q_a(t-\Delta t) + \frac{\Delta t}{2}\frac{1}{\tau}(1-\frac{\mu_\infty}{\mu_a})(S_{D33}^e(t) + e^{-\frac{\Delta t}{\tau}} S_{D33}^e(t-\Delta t)) \tag{A.6}$$

$$U_a(t) = e^{-\frac{\Delta t}{\tau}} U_a(t-\Delta t) + \frac{\Delta t}{2}\frac{1}{\tau}(1-\frac{\mu_\infty}{\mu_a})(S_{D22}^e(t) + e^{-\frac{\Delta t}{\tau}} S_{D22}^e(t-\Delta t)) \tag{A.7}$$

After the elimination of the integral by the above operations, equations (A.3) and (A.4) become a set of nonlinear algebraic equations. The Newton-Raphson method is used to find out the solution of the unknowns $\Lambda_1(t), \Lambda_2(t)$ with the stress prescribed.

Let consider (A.3) and (A.4) as $\mathbf{R}(\mathbf{\Lambda}) = \mathbf{0}$, where

$$\mathbf{R}(\mathbf{\Lambda}) = \begin{bmatrix} R_1(\Lambda_1, \Lambda_2) \\ R_2(\Lambda_1, \Lambda_2) \end{bmatrix}, \quad \mathbf{\Lambda} = \begin{bmatrix} \Lambda_1 \\ \Lambda_2 \end{bmatrix} \tag{A.8}$$

and the consistent tangent matrix is defined as $\mathbf{K} = \frac{\partial \mathbf{R}}{\partial \mathbf{\Lambda}}|_{\mathbf{\Lambda}_k}$. An iteration is needed to determine the components of the stretch tensor, which is summarized below:

(1) initialize $\mathbf{T} = \mathbf{T_0}$, $\mathbf{\Lambda} = \mathbf{\Lambda_0}$, $\mathbf{R} = \mathbf{0}$ (where $\mathbf{T_0}$, $\mathbf{\Lambda_0}$ are the stress and stretch when unloading begins)

(2) determine the initial $\mathbf{K}$

(3) iterate over the stress increment

- Determine the stress increment $\Delta\mathbf{T}$ (which is negative when unloading stress)
- Set $\mathbf{T} = \mathbf{T} + \Delta\mathbf{T}$
- Set $\mathbf{R} = \mathbf{R} - \Delta\mathbf{T}$
- Check for $\frac{\|\mathbf{R}\|}{\|\mathbf{T}\|} > tolerance$
    - Solve $\mathbf{Ku} = -\mathbf{R}$
    - Update $\mathbf{\Lambda} = \mathbf{\Lambda} + \mathbf{u}$; $\mathbf{K}$; $\mathbf{R}$

APPENDIX B

This appendix presents the derivation about the Cauchy stress and elasticity tensor of general hyperelastic model for Abaqus UMAT use and then neo-Hookean model is taken for demonstration. The strain energy function for a hyperelastic material with slight compressibility is

$$W(\mathbf{C}) = U(J) + \bar{W}(\bar{\mathbf{C}}) \tag{B.1}$$

where U , $\bar{W}$ are the volumetric and isochoric stored-energy potentials respectively. In order to get the formulation of Cauchy stress and material stiffness tensor, by substituting the above form of strain energy into the formulas and making use of the chain rule, it turns to be:

$$\begin{aligned}\mathbf{S} &= 2\frac{\partial U}{\partial J}\frac{\partial J}{\partial \mathbf{C}} + 2\frac{\partial \bar{W}}{\partial \bar{\mathbf{C}}}\frac{\partial \bar{\mathbf{C}}}{\partial \mathbf{C}} = J\frac{\partial U}{\partial J}\mathbf{C}^{-1} + 2J^{-2/3}\frac{\partial \bar{W}}{\partial \bar{\mathbf{C}}}(\mathbb{I} - \frac{1}{3}\mathbf{C}\otimes\mathbf{C}^{-1}) \\ &= J\frac{\partial U}{\partial J}\mathbf{C}^{-1} + 2J^{-2/3}[\frac{\partial \bar{W}}{\partial \bar{\mathbf{C}}} - \frac{1}{3}(\frac{\partial \bar{W}}{\partial \bar{\mathbf{C}}}\cdot\bar{\mathbf{C}})\bar{\mathbf{C}}^{-1}] \\ &= J\frac{\partial U}{\partial J}\mathbf{C}^{-1} + 2J^{-2/3}DEV[\frac{\partial \bar{W}}{\partial \bar{\mathbf{C}}}]\end{aligned} \tag{B.2}$$

where $DEV[\bullet] = [\bullet] - \frac{1}{3}([\bullet]\cdot\bar{\mathbf{C}})\bar{\mathbf{C}}^{-1}$.

Then accordingly, the material elasticity tensor $\mathbb{C}$ is:

$$
\begin{aligned}
\mathbb{C} &= 2\frac{\partial \mathbf{S}}{\partial \mathbf{C}} = 4\frac{\partial^2 W}{\partial \mathbf{C}\partial \mathbf{C}} = 2\frac{\partial}{\partial \mathbf{C}}\left(2\frac{\partial W}{\partial \mathbf{C}}\right) \\
&= 2\frac{\partial}{\partial \mathbf{C}}\{J\frac{\partial U}{\partial J}\mathbf{C}^{-1} + 2J^{-2/3}[\frac{\partial \bar{W}}{\partial \bar{\mathbf{C}}} - \frac{1}{3}(\frac{\partial \bar{W}}{\partial \bar{\mathbf{C}}}\cdot\bar{\mathbf{C}})\bar{\mathbf{C}}^{-1}]\} \\
&= J\frac{\partial U}{\partial J}(\mathbf{C}^{-1}\otimes\mathbf{C}^{-1} - 2\mathbb{I}_{\mathbf{C}^{-1}}) + J^2\frac{\partial^2 U}{\partial J^2}\mathbf{C}^{-1}\otimes\mathbf{C}^{-1} - \frac{4}{3}J^{-4/3}[\frac{\partial \bar{W}}{\partial \bar{\mathbf{C}}}\otimes\bar{\mathbf{C}}^{-1} + \bar{\mathbf{C}}^{-1}\otimes\frac{\partial \bar{W}}{\partial \bar{\mathbf{C}}}] \\
&\quad + \frac{4}{3}J^{-4/3}(\frac{\partial \bar{W}}{\partial \bar{\mathbf{C}}}\cdot\bar{\mathbf{C}})(J^{4/3}\mathbb{I}_{\mathbf{C}^{-1}} + \frac{1}{3}\bar{\mathbf{C}}^{-1}\otimes\bar{\mathbf{C}}^{-1}) + J^{-4/3}\bar{\mathbb{C}}_{\bar{W}}
\end{aligned}
\tag{B.3}
$$

Where

$\bar{\mathbb{C}}_{\bar{W}} = 4\frac{\partial^2 \bar{W}}{\partial \bar{\mathbf{C}}\partial \bar{\mathbf{C}}} - \frac{4}{3}[(\frac{\partial^2 \bar{W}}{\partial \bar{\mathbf{C}}\partial \bar{\mathbf{C}}}\cdot\bar{\mathbf{C}})\otimes\bar{\mathbf{C}}^{-1} + \bar{\mathbf{C}}^{-1}\otimes(\bar{\mathbf{C}}\cdot\frac{\partial^2 \bar{W}}{\partial \bar{\mathbf{C}}\partial \bar{\mathbf{C}}})] + \frac{4}{9}(\bar{\mathbf{C}}\cdot\frac{\partial^2 \bar{W}}{\partial \bar{\mathbf{C}}\partial \bar{\mathbf{C}}}\cdot\bar{\mathbf{C}})\bar{\mathbf{C}}^{-1}\otimes\bar{\mathbf{C}}^{-1}$, it is a part of $\mathbb{C}$ arised from the second derivative of $\bar{W}$ with respect to $\bar{\mathbf{C}}$. In the above procedure, some derivative results have been used:

$$
\frac{\partial J}{\partial \mathbf{C}} = \frac{1}{2}J\mathbf{C}^{-1},\quad \frac{\partial \bar{\mathbf{C}}}{\partial \mathbf{C}} = J^{-2/3}(\mathbb{I} - \frac{1}{3}\mathbf{C}\otimes\mathbf{C}^{-1}),\quad \frac{\partial \mathbf{C}^{-1}}{\partial \mathbf{C}} = -\mathbb{I}_{\mathbf{C}^{-1}},
$$

$$
\frac{\partial \bar{\mathbf{C}}^{-1}}{\partial \mathbf{C}} = J^{-2/3}(\frac{1}{3}\bar{\mathbf{C}}^{-1}\otimes\bar{\mathbf{C}}^{-1} - J^{4/3}\mathbb{I}_{\mathbf{C}^{-1}})
\tag{B.4}
$$

Where $\mathbb{I}$ is a fourth –order identity tensor, and $(\mathbb{I}_{\mathbf{C}^{-1}})_{ijkl} = -\frac{1}{2}(C^{-1}_{ik}C^{-1}_{jl} + C^{-1}_{il}C^{-1}_{jk})$.

Then by using the formulas (3.10)-(3.12) we can get the stiffness tensor and Cauchy stress required for Abaqus UMAT implementation.

And when isotropic neo-Hookean model is adopted, the strain energy function is in the form of:

$$
W = \frac{\mu}{2}(\bar{I}_1 - 3) + \frac{1}{D_1}(J-1)^2
\tag{B.5}
$$

According to the formulas derived above, we can easily get the following relations:

$$\frac{\partial \bar{W}}{\partial \bar{\mathbf{C}}}=\frac{\partial \bar{W}}{\partial \bar{I}_1}\frac{\partial \bar{I}}{\partial \bar{\mathbf{C}}}=\frac{\mu}{2}\mathbf{I}\ ,\ \frac{\partial U}{\partial J}=\frac{2}{D_1}(\mathrm{J}-1)\ ,\ \frac{\partial^2 U}{\partial J^2}=\frac{2}{D_1}\ ,\ \frac{\partial \bar{W}}{\partial \bar{\mathbf{C}}}\cdot\bar{\mathbf{C}}=\mathbf{I}\cdot\bar{\mathbf{C}}=\bar{I}_1$$

$$\frac{\partial^2 \bar{W}}{\partial \bar{\mathbf{C}}\partial \bar{\mathbf{C}}}=\frac{\partial}{\partial \bar{\mathbf{C}}}(\frac{\partial \bar{W}}{\partial \bar{\mathbf{C}}})=\frac{\partial}{\partial \bar{\mathbf{C}}}(\frac{\mu}{2}\mathbf{I})=\mathbf{0}\ ,\ \bar{\mathbb{C}}_{\bar{W}}=\mathbf{0} \tag{B.6}$$

And elasticity tensor is:

$$\begin{aligned}\mathbb{C}=&\frac{2}{D_1}J(J-1)\,(\mathbf{C}^{-1}\otimes\mathbf{C}^{-1}-2\mathbb{I}_{\mathbf{C}^{-1}})+\frac{2}{D_1}J^2\mathbf{C}^{-1}\otimes\mathbf{C}^{-1}\\&-\frac{2}{3}\mu J^{-2/3}[\mathbf{I}\otimes\mathbf{C}^{-1}+\mathbf{C}^{-1}\otimes\mathbf{I}]+\frac{2}{3}\mu\bar{I}_1(\mathbb{I}_{\mathbf{C}^{-1}}+\frac{1}{3}\mathbf{C}^{-1}\otimes\mathbf{C}^{-1})\end{aligned} \tag{B.7}$$

By transforming by $\mathbb{C}^{\tau c}_{ijkl}=F_{ip}F_{jq}F_{kr}F_{ls}\mathbb{C}_{pqrs}$, we can get the Oldroyd rate which is:

$$\mathbb{C}^{\tau c}=\frac{2}{D_1}J(J-1)\,(\mathbf{1}\otimes\mathbf{1}-2\mathbb{I})+\frac{2}{D_1}J^2\mathbf{1}\otimes\mathbf{1}-\frac{2}{3}\mu J^{-2/3}[\mathbf{B}\otimes\mathbf{1}+\mathbf{1}\otimes\mathbf{B}]+\frac{2}{3}\mu\bar{I}_1(\mathbb{I}+\frac{1}{3}\mathbf{1}\otimes\mathbf{1}) \tag{B.8}$$

The second Piola-Kirchhoff stress is:

$$\mathbf{S}=\frac{2}{D_1}J(J-1)\mathbf{C}^{-1}+\mu(J^{-2/3}\mathbf{1}-\frac{1}{3}\bar{I}_1\mathbf{C}^{-1}) \tag{B.9}$$

Then by pushing forward operations, we can get the stress at current configuration:

$$\boldsymbol{\tau}=\mathbf{F}\mathbf{S}\mathbf{F}^T=\frac{2}{D_1}J(J-1)\mathbf{I}+\mu(\bar{\mathbf{B}}-\frac{1}{3}\bar{I}_1\mathbf{I}) \tag{B.10}$$

$$\boldsymbol{\sigma}=J^{-1}\boldsymbol{\tau}=\frac{2}{D_1}(J-1)\mathbf{I}+\frac{\mu}{J}(\bar{\mathbf{B}}-\frac{1}{3}\bar{I}_1\mathbf{I}) \tag{B.11}$$

And the elasticity tensor is

$$\mathbb{C}^{\tau Z-J}=\mathbb{C}^{\tau c}+\frac{1}{2}(\delta_{\mathrm{ik}}\tau_{jl}+\tau_{ik}\delta_{\mathrm{jl}}+\delta_{\mathrm{il}}\tau_{jk}+\tau_{il}\delta_{\mathrm{jk}})\ \mathbf{e}_i\otimes\mathbf{e}_j\otimes\mathbf{e}_k\otimes\mathbf{e}_l \tag{B.12}$$

Or expressed in a form of index notation:

$$\mathbb{C}_{ijkl}^{\tau Z-J}=\mathbb{C}_{ijkl}^{\tau c}+\frac{1}{2}(\delta_{\mathrm{ik}}\tau_{jl}+\tau_{ik}\delta_{\mathrm{jl}}+\delta_{\mathrm{il}}\tau_{jk}+\tau_{il}\delta_{\mathrm{jk}})$$
$$=\frac{2}{D_1}J(J-1)(\delta_{ij}\delta_{kl}-\delta_{ik}\delta_{jl}-\delta_{il}\delta_{jk})+\frac{2}{D_1}J^2\delta_{ij}\delta_{kl}$$
$$-\frac{2}{3}\mu[B_{ij}\delta_{kl}+\delta_{ij}B_{kl}-\bar{I}_1(\frac{1}{2}(\delta_{ik}\delta_{jl}+\delta_{il}\delta_{jk})+\frac{1}{3}\delta_{ij}\delta_{kl})] \quad \text{(B.13)}$$

And

$$\mathbb{C}_{ijkl}^{MZ-J}=\frac{\mu}{J}[\frac{1}{2}(\delta_{\mathrm{ik}}\bar{B}_{jl}+\bar{B}_{ik}\delta_{\mathrm{jl}}+\delta_{\mathrm{il}}\bar{B}_{jk}+\bar{B}_{il}\delta_{\mathrm{jk}})+\frac{2}{3}(\frac{1}{3}\bar{I}_1\delta_{\mathrm{ij}}\delta_{\mathrm{kl}}-\bar{B}_{ij}\delta_{\mathrm{kl}}-\delta_{\mathrm{ij}}\bar{B}_{kl})]+\frac{2}{D_1}(2J-1)\delta_{\mathrm{ij}}\delta_{\mathrm{kl}}$$

(B.14)

APPENDIX C

This appendix presents the derivation about the Cauchy stress and elasticity tensor of anisotropic hyperelastic model for Abaqus UMAT use and then neo-Hookean model is taken for demonstration. The strain energy function of anisotropic hyperelastic model is:

$$W = W(I_3) + w(\bar{I}_1, \bar{I}_4, \bar{I}_5) \tag{C.1}$$

where $I_1 = tr\mathbf{C}, I_3 = J^2 = \det \mathbf{C}$, $J_1 = \boldsymbol{n}_0 \cdot \mathbf{C}\, \boldsymbol{n}_0$, $K_1 = \boldsymbol{m}_0 \cdot \mathbf{C}\, \boldsymbol{m}_0$, $\bar{I}_1 = J^{-2/3} I_1$, $\bar{I}_4 = J^{-2/3} J_1$, $\bar{I}_5 = J^{-2/3} K_1$.

The 2nd Piola-Kirchhoff stress can be derived as:

$$\begin{aligned} \frac{1}{2}\mathbf{S} &= W_3 I_3 \mathbf{C}^{-1} + w_1 (I_3^{-1/3}\mathbf{I} - \frac{1}{3}\bar{I}_1 \mathbf{C}^{-1}) + w_4 (I_3^{-1/3}\mathbf{N}_0 - \frac{1}{3}\bar{I}_4 \mathbf{C}^{-1}) + w_5 (I_3^{-1/3}\mathbf{M}_0 - \frac{1}{3}\bar{I}_5 \mathbf{C}^{-1}) \\ &= w_1 I_3^{-1/3}\mathbf{I} + [W_3 I_3 - \frac{1}{3}(w_1 \bar{I}_1 + w_4 \bar{I}_4 + w_5 \bar{I}_5)]\mathbf{C}^{-1} + w_4 I_3^{-1/3}\mathbf{N}_0 + w_5 I_3^{-1/3}\mathbf{M}_0 \end{aligned} \tag{C.2}$$

Where $W_i = \dfrac{\partial W}{\partial I_i}, i \in \{3\}$ and $w_i = \dfrac{\partial w}{\partial \bar{I}_i}, i \in \{1,4,5\}$

Some differential formulas have been used in above:

$$\begin{aligned} &\frac{\partial I_3}{\partial \mathbf{C}} = I_2\mathbf{I} - I_1\mathbf{C} + \mathbf{C}^2 = I_3\mathbf{C}^{-1} \\ &\frac{\partial I_1}{\partial \mathbf{C}} = I \qquad\qquad \Rightarrow \qquad \frac{\partial \bar{I}_1}{\partial \mathbf{C}} = I_3^{-1/3}\mathbf{I} - \frac{1}{3}\bar{I}_1\mathbf{C}^{-1} \\ &\frac{\partial I_4}{\partial \mathbf{C}} = \mathbf{n}_0 \otimes \mathbf{n}_0 = \mathbf{N}_0 \qquad \Rightarrow \qquad \frac{\partial \bar{I}_4}{\partial \mathbf{C}} = I_3^{-1/3}\mathbf{N}_0 - \frac{1}{3}\bar{I}_4\mathbf{C}^{-1} \\ &\frac{\partial I_5}{\partial \mathbf{C}} = \mathbf{m}_0 \otimes \mathbf{m}_0 = \mathbf{M}_0 \quad \Rightarrow \qquad \frac{\partial \bar{I}_5}{\partial \mathbf{C}} = I_3^{-1/3}\mathbf{M}_0 - \frac{1}{3}\bar{I}_5\mathbf{C}^{-1} \end{aligned} \tag{C.3}$$

The Cauchy stress can be obtained by push-forward operations of the equation (C.2)

$$\frac{1}{2}J\boldsymbol{\sigma} = w_1 I_3^{-1/3}\mathbf{B} + [W_3 I_3 - \frac{1}{3}(w_1\bar{I}_1 + w_4\bar{I}_4 + w_5\bar{I}_5)]\mathbf{I} + w_4 I_3^{-1/3} I_4 \mathbf{n}\otimes\mathbf{n} + w_5 I_3^{-1/3} I_5 \mathbf{m}\otimes\mathbf{m} \tag{C.4}$$

Where $\mathbf{n} = \lambda_n^{-1}\mathbf{F}\mathbf{n}_0$, $\mathbf{m} = \lambda_m^{-1}\mathbf{F}\mathbf{m}_0$ and λ_n, λ_m are the stretch quantities along the $\mathbf{n}_0$, $\mathbf{m}_0$ directions.

The following formula has been used in the push-forward operations:

$$\begin{aligned}
&\varphi^*(\mathbf{I}) = \mathbf{B} \\
&\varphi^*(\mathbf{C}) = \mathbf{B}^2 \\
&\varphi^*(\mathbf{C}^{-1}) = \mathbf{I} \\
&\varphi^*(\mathbf{N}_0) = I_4 \mathbf{n}\otimes\mathbf{n} \\
&\varphi^*(\mathbf{M}_0) = I_5 \mathbf{m}\otimes\mathbf{m}
\end{aligned} \tag{C.5}$$

Now we come to derive the elasticity tensor, the spatial form is obtained first by derivative of the second Piola-Kirchhoff stress $\mathbf{S}$ with respect to stretch tensor $\mathbf{C}$ as expressed in the equation (C.6):

$$\begin{aligned}
\frac{1}{4}\mathbb{C} &= I_3^{-2/3} w_{11}\mathbf{1}\otimes\mathbf{1} \\
&+ (-\frac{1}{3}I_3^{-1/3}\bar{I}_1 w_{11} - \frac{1}{3}I_3^{-1/3} w_1 - \frac{1}{3}I_3^{-1/3}\bar{I}_4 w_{14} - \frac{1}{3}I_3^{-1/3}\bar{I}_5 w_{15})(\mathbf{I}\otimes\mathbf{C}^{-1} + \mathbf{C}^{-1}\otimes\mathbf{I}) \\
&+ [I_3^2 W_{33} + I_3 W_3 + \frac{1}{9}(\bar{I}_1 w_1 + \bar{I}_4 w_4 + \bar{I}_5 w_5 + \bar{I}_1^2 w_{11} + \bar{I}_4^2 w_{44} + \bar{I}_5^2 w_{55} + 2\bar{I}_1\bar{I}_4 w_{14} \\
&+ 2\bar{I}_1\bar{I}_5 w_{15} + 2\bar{I}_4\bar{I}_5 w_{45})]\mathbf{C}^{-1}\otimes\mathbf{C}^{-1} \\
&+ I_3^{-2/3} w_{14}(\mathbf{1}\otimes\mathbf{N}_0 + \mathbf{N}_0\otimes\mathbf{1}) + I_3^{-2/3} w_{15}(\mathbf{1}\otimes\mathbf{M}_0 + \mathbf{M}_0\otimes\mathbf{1}) \\
&+ (-\frac{1}{3}I_3^{-1/3}\bar{I}_1 w_{14} - \frac{1}{3}I_3^{-1/3}\bar{I}_4 w_{44} - \frac{1}{3}I_3^{-1/3} w_4 - \frac{1}{3}I_3^{-1/3}\bar{I}_5 w_{45})(\mathbf{C}^{-1}\otimes\mathbf{N}_0 + \mathbf{N}_0\otimes\mathbf{C}^{-1}) \\
&+ (-\frac{1}{3}I_3^{-1/3}\bar{I}_1 w_{15} - \frac{1}{3}I_3^{-1/3}\bar{I}_5 w_{55} - \frac{1}{3}I_3^{-1/3} w_5 - \frac{1}{3}I_3^{-1/3}\bar{I}_4 w_{45})(\mathbf{C}^{-1}\otimes\mathbf{M}_0 + \mathbf{M}_0\otimes\mathbf{C}^{-1})
\end{aligned}$$

$$
\begin{aligned}
&+ I_3^{-2/3} w_{44} \mathbf{N}_0 \otimes \mathbf{N}_0 + I_3^{-2/3} w_{55} \mathbf{M}_0 \otimes \mathbf{M}_0 \\
&+ I_3^{-2/3} w_{45} (\mathbf{N}_0 \otimes \mathbf{M}_0 + \mathbf{M}_0 \otimes \mathbf{N}_0) \\
&+ [W_3 I_3 - \frac{1}{3}(\bar{I}_1 w_1 + \bar{I}_4 w_4 + \bar{I}_5 w_5)] \mathbf{I}_{\mathbf{C}^{-1}}
\end{aligned} \tag{C.6}
$$

By push-forward operation using the above formula and

$\varphi^*(\mathbf{I}_{\mathbf{C}^{-1}}) = (-\frac{1}{2})(\delta_{ik}\delta_{jl} + \delta_{il}\delta_{jk})\mathbf{e}_i \otimes \mathbf{e}_j \otimes \mathbf{e}_k \otimes \mathbf{e}_l$, we have

$$
\begin{aligned}
\frac{1}{4}\mathbb{C}^{tc} &= I_3^{-2/3} w_{11} \mathbf{B} \otimes \mathbf{B} \\
&+ (-\frac{1}{3} I_3^{-1/3} \bar{I}_1 w_{11} - \frac{1}{3} I_3^{-1/3} w_1 - \frac{1}{3} I_3^{-1/3} \bar{I}_4 w_{14} - \frac{1}{3} I_3^{-1/3} \bar{I}_5 w_{15})(\mathbf{B} \otimes \mathbf{1} + \mathbf{1} \otimes \mathbf{B}) \\
&+ [I_3^2 W_{33} + I_3 W_3 + \frac{1}{9}(\bar{I}_1 w_1 + \bar{I}_4 w_4 + \bar{I}_5 w_5 + \bar{I}_1^2 w_{11} + \bar{I}_4^2 w_{44} + \bar{I}_5^2 w_{55} + 2\bar{I}_1\bar{I}_4 w_{14} \\
&+ 2\bar{I}_1\bar{I}_5 w_{15} + 2\bar{I}_4\bar{I}_5 w_{45})] \mathbf{1} \otimes \mathbf{1} \\
&+ I_3^{-2/3} w_{14} (\mathbf{B} \otimes I_4 \mathbf{n} \otimes \mathbf{n} + I_4 \mathbf{n} \otimes \mathbf{n} \otimes \mathbf{B}) + I_3^{-2/3} w_{15} (\mathbf{B} \otimes I_5 \mathbf{m} \otimes \mathbf{m} + I_5 \mathbf{m} \otimes \mathbf{m} \otimes \mathbf{B}) \\
&+ (-\frac{1}{3} I_3^{-1/3} \bar{I}_1 w_{14} - \frac{1}{3} I_3^{-1/3} \bar{I}_4 w_{44} - \frac{1}{3} I_3^{-1/3} w_4 - \frac{1}{3} I_3^{-1/3} \bar{I}_5 w_{45})(\mathbf{1} \otimes I_4 \mathbf{n} \otimes \mathbf{n} + I_4 \mathbf{n} \otimes \mathbf{n} \otimes \mathbf{1}) \\
&+ (-\frac{1}{3} I_3^{-1/3} \bar{I}_1 w_{15} - \frac{1}{3} I_3^{-1/3} \bar{I}_5 w_{55} - \frac{1}{3} I_3^{-1/3} w_5 - \frac{1}{3} I_3^{-1/3} \bar{I}_4 w_{45})(\mathbf{1} \otimes I_5 \mathbf{m} \otimes \mathbf{m} + I_5 \mathbf{m} \otimes \mathbf{m} \otimes \mathbf{1}) \\
&+ I_3^{-2/3} w_{44} I_4^2 \mathbf{n} \otimes \mathbf{n} \otimes \mathbf{n} \otimes \mathbf{n} + I_3^{-2/3} w_{55} I_5^2 \mathbf{m} \otimes \mathbf{m} \otimes \mathbf{m} \otimes \mathbf{m} \\
&+ I_3^{-2/3} w_{45} I_4 I_5 (\mathbf{n} \otimes \mathbf{n} \otimes \mathbf{m} \otimes \mathbf{m} + \mathbf{m} \otimes \mathbf{m} \otimes \mathbf{n} \otimes \mathbf{n}) \\
&+ [W_3 I_3 - \frac{1}{3}(\bar{I}_1 w_1 + \bar{I}_4 w_4 + \bar{I}_5 w_5)](-\frac{1}{2})(\delta_{ik}\delta_{jl} + \delta_{il}\delta_{jk})\mathbf{e}_i \otimes \mathbf{e}_j \otimes \mathbf{e}_k \otimes \mathbf{e}_l
\end{aligned} \tag{C.7}
$$

Now for Neo-Hookean model, substitute the specific form of $W = \frac{1}{D}(I_3^{1/2} - 1)^2$ and

$w = \frac{\mu}{2}(\bar{I}_1 - 3) + C_{201}(\bar{I}_4 \text{-} 1)^2 + C_{202}(\bar{I}_5 \text{-} 1)^2$ into the above relations， we can have

$W_3 = \frac{1}{D}(1 - I_3^{-1/2})$， $W_{33} = \frac{1}{2D} I_3^{-1/2-1}$

$$
\begin{aligned}
&w_1 = \frac{\mu}{2}, \quad w_{11} = 0, \; w_{14} = 0, \; w_{15} = 0 \\
&w_4 = 2C_{201}(\bar{I}_4 - 1), \; w_{41} = 0, \; w_{44} = 2C_{201}, \quad w_{45} = 0 \\
&w_5 = 2C_{202}(\bar{I}_5 - 1), \; w_{51} = 0, \; w_{54} = 0, \quad w_{55} = 2C_{202}
\end{aligned} \tag{C.8}
$$

Thus,

$$
\begin{aligned}
\frac{1}{4}\mathbb{C}^{rc} = &-\frac{\mu}{6} I_3^{-1/3}(\mathbf{B}\otimes\mathbf{1} + \mathbf{1}\otimes\mathbf{B}) \\
&+ [\frac{1}{2D} I_3^{1/2} + \frac{1}{D}(I_3 - I_3^{1/2}) + \frac{1}{9}(\frac{\mu}{2}\bar{I}_1 + 2C_{201}(\bar{I}_4 - 1)\,\bar{I}_4 + 2C_{202}(\bar{I}_5 - 1)\bar{I}_5 + 2C_{201}\bar{I}_4^2 \\
&+ 2C_{202}\bar{I}_5^2)]\mathbf{1}\otimes\mathbf{1} \\
&+ (-\frac{2}{3}C_{201} I_3^{-1/3}\bar{I}_4 - \frac{2}{3}C_{201}(\bar{I}_4 - 1) I_3^{-1/3})(\mathbf{1}\otimes I_4\mathbf{n}\otimes\mathbf{n} + I_4\mathbf{n}\otimes\mathbf{n}\otimes\mathbf{1}) \\
&+ (-\frac{2}{3}C_{202} I_3^{-1/3}\bar{I}_5 - \frac{2}{3}C_{202}(\bar{I}_5 - 1) I_3^{-1/3})(\mathbf{1}\otimes I_5\mathbf{m}\otimes\mathbf{m} + I_5\mathbf{m}\otimes\mathbf{m}\otimes\mathbf{1}) \\
&+ 2C_{201} I_3^{-2/3} I_4^2 \mathbf{n}\otimes\mathbf{n}\otimes\mathbf{n}\otimes\mathbf{n} + 2C_{202} I_3^{-2/3} I_5^2 \mathbf{m}\otimes\mathbf{m}\otimes\mathbf{m}\otimes\mathbf{m} \\
&+ [\frac{1}{D}(1 - I_3^{-1/2}) I_3 - \frac{1}{3}(\frac{\mu}{2}\bar{I}_1 + 2C_{201}(\bar{I}_4 - 1)\,\bar{I}_4 + 2C_{202}(\bar{I}_5 - 1)\,\bar{I}_5)] \\
&(-\frac{1}{2})(\delta_{ik}\delta_{jl} + \delta_{il}\delta_{jk})\mathbf{e}_i\otimes\mathbf{e}_j\otimes\mathbf{e}_k\otimes\mathbf{e}_l
\end{aligned} \tag{C.9}
$$

For Abaqus user material subroutine use,

$$
\begin{aligned}
\mathbb{C}^{MZ-J} &= \frac{1}{J}\mathbb{C}^{\tau c} + \frac{1}{2}(\delta_{ik}\sigma_{jl} + \sigma_{ik}\delta_{jl} + \delta_{il}\sigma_{jk} + \sigma_{il}\delta_{jk})\mathbf{e}_i \otimes \mathbf{e}_j \otimes \mathbf{e}_k \otimes \mathbf{e}_l \\
&= -\frac{2\mu}{3J}(\bar{\mathbf{B}} \otimes \mathbf{1} + \mathbf{1} \otimes \bar{\mathbf{B}}) \\
&+ [\frac{2}{D}(2J-1) + \frac{4}{9J}(\frac{\mu}{2}\bar{I}_1 + 2C_{201}(\bar{I}_4 - 1)\,\bar{I}_4 + 2C_{202}(\bar{I}_5 - 1)\bar{I}_5 + 2C_{201}\bar{I}_4^2 + 2C_{202}\bar{I}_5^2)]\mathbf{1} \otimes \mathbf{1} \\
&- \frac{8}{3J}C_{201}(2\bar{I}_4 - 1)\bar{I}_4(\mathbf{1} \otimes \mathbf{n} \otimes \mathbf{n} + \mathbf{n} \otimes \mathbf{n} \otimes \mathbf{1}) \\
&- \frac{8}{3J}C_{202}(2\bar{I}_5 - 1)\bar{I}_5(\mathbf{1} \otimes \mathbf{m} \otimes \mathbf{m} + \mathbf{m} \otimes \mathbf{m} \otimes \mathbf{1}) \\
&+ \frac{8}{J}C_{201}\bar{I}_4^2\mathbf{n} \otimes \mathbf{n} \otimes \mathbf{n} \otimes \mathbf{n} + \frac{8}{J}C_{202}\bar{I}_5^2\mathbf{m} \otimes \mathbf{m} \otimes \mathbf{m} \otimes \mathbf{m} \\
&+ [\frac{4}{D}(J-1) - \frac{4}{3J}(\frac{\mu}{2}\bar{I}_1 + 2C_{201}(\bar{I}_4 - 1)\,\bar{I}_4 + 2C_{202}(\bar{I}_5 - 1)\,\bar{I}_5)] \\
&(-\frac{1}{2})(\delta_{ik}\delta_{jl} + \delta_{il}\delta_{jk})\mathbf{e}_i \otimes \mathbf{e}_j \otimes \mathbf{e}_k \otimes \mathbf{e}_l \\
&+ \frac{1}{2}(\delta_{ik}\sigma_{jl} + \sigma_{ik}\delta_{jl} + \delta_{il}\sigma_{jk} + \sigma_{il}\delta_{jk})\mathbf{e}_i \otimes \mathbf{e}_j \otimes \mathbf{e}_k \otimes \mathbf{e}_l
\end{aligned}
\tag{C.10}
$$

And

$$
\begin{aligned}
\boldsymbol{\sigma} &= \frac{\mu}{J}\bar{\mathbf{B}} + [\frac{2}{D}(J-1) - \frac{2}{3J}(\frac{\mu}{2}\bar{I}_1 + 2C_{201}(\bar{I}_4 - 1)\,\bar{I}_4 + 2C_{202}(\bar{I}_5 - 1)\bar{I}_5)]\mathbf{1} \\
&+ \frac{4C_{201}}{J}(\bar{I}_4 - 1)\,\bar{I}_4\mathbf{n} \otimes \mathbf{n} + \frac{4C_{202}}{J}(\bar{I}_5 - 1)\bar{I}_5\mathbf{m} \otimes \mathbf{m}
\end{aligned}
\tag{C.11}
$$